INTERACTION OF BRIDGE CONTRACTION SCOUR AND PIER SCOUR IN A LABORATORY RIVER MODEL

A Thesis
Presented to
The Academic Faculty

by

SeungHo Hong

In Partial Fulfillment
Of the Requirements for the Degree
Master of Science in Civil Engineering

Georgia Institute of Technology
December 2005

INTERACTION OF BRIDGE CONTRACTION SCOUR AND PIER SCOUR IN A LABORATORY RIVER MODEL

Approved by

Dr. Terry W. Sturm, Chairman
School of Civil and Environmental Engineering
Georgia Institute of Technology

Dr. Marc Stieglitz
School of Civil and Environmental Engineering
Georgia Institute of Technology

Mark N. Landers
U.S. Geological Survey

Date Approved: **November 17, 2005**

ACKNOWLEDGEMENTS

The writer wishes to express his sincere appreciation to all who had a part in making this thesis possible. Firstly, special appreciation is expressed to Dr. Terry W. Strum, thesis advisor and chairman of the reading committee, who initially suggested the topic and offered excellent guidance throughout the duration of the study. Gratitude is expressed to Dr. M. Stieglitz, Georgia Institute of Technology, and to M.N. Landers, U.S. Geological Survey, for their assistance and their time in reviewing and commenting on this thesis. Sincere thanks are due to Andy Udell whose assistance in the construction of the model was indispensable. Finally, I appreciated to my parents and lovely my wife, Hae sun.

TABLE OF CONTENTS

LIST OF TABLES

LIST OF FIGURES

SUMMARY

Existing scour depth equations recommended by the Federal Highway Administration (FHWA) generally give excessively conservative estimates of the scour depth because these equations are based primarily on idealized laboratory experiments in rectangular flumes. In addition to idealized laboratory experiments, another possible reason for scour depth overprediction is the current practice of adding separate estimates of contraction scour and local scour when in fact these processes occur simultaneously and interact. The experiments were conducted to address the interaction between contraction scour and local scour (pier scour) using a 1:45 scale hydraulic model of the Ocmulgee River bridge at Macon, Georgia including the river bathymetry. The results show that the time development of contraction scour is much slower than pier scour, and that the specific discharge distribution causing contraction scour is affected by pier scour. The comparison between laboratory and field measurements of local pier scour showed good agreement for maximum scour depth. The comparison between measured laboratory contraction scour and predicted clear-water contraction scour using accepted theoretical formulas also resulted in close agreement provided that adjustments were made for residual contraction scour. However, laboratory and field measurements of contraction scour showed some discrepancy for a historic discharge based on only one field-measured cross section upstream of the bridge. The field results indicate that contraction scour is very dynamic and constantly adjusting to the incoming sediment load, and that the assumption of a long contraction that underpins the theoretical contraction scour formulas is not entirely accurate. More detailed spatial and temporal field data is

needed for a large prototype discharge so that it can be modeled directly in the laboratory to obtain more definitive comparisons.

CHAPTER I

INTRODUCTION

While flood damages typically involve widespread inundation of agricultural land, destruction of homes and businesses, and disruption of economic activity, a less obvious threat is the existence of bridges over waterways that cause flow obstruction and scour around the bridge foundations with possible failure of the bridges. The mechanism of bridge foundation failure is due to processes of (1)local scour at the base of abutments and piers caused by flow obstruction, downflow, and formation of a horseshoe vortex that wraps around the obstructions and (2)contraction scour across the entire channel due to the flow contraction caused by the bridge opening and deflection of floodplain flow into the main channel.

In recent years, flood waters have closed many highways and local roads as well as interstate highways, and caused scour that damaged many bridges and even resulted in loss of life. For example, intense thunderstorms in Iowa in 1992 caused 6m of contraction scour at the State Highway 14 bridge over Wolf Creek (Fischer, 1993). One thousand bridges have collapsed over the last 30 years in the United States and the leading cause is hydraulic failure, resulting in large financial losses. In Georgia, the total financial loss

from tropical storm Alberto in 1994 was approximately $130 million because more than 100 bridges had to be replaced and repaired due to flooding (Richardson and Davis, 2001). During the 1993 upper Mississippi River basin flooding, more than 258 million dollars in federal assistance was requested for repair and/or replacement of bridges, embankments, and roadways (Parola et al. 1997). Bridge failures can be also lead to loss of life such as in the 1987 failure of the I-90 bridge over Schoharie Creek near Albany, New York, the US 51 bridge over the Hatchie River in Tennessee in 1989, and the I-5 bridges over Arroyo Pasajero in California in 1995 (Morris and Pagan-Ortiz, 1999).

The engineering design of a hydraulic structure such as a river bridge requires consideration of the factors that affect the safety of the structure. Among them, two of the most important variables are bridge foundation scour and construction cost. However, engineering experience seems to indicate that computation of scour depth using current scour formulas tends to overpredict scour in comparison to field measurements. The result can be overdesigned bridge foundations that increase the cost of the bridge. In fact, achieving a balance between safety and cost is a very difficult problem which is why the Federal Highway Administration has mandated the use of scour prediction formulas that have a very large factor of safety to compensate for a lack of understanding of the complex physics of the scour process. These scour prediction formulas are based

primarily on idealized (uniform and non-cohesive sediments and steady flow) laboratory experiments in rectangular flumes. To predict more accurate scour depths and to suggest more economical methods of designing bridge foundations, laboratory experiments should be done with physical models that reproduce the pier and abutment geometry as well as the river bathymetry, but only in a few cases has this been done. (Hunt et al. 1998)

In addition to idealized laboratory experiments, another possible reason for scour depth overprediction is the current practice of adding separate estimates of contraction scour and local scour when in fact these processes occur simultaneously and interact. Local scour occurs at the location of a bridge pier or abutment due to obstruction of the flow and the development of complex, three-dimensional horseshoe vortices at the base of the foundation that entrain and carry sediment away. Contraction scour, on the other hand, tends to occur across the entire bridge section due to contraction of the flow. During a flood, velocities increase as depths increase but they are also affected by changes in the distribution of discharge between the main channel and floodplain especially within the contracted bridge section. In addition, the time history and time development of contraction scour and local scour are not the same. As a result, the influence of local scour on contraction scour, for example, is time dependent. Some

researchers have studied the relationship between local scour and contraction scour (Niezgoda et al.1999 and Schreider et al. 2001). However, those studies were limited to the interaction between abutment scour and contraction scour and so did not consider the relationship between pier scour and contraction scour. As a matter of fact, very few laboratory studies have been conducted on contraction scour which is the focus of this thesis.

In the present study, laboratory experiments were conducted using a 1:45 scale hydraulic model of the Ocmulgee River bridge at Macon, Georgia including the river bathymetry over a 850 ft length reach of the river. Initially, the contraction scour was measured without the bridge piers in place using the historic floods having recurrence intervals of 20 yr (65,000cfs) and 50yr (79,200cfs). In these experiments, the time history of the scour and of the velocity in the bridge section were measured. Then the piers were placed at the bridge cross- section in the flume, and the same measurements were made. The movable-bed section was fixed by using polyurethane to enable measurement of the initial velocities before scour at the bridge approach section and in regions of pier and contraction scour. These velocity measurements were repeated after scour had reached an equilibrium state which was approximately 48-72 hours for pier scour and as much as 100hrs for contraction scour. Detailed scour depths were measured for both local and

contraction scour at the end of each experiment. The experiment procedure was carried out for a historical flood for which field measurements were available. For this case, comparisons are made among field measurements of scour depth, experimental results and computed scour depth using existing scour-prediction formulas. In addition, experiments were conducted for design discharges including the 50yr flood and 100yr flood to determine the effect of discharge on the results. The experimental results are used to assess the relative contribution of contraction scour and local pier scour to the final design of the bridge foundation depth.

Chapter II is a review of basic concepts of scour formula and current literature related to comparison between field measurement and result calculated by the scour prediction formula. River modeling in the lab and experimental procedures are described in Chapter III. Results and analysis are found in Chapter IV, and the final chapter provides conclusions and recommendations.

CHAPTER II

LITERATURE REVIEW

2.1 Introduction

Long roadway approach sections and narrow bridge openings force floodplain waters to re-enter the main channel at the bridge, causing a severe contraction in flow area that results in both contraction and local scour. This severe contraction in flow area produces a mixed flow pattern under the bridge, with increased velocities, shear stresses, and turbulence around the bridge pier. As a result, it is difficult to separate contraction scour and local scour processes. However, current scour practice assumes that contraction and local scour processes are independent and thus are determined separately and summed for total scour depth (Richardson and Davis, 2001). Furthermore, existing contraction scour prediction equations are based on theories of flow continuity and sediment transport in an idealized long contraction, while existing local scour prediction equations are based primarily on laboratory data, making many of the existing contraction and local scour prediction equations unsuitable with respect to field conditions. Idealized laboratory experiments which often employ rectangular channels and uniform sediment while ignoring effects of some important dimensionless parameters

may limit the accuracy of scour depth estimate when applied to actual field conditions.

2.2 Contraction scour

When the flow area at flood stage is reduced by a natural contraction or bridge opening, the velocity and bed shear stress will be increased as required by continuity and momentum considerations. The higher velocity results in an increased erosive force so that more bed material is removed from the contracted reach. As a result, the bed elevation is lowered and a scour hole develops over the general bridge cross section, which is called contraction scour. Contraction scour is classified as either clear-water or live-bed. In the clear-water case, no sediment transport occurs upstream of the contraction, while in the live-bed case, sediment is transported from upstream through the contraction scour area.

2.2.1 Live bed contraction scour

Laursen(1958) developed expressions for both live-bed and clear-water contraction scour. He assumed that the contraction was long so that the flow is uniform and sediment transport occurs only in the main channel for the live-bed case. To satisfy continuity at the equilibrium state, he expressed conservation of sediment mass with

reference to Fig 2.1 as

$$C_{t1} Q_c = C_{t2} Q_T \tag{2.1}$$

where, C_{t1} is mean sediment concentration in the approach section; Q_c is approach channel discharge; C_{t2} is mean sediment concentration in the contracted section; Q_T is total discharge in the contracted section; Q_o is the overbank discharge.

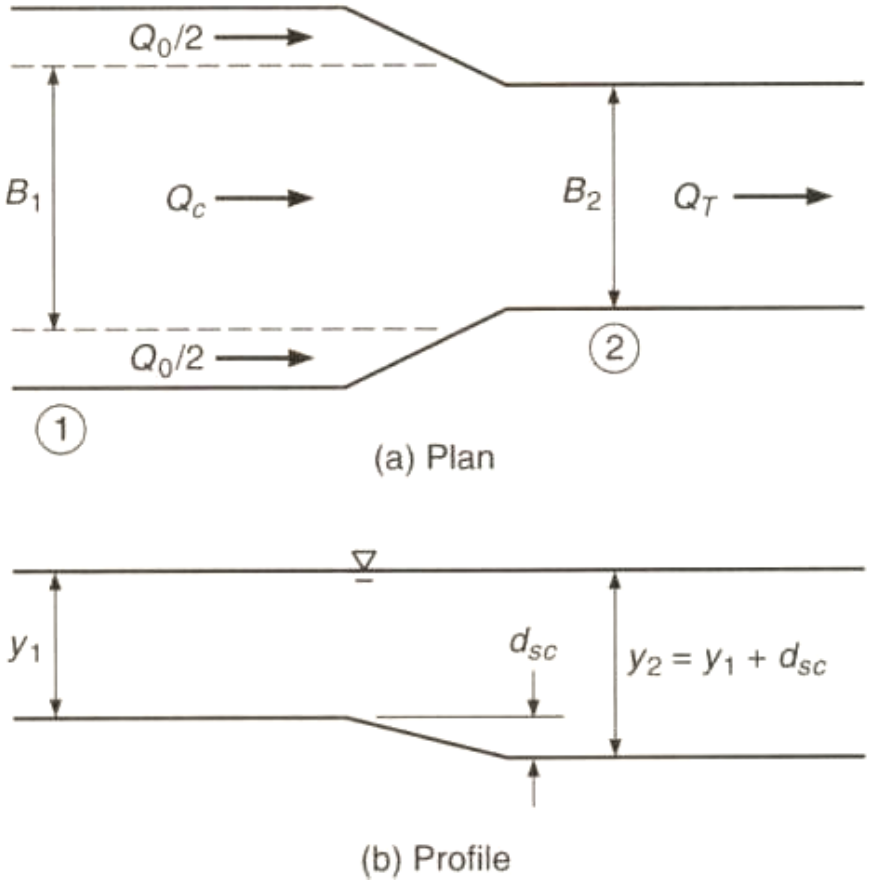

Figure 2.1 Scour in an idealized long contraction

Laursen then applied his total sediment discharge formula given by

$$C_{t,ppm} = (1*10^4)\left[\frac{d_{50}}{y_0}\right]^{7/6}\left(\frac{\tau'_0}{\tau_c}-1\right)f(\frac{u_*}{w_f}) \qquad (2.2)$$

where, C_t is total sediment concentration in ppm by weight; d_{50} is median grain size; y_0 is uniform flow depth; $\tau_0^{/}$ is grain shear stress; τ_c is critical shear stress; and $f(u_*/w_f)$ is the specified graphical function of the ratio of shear velocity to fall velocity which Laursen determined from experiment. To determine the value of τ'_0/τ_c, Manning's equation and Strickler's equation are used. In this procedure Laursen assumed that the channel is wide enough to use y_0 (uniform flow depth) instead of using R (hydraulic radius) in Manning's equation, and that no bedforms exist so that Stricker's equation is valid for flow resistance as a function of grain resistance alone. Also, he assumed $f(u_*/w_f)$ to be a power function expressed as $\left(u_*/w_f\right)^a$. Substituting the formula for the sediment discharge equation (2.2) into the sediment continuity equation (2.1) results in the final equation developed by Laursen for live bed scour

$$\frac{y_2}{y_1} = \left(\frac{Q_T}{Q_c}\right)^{6/7}\left(\frac{B_1}{B_2}\right)^{k_1}\left(\frac{n_2}{n_1}\right)^{k_2} \qquad (2.3)$$

with the depth of contraction scour defined by

$$d_{sc} = y_2 - y_1 \tag{2.4}$$

where the variables are defined by,

y_1	=	average water depth in the upstream main channel, m
y_2	=	average water depth in the contracted section, m
Q_T	=	total flow in the contracted channel, m^3/s
Q_c	=	flow in the upstream main channel transporting sediment, m^3/s
B_1	=	width of the upstream main channel, m
B_2	=	width of the main channel in the contracted section, m
n_1	=	Manning's n for upstream main channel
n_2	=	Manning's n for contracted section
k_1 *and* k_2	=	exponents determined depending on the mode of bed material transport as given in Table 2.1

The exponents given in Table 2.1 depend on the ratio of shear velocity to sediment fall velocity (u_*/w_f), which reflects the relative capacity of the flow to suspend the sediment. It should be noted that Equation 2.4 implicitly neglects the velocity head change between the approach and contracted sections.

Table 2.1 Exponents for the live-bed contraction scour equation

u_* / w_f	k_1	k_2	Mode of bed material transport
≤ 0.50	0.59	0.066	Mostly contact bed material discharge
0.50 *to* 2.0	0.64	0.21	Some suspended bed material discharge
≥ 2.0	0.69	0.37	Mostly suspended bed material discharge

2.2.2 Clear water contraction scour

For the clear-water scour condition, scour increases in the contracted section until the shear stress (τ_0) on the bed is equal to the critical shear stress (τ_c). Laursen started from this equilibrium condition to derive the clear water contraction scour equation. At equilibrium, we have

$$\tau_0 = \tau_c \tag{2.5}$$

where, τ_0 is average bed shear stress at contracted section; and τ_c is the critical bed shear stress at incipient motion.

Now for uniform flow, the mean boundary shear stress in the contracted section is given by

$$\tau_0 = \gamma\, y_2\, S = \frac{\rho\, g\, n^2\, V^2}{y_2^{1/3}} \tag{2.6}$$

where depth y_2 is used for the hydraulic radius R because the channel is assumed very wide, and Manning's equation is used to substitute for the slope S.

For noncohesive bed material and fully developed clear-water scour, the critical shear stress can be estimated using *Shields'* relation given by

$$\tau_c = \tau_{*c} \, (\gamma_s - \gamma) \, d_{50} \tag{2.7}$$

in which, τ_{*c} is the critical value *Shields'* parameter. Equation (2.6) and (2.7) can be substituted into equation (2.5) to derive:

$$\begin{aligned} y_2 &= \left[\frac{n^2 \, V_2^{\,2}}{\tau_{*c} \, (SG-1) \, d_{50}} \right]^3 = \left[\frac{n^2 \, Q^2}{\tau_{*c} \, (SG-1) \, d_{50} \, B_2^{\,2}} \right]^{3/7} \\ y_2 &= \left(\frac{c_n^2 \, g}{K_n^2} \right)^{3/7} \left[\frac{q_2^2}{\tau_{*c} \, (SG-1) g d_{50}^{2/3}} \right]^{3/7} \end{aligned} \tag{2.8}$$

in which the variables are defined by:

y_2 = average equilibrium water depth in the contracted section after scour, m

V_2 = average velocity in the contracted section, m/s

d_{50} = median sediment diameter, m

Q = total discharge, m^3/s

B_2 = width of the main channel in the contracted section, m

SG = specific gravity of sediment (2.65 for quartz)

n = Manning's roughness coefficient

τ_{*c} = critical value of *Shields'* parameter for incipient sediment motion

c_n = Strickler constant ($= n / d_{50}^{1/6}$)

K_n = Manning equation constant (1.49 in English units and 1.0 in SI units)

q_2 = Q/B_2 (Discharge per unit of width)

Then the average contraction scour depth is obtained from

$$d_{sc} = y_2 - y_0 \tag{2.9}$$

in which d_{sc} is average scour depth; and y_0 is average existing water depth in the contracted section before scour.

2.2.3 Reference bed elevation assessment

The depth of contraction scour is the difference in average streambed elevations with and without the contraction in place and is defined generally as the difference between average streambed elevations of the contracted and uncontracted sections (Landers and Mueller, 1993). The preferred method for deciding the reference elevation for uncontracted conditions is to pass a line through the average streambed elevations of the uncontracted sections upstream and downstream of the bridge. For clear water contraction scour, the bed elevation upstream of bridge and scour hole will remain the same geometry after the passage of the flood. Therefore, post flood surveys can be used to decide the reference elevation and to measure clear water contraction scour depth. However, for live-bed contraction scour, the spatial and temporal distribution of data collected must include the data needed to identify the reference surfaces to eliminate effects from aggradation, degradation, and short-term scour. (Mueller and Wagner, 2005)

To decide the reference elevation for contraction scour without the preconstruction contour, Hayes (1996) suggested the plot of the average streambed elevations with time to review the trend of bottom elevation. Trends in the data indicate changes in stream conditions, resulting from general scour or fill. Data from periods of

time where trends exist were eliminated. Data from periods of time where no trends exist were reviewed and retained if appropriate vertical datums could be applied.

Blodgett and Harris (1993) used the channel thalweg (lowest point in a cross section) to decide the reference elevation. Channel thalweg profiles at the Sacramento River at Hamilton City, California have been surveyed since 1979. From the thalweg point at the approach cross-sections, a straight line is projected over the channel bed where the contraction scour occurs. The contraction scour was measured as the difference between this reference surface and the thalweg of the contracted bridge section. The result from using the Blodgett's reference elevation represented a worst-case condition because the contraction scour depth from this method was the predicted difference between the reference surface elevation and thalweg (the lowest point in the cross section) elevation, not between the reference surface elevation and the average surface elevation at the contracted section.

The method to determine the reference surface for live-bed conditions is very difficult. Landers and Mueller (1993) acknowledged several potential problems (Mueller and Wagner, 2005)

- Identification of the bottom width is often difficult because of irregular cross section geometry.

- Upstream and downstream cross sections may be in natural contractions or expansions because of channel bends or other factors, so there can be problems in establishing an uncontracted reference surface at the bridge.
- Measured contraction scour may not represent equilibrium scour if the scour develops over many years because of the infrequency of channel-formative flows and the resistance of the bed to scour.

2.2.4 Contraction scour case studies

Many bridges have collapsed in the United States and many researchers have tried to find a general solution for scour prediction so as to prevent bridge foundation failure due to scour. A brief summary of field data for contraction scour is presented.

Fischer(1993) presented contraction scour data occurring at the State Highway 2 bridge over the Weldon River in Iowa. The bridge is 68 m long and supported by two monolithic piers and concrete abutments. The piers and abutments are supported by steel pilings driven into the underlying glacial clay. The drainage area is 188 km^2 and a major tributary, Jonathan Creek, drains into the Weldon River about 30 m upstream of the bridge. Because the watershed consists of rolling hills that surround a wide valley, the difference between the highest point in the drainage basin and the elevation at the

basin outlet is approximately 70 m, which results in high river velocities and significant contraction at the bridge. The peak discharge was 1,930 m^3/s in September 14 and 15, 1992 and this was about 4 times the 100-year design flood. Floodwaters covered the road and bridge deck for several hours, resulting in pressure flow conditions as the water surface came into contact with the bridge structure. The difference between the upstream and downstream high water levels was 1.45 m. Contraction scour of about 1.5 m occurred upstream and downstream of the bridge as shown in Figure 2.2. Contraction scour exposed the pier footing, the entire stream face of the left abutment, and about 3 m of the left abutment pilings. No evidence was found that any pier footing piling was exposed because the clay layer was resistant to vertical scour which forced the scouring process to erode the channel at the left abutment. The bridge subsequently was closed to traffic until the scour damage at the left abutment could be repaired.

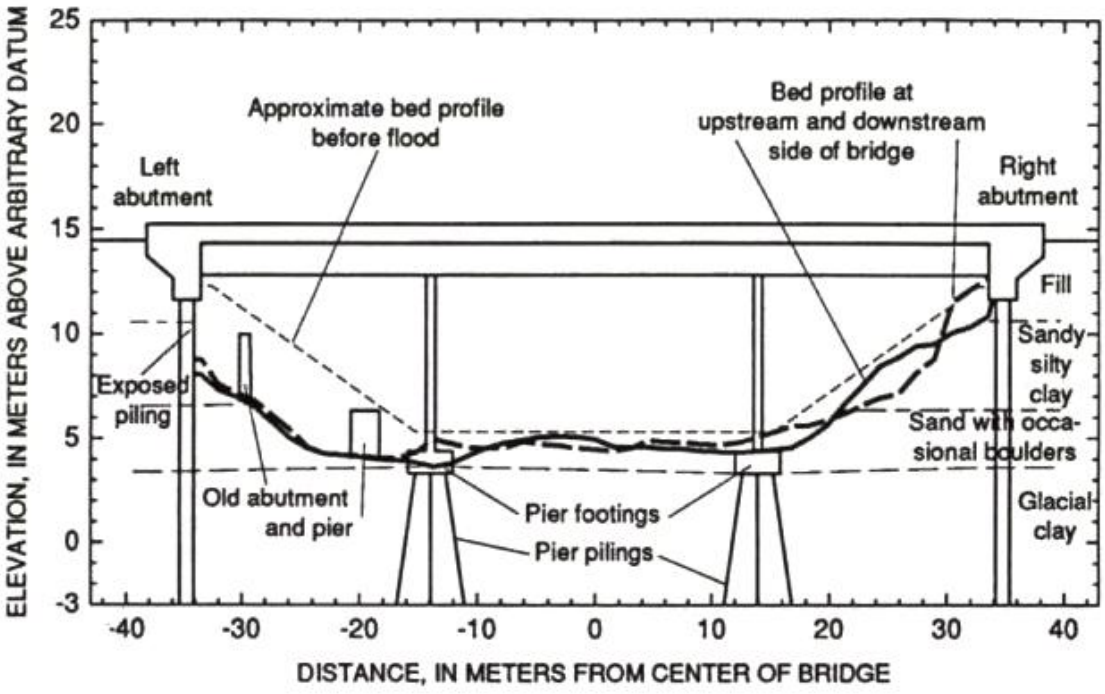

Figure 2.2 Looking downstream view of cross section at State Highway 2 bridge over the Weldon River, Iowa, 1992 (Fischer, 1993)

Flooding of the Iowa River in July and August of 1993 caused extensive contraction scour at the State Highway 99 bridge over the Iowa River at Wapello, Iowa (Fishcer, 1994). The State Highway 99 bridge is a multiple span structure that is 371 m long and 9.1 m wide. The piers are concrete and are supported on footings that cap wood piling. The streambed in the main channel is sand and gravel and the sand and gravel is underlain by glacial clay. The drainage area is 32,372 km ^{2}and there is dense tree cover in the flood plain. The peak discharge for the 1993 flood was 3,140 m^3/s. It is the greatest peak discharge in 79 years of stream flow record collected at the site. An

irregular characteristic of this flood is the long duration of high water, a period of 106 days. Because the stream bed was not filling in under the bridge due to sediment deposition after the flood had receded, the channel was sounded upstream and downstream to determine the extent of the scoured bed. Bed profiles measured after the flood are shown in Figure 2.3. The lines of equal bed elevation show that the contraction in the width of the flood plain caused flood waters to scour the streamebed for a distance of about 500 m upstream of the bridge. Contraction scour of about 4 m occurred in the main channel and at least 3.3 m of piling was exposed. The resistance to flow caused by the vegetation in the flood plain also contributed to the contraction in the flow area as shown in the Figure 2.3.

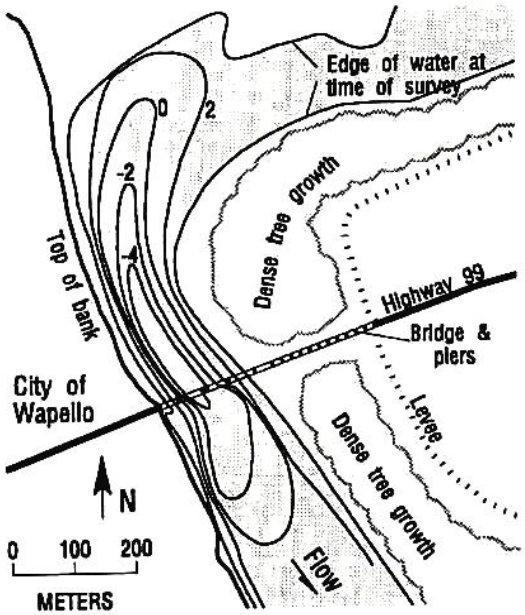

Figure 2.3 Lines of equal bed elevation in the Iowa River at the State Highway 99 bridge, 1993 (Fischer, 1994)

2.3 Pier scour

To compute the pier scour depth, HEC-18 recommended the equation based on the CSU equation for both live-bed and clear-water pier scour. The pier scour is obtained from

$$\frac{d_s}{b} = 2.0 K_s K_\theta K_b K_a (\frac{y_1}{b})^{0.35} Fr_1^{0.43} \quad (2.10)$$

in which, d_s is pier scour depth, b is pier width, K_s is pier shape factor, K_θ is skewness factor, K_b is correction factor for bed condition, K_a is bed armoring factor, y_1 is approach flow depth for pier scour and Fr_1 is approach Froude number for pier scour.

2.4 Discrepancy between predicted and observed scour depths

Most scour equations are either based on theories or based primarily on laboratory data. As a result, a lot of important factors that must be considered to predict scour depth are ignored. For example, laboratory experiments are usually conducted in the rectangular straight channel with non-cohesive uniform sediment and steady uniform flow. Although the local scour and contraction scour may be interrelated, these components are assumed independent in most experiments. Oversimplifying and neglecting many of the complexities that exist in the real world may account for some

of the discrepancy between the predicted and measured scour depths.

Holnbeck et al. (1993) presented contraction scour and abutment scour data occurring at U.S. 87 over Razor Creek in Montana and they compared computed results from scour prediction equations to the measured data. The bridge at U.S. 87 over Razor Creek is 22.9 m long and supported by two pile bents at 7.6 m spacing, each consisting of seven timber piles. The drainage area is 44.3 km^2 and the streambed consists of a sand and gravel layer. Very dense, tan sandstone and weathered shale underlie the sand and gravel. Two large floods occurred in 1986 and 1991. Holnbeck et al. compared the surveyed data after the 1991 flood with a 1955 design section. Residual scour from floods prior to 1986 was assumed to be negligible because large floods were not recorded for this area during that period. Also, scour for the 1986 flood was believed to be less than for the 1991 flood. Observed total scour was 2.23 m at the right abutment, 0.85 m at the left abutment, and 0.94 m at the pile bents as shown in Figure 2.4. However, calculated scour depths were larger than the observed result. The output from the computer model WSPRO was used to calculate the contraction, pier and abutment scour. Holnbeck et al. used the Laursen lived-bed equation to compute contraction scour, the Froehlich live-bed equation for abutment scour, and the Colorado State University equation for pier scour. The observed total scour is

compared to the calculated total scour at three locations as shown in Table 2.2. The results indicate that the equations for scour overpredict total scour for this study. The observed total scour depth is about 25 % of the total computed scour depth at the left abutment and 48 % at the right abutment. For the pier scour, the observed result is about 55 % smaller than the calculated result.

Table 2.2 Comparison of computed and measured scour at U.S. 87 on Razor Creek, Montana, 1991 (Holnbeck et al. 1993)

Location	Computed scour (m)			Observed total Scour (m)
	Contraction	Local	Total	
Left abutment	0.70	2.50	3.20	0.85
Right abutment	0.70	3.66	4.36	2.23
Pile bents	0.70	1.43	2.13	0.94

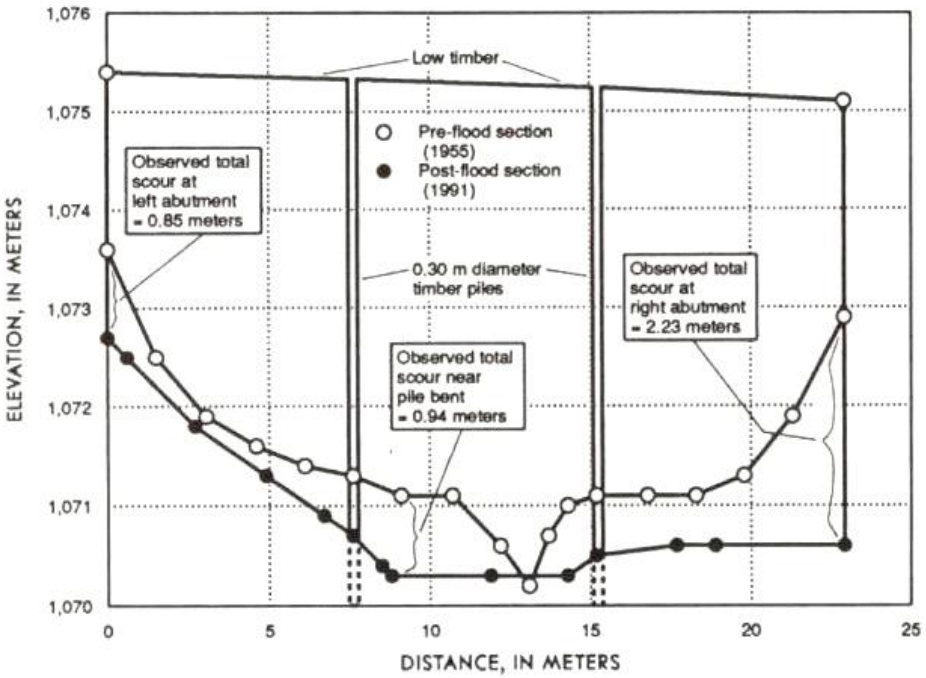

Figure 2.4 Looking downstrean view of cross sections at upstream face of bridge. Razor Creek, Montana, 1991 (Holnbeck et al. 1993)

Fischer (1995) presented a case study of contraction scour at the State Highway 14 bridge over Wolf Creek in Iowa. The bridge is a 30.5m single-span steel structure supported by vertical-wall concrete abutments with wingwalls. The drainage area is 138 km^2 and the drainage basin is surrounded by the rolling hills. The peak discharge of the 1992 flood was 2,200 m^3/s. To determine the contraction scour depth, Fischer used the stream bed profile shown in the bridge plan (1946) as a reference and concluded that contraction scour lowered the streambed in the bridge opening about 6m. However, when he used the live-bed scour equation for contraction scour, the result was 9.1 m as shown in Table 2.3 which is 50 % grater than the observed value.

Table 2.3 Comparison of computed and measured scour depth at State highway 14 bridge at Wolf Creek, Iowa, 1992 (Fischer, 1995)

Observed contraction scour depth (m)	Computed contraction scour depth (m)
6	9.1

Brabet (1994) analyzed the process of scour through twelve bridges located along the Copper River Highway, Alaska. Among them, the comparison of observed and computed contraction scour was at the two bridges, Bridge 331 and Bridge 1187. The approach cross sections in uncontracted areas and contracted areas for these two sites had been obtained in May 1992. Comparison between the mean bed elevations of the channel measured in 1968 and 1992 shows the average contraction scour depth since 1968. In 1968, the mean bed elevation of the channel was 13.6ft at the Bridge 331 and May 21, 1992 it was 4.5ft, indicating that about 9 ft of scour had occurred since 1968. For the Bridge 1187, the mean bed elevation in 1968 was 11.8 ft and in June 1992, the mean bed elevation was 9.6 ft, indicating that about 2ft of scour has occurred during this time. As shown in Table 2.4, Brabet used the Straub, Laursen, and Komura contraction scour equations to predict contraction scour. The equation was solved for the mean depth of flow at the contracted section. At Bridge 331, all three contraction scour equations overestimated the mean depth of flow. In particular, the

Komura contraction scour equation predicted a 50 % larger value than the measured mean depth of flow. However, at Bridge 1187, the results were quite close to the measured mean depth of flow, 7.8ft as shown in the Table 2.4. All predicted values were within 1.0 ft

Table 2.4 Comparison of computed and measured scour depth at Bridges 331 and 1187 on the Copper River-highway, May 1992 (Brabets, 1994)

Bridge	Measured mean depth of flow (ft)	Computed mean depth of flow from equation (ft)		
		Straub	Laursen	Komura
331	10.8	13.8	13.4	15.8
1187	7.8	8.2	8.1	8.8

Norman (1975) also presented detailed data for contraction scour at seven sites in Alaska. Norman used Straub, Laursen and Komura contraction scour equations to compute the contraction scour and to compare the computed value and measured value. The results are shown in the Table 2.5. The same as in Brabets case, the computed scour depth computed by the Komura equation had the greatest difference compared to the measured depth. The interesting thing is that the results by the Komura contraction scour equation underestimate the contraction scour depth in the 524 Bridge at Tanana

River. However, in this data set, the computed scour depth is usually larger than the measured scour depth.

Table 2.5 Comparison of computed and measured contraction scour depth at seven sites, Alaska, (Mueller and Wagner, 2005)

Location	Section Number	Measured depth (m)	Computed scour depth (m)		
			Straub	Laursen	Komura
Susitna River, bridge 254, 1971	1	4.51	Uncontracted section		
	2	4.78	4.94	4.97	5.09
	4	5.49	6.10	6.25	6.89
	5	5.61	6.16	6.34	7.04
Tazlina River, bridge 573, 1971	1	2.8	-	-	-
	2	3.14	2.99	2.99	3.60
Tanana River, bridge 524, 1971	1	3.96	Uncontracted section		
	2	4.69	5.09	5.09	2.99

On the other hand, Hayes' (1996) analysis shows that the equations for contraction scour frequently underestimate the actual scour depth. Hayes evaluated the contraction scour equation with river data measured in Delaware, Maryland, and Virginia. The uncontracted condition was determined from preconstruction contours obtained from the bridge plan for the reference elevation for contraction scour. Figure 2.5 shows the result of the comparison between measured contraction scour and

computed contraction scour for clear-water scour condition. Hayes used the Laursen's clear-water contraction scour equation to compute the contraction scour depth. As shown in Figure 2.5, all scour measurements were underestimated except for two. Figure 2.6 shows the live-bed contraction scour case. To compute the live-bed contraction scour depth, Hayes used the Laursen's live-bed contraction scour equation. As shown in the Figure 2.6, the equation underestimated contraction scour depth for 10 measurements and overestimated contraction scour for 4 measurements. The error between measured and predicted contraction scour was less than 1.0 ft for all 10 measurements that were underestimated. The predicted values that overestimated the measured values did not overestimate by large amounts.

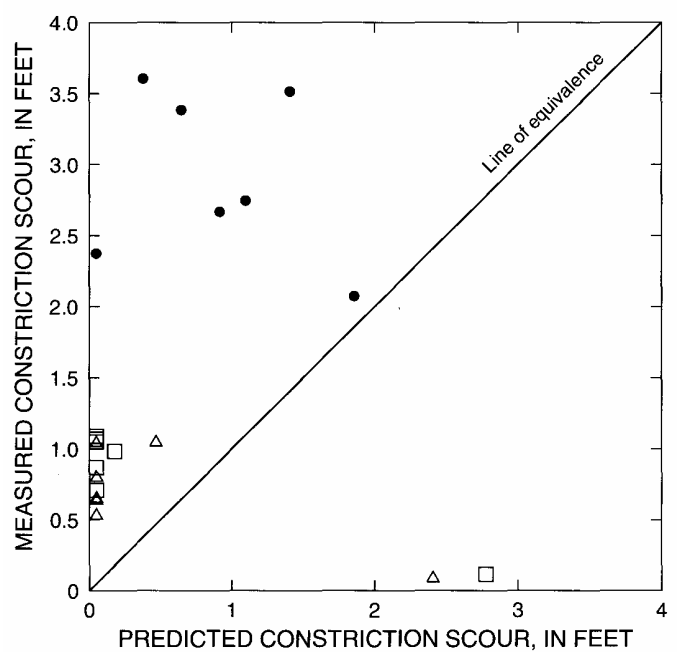

Frgure2.5 Relation of measured contraction scour to predicted contraction scour for clear-water scour condition in Maryland (Hayes, 1996)

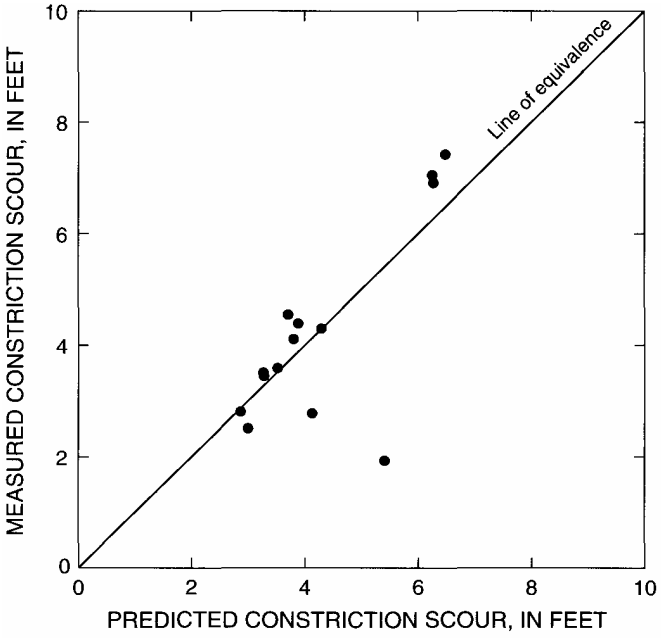

Frgure2.6 Relation of measured contraction scour to predicted contraction scour for live- bed scour condition in Virginia (Hayes, 1996)

2.5 The effect of interrelation between local scour and contraction scour

Using the current total scour prediction equations usually results in over-estimation of total scour depth. There are some reasons. The majority of work on contraction scour prediction has focused primarily on Straub's (1934) discharge and sediment transport theory. Straub assumed that the sediment was transported in a long rectangular contraction and that the sediment was in equilibrium transport. However, contractions in actual field conditions are more likely to have shapes that could be classified as short contractions or abrupt contractions. In addition, flow and sediment transport conditions change continuously during flood passage. In terms of the local scour component of total scour, the local scour prediction equations are derived from experimental data based on simplified experimental conditions different from real field situations. One other important consideration is that the current total scour prediction formulas assume that local and contraction scour processes are independent. In general, contraction scour is a result of acceleration of flow due to a contraction in flow area, while local scour is caused by the pile-up of water upstream of an obstruction that forces the downward acceleration of flow and the removal of sediment from the base of the obstruction. However, the contraction in flow area tends to cause scour processes to act concurrently; thus, two components, local scour and contraction scour, are time

dependent. However, the HEC-18, widely used in the scour prediction, recommends that the local scour and contraction scour are independent and the total scour depth can be predicted by the summation of local scour depth and contraction scour depth calculated separately.

The Maryland State Highway Administration (MDSHA) developed an abutment scour equation for small, severely contracted bridges called ABSCOUR (Niezgoda and Johnson, 1999). That equation involves relating abutment scour to contraction scour which was first suggested by Laursen (1962). Sturm (1999) also derived an abutment scour equation based on Laursen's contraction scour equation but tailored it to the change in distribution of flow between the main channel and floodplain as the bridge contraction is approached. Sturm (1999) correlated extensive laboratory results in a compound channel using the proposed equation and showed good agreement with field measurements in Minnesota.

The Federal Highway Administration's HEC-18 scour guidelines suggest the use of Froehlich's (1989) local abutment scour equations that were developed through the regression analysis of laboratory experiments in rectangular channels. However, Sturm (1999) showed that Froehlich's equation over-predicts his laboratory data for abutment scour in a compound channel because Froehlich's equation is based on

idealized experiments in rectangular channels.

The Maryland ABSCOUR program incorporates adjustment factors to account for the higher velocity and spiral flow conditions around the abutment. Niezgoda and Johnson (1999) applied the ABSCOUR program to several Pennsylvania bridges to determine its capabilities. The results were more reasonable than using the HEC-18 formulas of Laursen to calculate scour depth at small, severely contracted bridges. Results are shown in Table 2.6. The results show that the ABSCOUR prediction of 4.18 m provides a more reasonable scour depth estimate than the HEC-18 prediction when compared to the field scour depth estimate of 2.25 m. The results at other locations by the ABSCOUR prediction were quite close to the measured scour depth as shown in Table 2.6. This can be attributed to the interrelation of scour processes by the ABSCOUR program, which agrees well with scour development at the severely contracted bridge.

Table 2.6 Comparison of computed and measured scour depth at Pennsylvania (Niezgoda, 1999)

Location / Method	Piney-creek	Brush Run	Little Creek
Field scour depth (m)	2.25	1.92	3.05
HEC-18 (m)	7.62	-	-
ABSCOUR (m)	4.18	2.13	3.81

Schreider et al (2001) suggested from laboratory experiments a new method to compute the total scour depth when both local scour and contraction scour occur. Their experiments showed a significant difference in time development between contraction scour and abutment scour (Figure 2.7). Contraction scour occurred over a much longer time than abutment scour which reached equilibrium more quickly. In addition, the effect of guide banks on abutment scour and contraction scour was studied. The contraction scour was maximum when abutment scour was avoided by means of a guide bank. When one guide bank was withdrawn, the maximum contraction scour was about 50% of the scour when there was no abutment scour and when both guide banks were withdrawn, the maximum contraction scour was only about 25% of the scour depth measured in the case without abutment scour (Figure 2.8). Based on these lab data, Schreider(2001) suggested a new method to predict the total

scour depth. The proposed method involves the use of a discharge redistribution graph. This graph shows how the discharge that flows out of the abutment scour hole is smaller when the abutment scour depth is larger. Schreider suggested that the adjusted discharge should be used to calculate the contraction scour depth

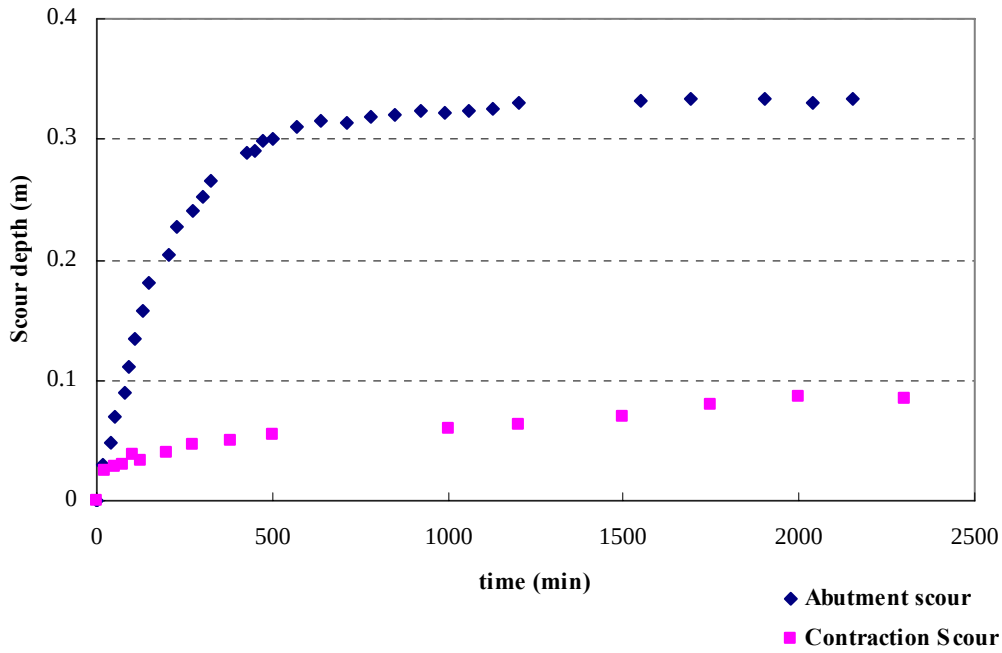

Figure2.7. Time evolution of the contraction and abutment scour (Schreider, 2001)

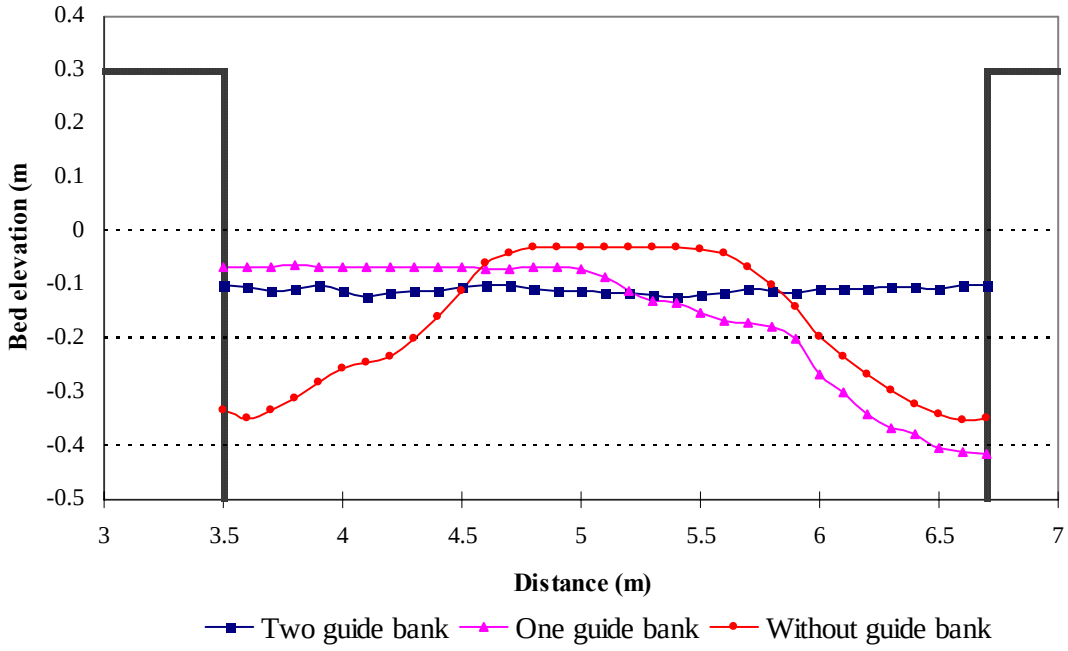

Figure2.8. Final erosion section of Schreider's experiment (2001)

In Figure 2.7, abutment scour develops fasters than the contraction scour. Whereas the abutment scour depth reaches about 85% of its final value after 500 minutes from the beginning of the experiments, the contraction scour just reaches 50% of its final value during the same time period. That means the discharge distribution at the beginning of scour that affects the contraction scour, changes as the abutment scour hole is developed. The discharge that flows outside the local abutment scour holes is reduced with respect to the initial discharge in the same part of the cross section. (Schreider et al (2001)).

In general, to compute the total scour depth, contraction scour and local scour (pier scour and abutment scour) are computed in an isolated way using the initial discharge and then, they are added. However, when the abutment is located on the bank of the main channel in a compound channel, both contraction and abutment scour occur simultaneously (Sturm, 1999). In this case, a single equation was suggested to predict the combined abutment and contraction scour due to acceleration of the flow caused by entrainment of the floodplain discharge into the the main channel flow as the bridge contraction is approached.

CHAPTER III

LABORATORY INVESTIGATION

3.1 Introduction

In this study, a full three-dimensional laboratory scale model of the Fifth Street Bridge over the Ocmulgee River at Macon, Georgia including upstream and downstream river reaches was constructed in the hydraulics laboratory in the School of Civil Engineering at the Georgia Institute of Technology, Atlanta, GA. The field data for this research were obtained through field monitoring by the USGS, as shown in Figure 3.1. The USGS has been gaging streamflow at this site since 1895, but detailed monitoring including continuous measurement (30-minute intervals) of pier scour using six fathometers has been underway since 2002 as part of a larger scour study for the Georgia DOT (Sturm et al, 2004).

The drainage area at the Ocmulgee River gaging station in Macon is 2,240 square miles. A discharge measurement of 65,000 cfs was made by the USGS in March of 1998 including velocities and cross-section bed elevations at the upstream side of the bridge. In comparison with cross sections collected in 2003, approximately 10 ft of contraction scour occurred for this event (Sturm et al. 2004). The 50-yr peak discharge

for the site is 79,200 cfs, and the 100-yr discharge is 88,300 cfs.

The pier bents as shown in Figure 3.1 consist of four cylindrical piers each with a diameter of 6 ft and a streamwise spacing of 23 ft. Bed material samples were collected upstream of the bridge and at the bridge section. The median particle size (d_{50}) ranged from 0.7 to 0.8 mm, with a value of 0.8 mm at the bridge.

Seven cross sections, as shown in Figure 3.2, were surveyed on Feb 26, 2002 throughout the channel reach. With that data, the laboratory model was constructed at an undistorted scale of 1:45 including the complete river bathymetry as well as the bridge pier bents and bridge abutments. To separate out the effect of the bridge piers on the contraction scour depth, the first set of experiments was conducted with the piers in place and the second set of experiments was conducted without the piers.

The velocity field and scour contours were measured in the laboratory with an acoustic Doppler velocimeter. To calculate the predicted scour depth with the contraction scour equation for comparison with field and laboratory results, the Hydrologic Engineering Center's River Analysis System (HEC-RAS) output results were used to obtain the approach discharge distribution, mean velocity, hydraulic depth, and other hydraulic variables.

Figure 3.1 Ocmulgee River at Macon, Georgia

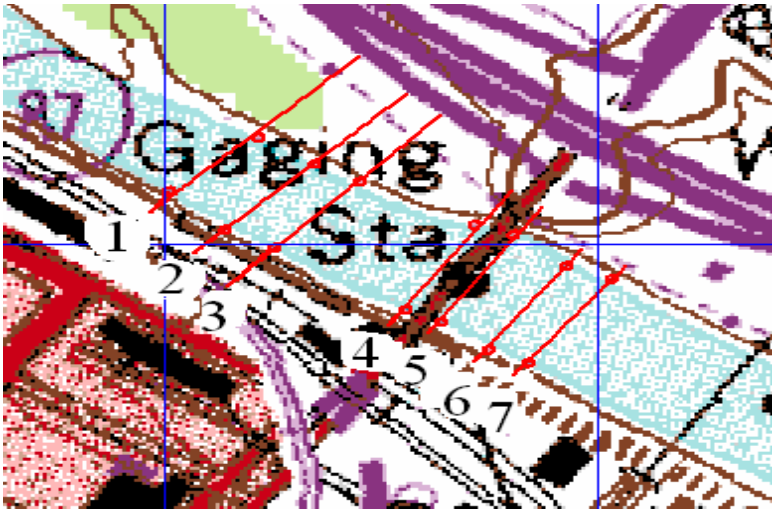

Figure 3.2 Layout of surveyed cross-sections at Macon

3.2 Experimental equipment

3.2.1 Flume

The scaled down river model was constructed in a steel flume, which is 80 ft long, 14 ft wide and 2.5 ft deep. The existing flume consists of a level concrete bed with vertical steel walls bolted down to the floor and water-sealed.

Water enters the flume from a 12-in. diameter pipe, which discharges vertically into the forebay section of the flume. Figure 3.3 shows a general view of the forebay section. Turbulence at the pipe outlet is reduced by two rolls of chain link fence. An overflow wier, baffles and a steel plate having 5/16-in. holes spaced 5/8-in apart serve to minimize entrance effects and produce a uniform flume inlet velocity distribution. At the downstream end of the flume, there is an adjustable flap tailgate for controlling the tailwater elevation. The water supply is provided by a constant-head tank. Water flows through the flume and recirculates through the laboratory sump where it is continuously pumped by two pumps with a total capacity of 10 cfs to the head tank which overflows back to the sump.

Adjustable rails on the top of the flume walls provide a level track for an instrument carriage. The instrument carriage is moved along the rails by a system of cables driven by an electric motor. The Acoustic Doppler Velocimeter (ADV), which is used for

velocity and bottom elevation measurement, and the point gage for the water surface elevation measurement, are mounted on the carriage and can be moved in three dimensions freely.

Figure 3.3 Photograph showing the forebay section of the flume

3.2.2 Measurement instrumentation

3.2.2.1 Magnetic flow meter

The flow rate in the 12-in. supply pipe is measured by a magnetic flow meter which has an expected uncertainty of ± 0.01 cfs.

3.2.2.2 Acoustic Doppler Velocimeter (ADV)

Velocities and bed elevations were measured with a 3D-down looking SonTek 10 MHz Acoustic Doppler Velocimeter (ADV) as well as a 2D-side-looking SonTek Micro ADV. The operation principle of the ADV is based on the Doppler frequency shift. The ADV measures the velocity in the sampling volume located at the intersection of the transmitted and received acoustic beam as shown in Figure 3.4. A short pulse of sound from the transmitter propagates through the water and is reflected in all directions within the sampling volume by sediment particles. Some portion of the reflected pulse travels back along the receiver axis where it is sampled by the ADV and the processing electronics measure the change in frequency. The Doppler frequency shift measured by the receiver is proportional to the velocity of the reflecting particle that is assumed to move with the same velocity as water.

The 3D down-looking ADV receivers used in these experiments are focused in a sampling volume located 5cm below the transmitter. When measurements need to be made in shallow water and close to the bottom, the 2D-side-looking ADV probe having a 5 cm distance to the measuring volume is used. The bottom elevation can also be measured by the ADV. The ADV can detect the distance from the center of the sampling volume to a solid boundary with ± 1 mm uncertainty. However, sometimes the

(a) 3D 16 MHz Micro ADV

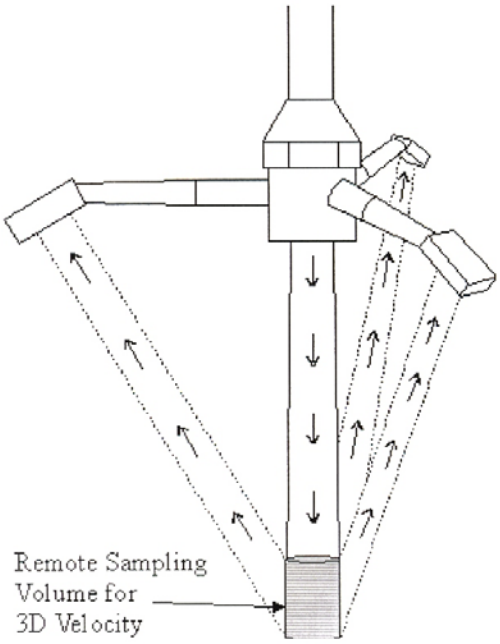

(b) 3D-down looking ADV probe

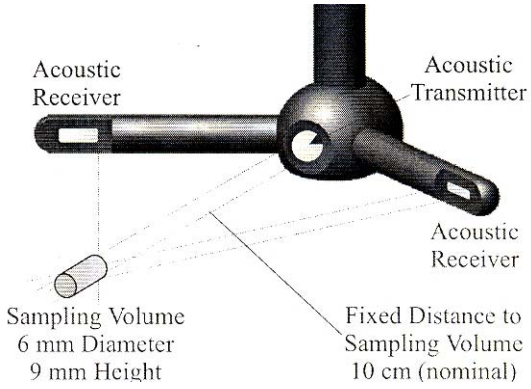

(c) 2D-side looking ADV probe

Figure 3.4 Acoustic Doppler Velocimeter

ADV is not able to detect precisely the bed elevation along a steep slope so that measurements with a point gage are needed. The elevation of a reference point can be determined by a point gage and compared to the elevation measured by the ADV before measuring all bed elevations to provide a common elevation datum.

The existence of Doppler noise from the ADV always can occur when measuring the velocity, especially when the flow velocity exceeds the pre-set velocity range or when there is contamination from the previous acoustic pulse reflected from boundaries of complex geometries. Noise also occurs when a high level of turbulence exists at the measuring location. Hence, the examination and filtering of the signal is needed before analyzing the mean point velocity and turbulent kinetic energy. Also, addition of seeding particles helps to measure the turbulence characteristics in highly turbulent flow or highly aerated water because the correlation values and signal strength, which are quality control parameters for acceptance or rejection of the ADV signal, will be higher.

In these experiements, the measurements below a level of about 1.2 in. above the bed caused problems because ADV signal noise occurred in this zone. This noise is attributed to high levels of both turbulence and mean velocity shear near the bed as well as errant reflections from the bed and boundary interference when the return signal from the boundary interferes with the signal from the measuring volume (Lane et al. 1998).

One method of dealing with this noise is to filter the data according to the value of a correlation coefficient that is a measure of the coherence of the return signals from two successive acoustic pulses (Martin et al. 2002, Wahl 2002). The data were filtered by requiring that the correlation coefficient of each sample in the 2-minute time record exceed a value of 70 percent as recommended by the manufacturer (SonTek 2001) for obtaining turbulence statistics.

3.3 Model construction

The experimental studies were conducted in an undistorted geometric scale model (1:45) constructed in a laboratory flume. All of the prototype data, including discharge, stage, velocity distributions and river bathymetry were measured by the USGS. Dynamic similarity was obtained by equating Froude numbers in the model and prototype. Calculation of model flow rates from the prototype followed the Froude number law. The prototype bathymetric data from the USGS was scaled so that the model would fit in the laboratory flume. A scale ratio of 1:45 was selected based on the limiting dimensions of the flume. The model sediment size of d_{50} = 1.1 mm with σ_g = 1.3 was chosen such that the ratio of pier size to sediment size b/d_{50} was in the range of 25-50 where it has no influence on pier scour (Melville and Coleman, 2000), and the value of the sediment

mobility parameter given by the ratio of approach velocity to critical velocity for incipient sediment motion V/V_c was close to one for the occurrence of maximum clear water scour (Lee et al. 2004).

The complete river bathymetry was modeled with a fixed-bed approach channel followed by a mobile-bed working section in which the bridge pier, embankment and abutment were placed as shown in Figure 3.5. The approach section was approximately 30-ft long with a 20-ft long working section followed by an approximately 10-ft long exit section for sediment deposition.

In the approach section, river bathymetry was modeled by cutting plywood templates that reproduced the surveyed cross-sections. The templates were nailed into wooden cleats attached to the floor of the flume. The bed material was leveled carefully by hand to match the templates as shown in Figure 3.6 (a). The templates were left in place in the fixed-bed section, but in the moveable bed section (from R.S. 8.0 to R.S. 1.0 in Figure 3.5) they were installed and removed after the bed was shaped for each experimental run. To accomplish that task in the moveable-bed section, the river bathymetry was molded to thin aluminum panels that could be extracted without disturbing the bed as shown in Figure 3.6 (b).

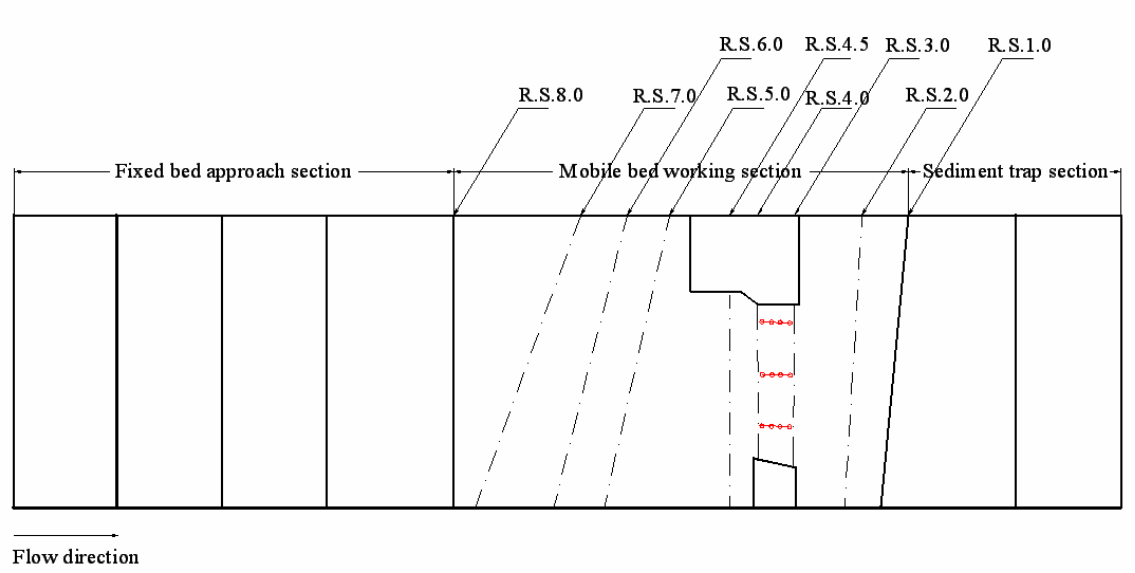

Figure 3.5 Plan view of flume for model construction

(a) Approach fixed bed section, looking downstream from right floodplain

(b) Working moveable bed section, looking downstream from left floodplain

Figure 3.6 Model construction

In the fixed-bed approach section, the full depth of a 3.3-mm gravel bed was shaped to the plywood templates, and a surface layer was fixed with polyurethane. In the moveable-bed working section, the full depth of the 1.1-mm sand bed was available to measure the bed deformation by scour. In the sediment trap section, the surface layer of a 3.3-mm gravel bed was fixed with polyurethane just as in the approach section to trap the sediment transported out of the working section.

The model values for stream stations and prototype values for flow distance between the river sections shown in Figure 3.5 are given in Table 3.1.

3.4 Experimental procedure

After completion of the model construction, the scour experiments were conducted. The flume was slowly filled with water from a downstream supply hose so that the sand was saturated safely and the initial bottom contours were unchanged. After complete saturation, the initial bottom elevation of the entire working movable-bed section was measured by the ADV and point gage in detail. The initial bottom elevation was measured every 0.2-ft in the streamwise direction from R.S. 7.0 to R.S. 2.0 and every 0.1-ft laterally from the left to the right wall. The required discharge was then set using the magnetic flow meter. A flow depth larger than the target value was used by the

tailgate so as to prevent scour while the test discharge was set. Then the tailgate was lowered to achieve the desired depth of flow. During this time, the point gage on the instrument carriage was used to measure the flow depth.

Table 3.1 Model and prototype flow distance between the river sections (L.W.E: Left water edge, R.W.E: Right water edge)

River station	Model		Prototype	
	Cumulative distance from flume entrance		Distance between cross sections	
	L.W. E (ft)	R.W.E (ft)	L.W. E (ft)	R.W. E (ft)
R.S. 8.0	31.00	31.00		
R.S. 7.0	37.13	32.08	275.85	48.60
R.S. 6.0	39.36	35.84	129.90	149.34
R.S. 5.0	41.40	38.26	101.15	108.67
R.S. 4.5	43.90	43.93	175.64	222.62
R.S. 4.0	45.62	45.64	76.32	81.94
R.S. 3.0	47.44	47.30	81.60	76.97
R.S. 2.0	50.63	49.79	132.30	118.85
R.S. 1.0	52.85	51.55	95.73	85.49

Three different discharges were used to conduct the experiments. The historic discharge of 4.79cfs (65,000cfs in prototype scale) that occurred in March of 1998 was used for the first experimental run as shown in Figure 3.7 and then the 100-yr discharge of 6.50cfs (88,300cfs in prototype scale) and the 50-yr discharge of 5.83cfs (79,200cfs in prototype scale) were utilized in the second and third runs respectively. To satisfy the dynamic similarity of model and prototype, Froude number similarity was used. Table 3.2 shows the prototype value and the model value that is used in the experiment.

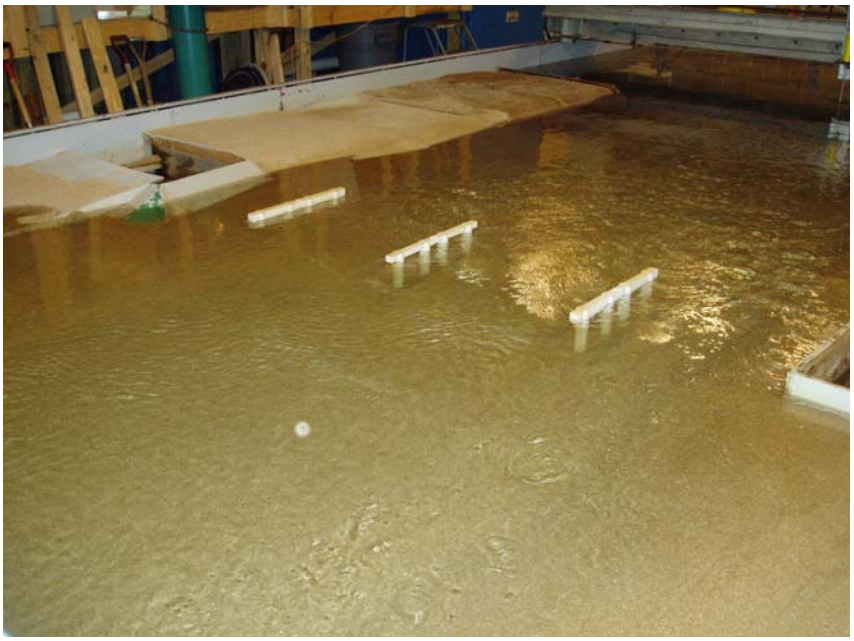

Figure 3.7 River and bridge looking downstream from right floodplain (4.79cfs in model, 65,000cfs in prototype value)

Table 3.2 Discharge and water surface elevation of prototype and model

Discharge (cfs)	Water surface elevation (ft)	Discharge in model (cfs)	Water surface elevation in model (cfs)
65,000	299.75	4.79	2.078
79,200	301.38	5.83	2.109
88,300	302.95	6.50	2.147

The first set of experiments was conducted with the piers in place. In these experiments, the time history for contraction scour and pier scour and the time history of velocity at selected locations were measured. The velocities at the selected points were measured to compare the velocity change before and after scouring. After finishing the velocity measurements, the entire bed bathymetry was measured with the ADV and point gage following the same procedure as for the initial bed elevation measurements. These experiments were conducted with the three different model discharges of 4.79cfs (65,000 cfs), 5.83 cfs (79,200 cfs) and 6.50cfs (88,300 cfs).

The second set of experiments was conducted with a fixed bed. To determine the initial velocity distribution before scour, the entire moveable-bed section was fixed by spraying polyurethane on the surface. The initial approach velocity for contraction scour was measured every 0.5 ft laterally at 10 locations in the vertical profile at R.S. 5.0 to

determine the initial velocity distribution across the cross section. For the pier scour, the initial approach velocity was measured in the same way as for contraction scour but at R.S. 4.5. These experiments were also conducted with the same three discharges given in Table 3.2 to know the initial velocities for each case.

The third set of experiments was conducted without piers. The fixed layer of the bed was removed as were the three pier bents. The moveable-bed section was leveled to match the templates without the piers in place. For this series of experiments, the time histories for contraction scour and velocity were measured using two different discharges, 4.79 cfs and 5.83 cfs. As the contraction scour approached equilibrium, the velocities at some pertinent points were measured and then the bed elevations were measured as in earlier experiments at the same points.

3.4.1 Time development of scour

Once the target flowrate and depth were reached, measurements of scour depth and velocity as a function of time at a several fixed points were measured with the ADV. The time history for pier scour was measured at point A having flume coordinates of 45.72 ft (streamwise direction from flume entrance) and 7.54 ft (lateral direction from the left wall) as shown in Figure 3.8. Point A is located in front of the leading pier of the

center pier bent which is assumed to be the location of maximum pier scour. The time history for the contraction scour was measured at 4 points, as shown in Figure 3.8: B (45.91, 6.75), C (45.92, 8.37), D (47.34, 8.42) and E (47.35, 7.25).

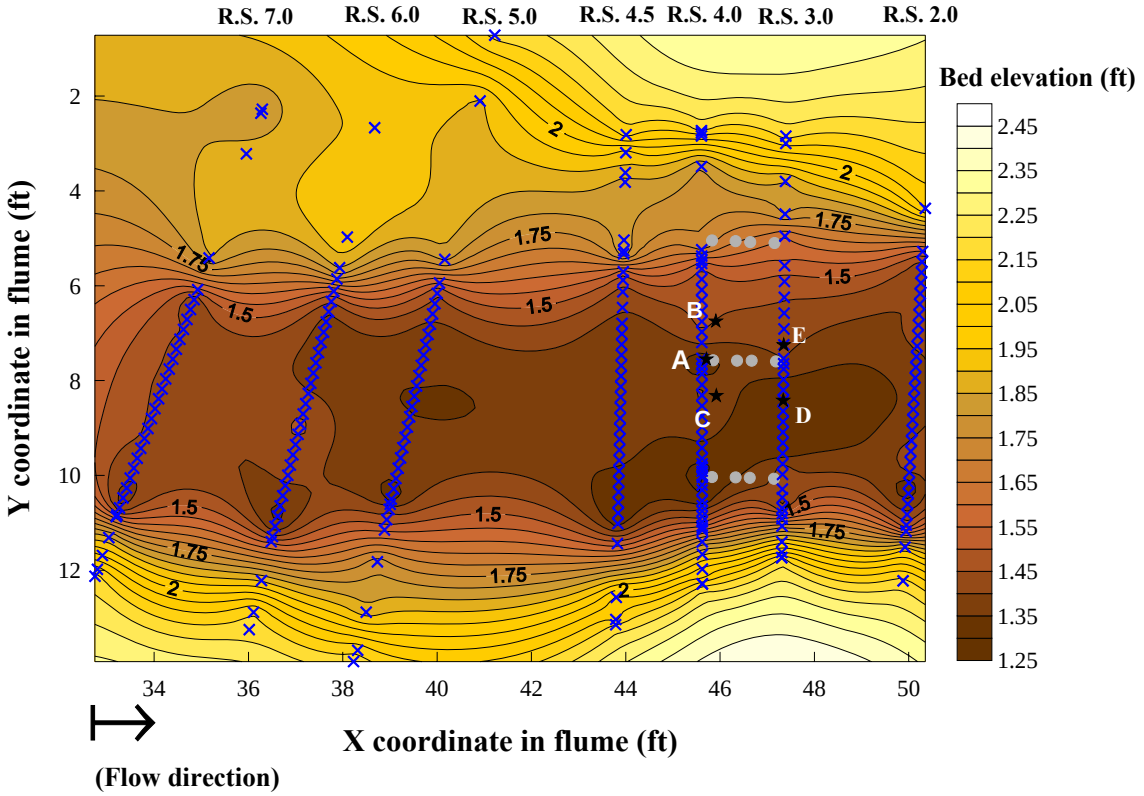

Figure 3.8 Plan view of measuring points A, B, C, D and E (Blue x shows the cross -section location)

The locations chosen for measurement of contraction scour time history measurement were decided by comparison of historic cross section data from the USGS. The "x" mark as shown in Figure 3.8 shows the cross section at R.S. 4.0. In this cross

section, the maximum contraction scour occurred at point C (241 ft from the left embankment at prototype scale) during the historic flood of 65,000cfs which was recorded on Mar, 10, 1998. The cross section elevations at R.S. 4.0 for the historic flood and also on February 26, 2002 for comparison are given in Figure 3.9 to show the measuring points B and C where contraction scour occurred.

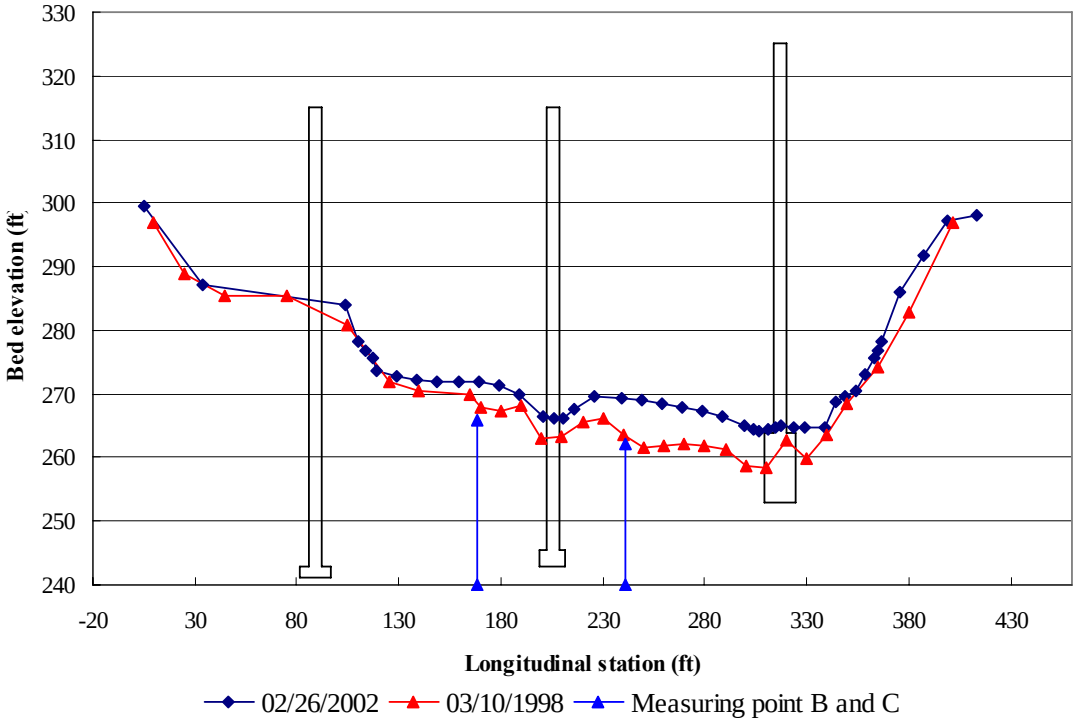

Figure 3.9Cross section comparison using historic data (Q=65,000 cfs and W.S. elevation=299.75 ft)

Time development of pier scour depth is an asymptotic process (Melville and Coleman 2000). Thus, the change of bottom elevations with time should be measured over shorter intervals at the beginning of the experiment. The time development of scour was measured every 5 minutes during the first hour and then every 10 minutes for the second hour. Measurements were conducted every 30 minutes for the two following hours and then hourly measurements were conducted until the scour depth reached equilibrium.

Time development of velocities was measured at the same point as the maximum contraction scour (Point C). Point velocities were measured at relative heights above the bed of approximately 0.01, 0.02, 0.04, 0.08, 0.1, 0.2, 0.4, and 0.6 times the flow depth. A sampling duration of 2 minutes was used at each measuring location. Because the time development of scour depth was measured every 5 or 10 minutes during the first two hours, there was not enough time to set up the velocity probe and measure velocity profiles in addition to bed elevations, so the velocity time development was measured starting two hours after the beginning of the experiment.

3.4.2 Critical velocity assessment

Critical velocity (V_c) is the flow velocity for initiation of motion of sediment

grains in a channel bed. To determine whether clear-water or live-bed scour conditions exist, and to estimate the sediment mobility parameter, V/V_c, the critical velocity has to be calculated.

Keulegan applied the logarithmic velocity distribution for fully-rough turbulent flow to open channels. He assumed that the shape of the cross section is trapezoidal and then integrated the Nikuradse fully-rough turbulent velocity distribution over the whole cross section to give the expression

$$\frac{V}{u_*} = 5.75 \log \frac{12.2\, R}{k_s} \tag{3.1}$$

where V is mean cross-sectional velocity; u_* is shear velocity = $(\tau_0/\rho)^{1/2}$; τ_0 is mean boundary shear stress; ρ is fluid density; R is hydraulic radius; and k_s is equivalent sand-grain roughness height.

To calculate the critical velocity, the shear velocity u_* should be replaced by the critical value of shear velocity u_{*c} as given by

$$u_{*c} = \sqrt{\tau_{*c}(SG-1)\, g\, d_{50}} \tag{3.2}$$

where, u_{*c} is critical value of shear velocity; τ_{*c} is Shields parameter; which is equal to $\tau_c/[(\gamma_s - \gamma)\, d_{50}]$; τ_c is critical shear stress for incipient sediment motion; γ_s is the specific weight of sediment; γ is the specific weight of fluid; d_{50} is median grain size; SG is specific gravity; and g is gravitational acceleration.

Shields parameter is related to the threshold of sediment movement as defined by the critical shear stress. Shields collected experimental data on the initiation of motion and bedload transport of sediment and presented the Shields diagram using a dimensionless parameter τ_{*c} to express the initiation of sediment motion as a function of the boundary Reynolds number which is affected by viscosity and sediment size. Later, the Shields diagram was modified by the many other researchers, including Rouse(1939), Yalin(1979) and Karahan(1979). The modified Shields diagram is shown in Fig. 3.10 in terms of a dimensionless grain diameter d_* which is defined by.

$$d_* = \left(\frac{(SG-1)\, g\, d^3}{\nu^2} \right)^{1/3} \tag{3.3}$$

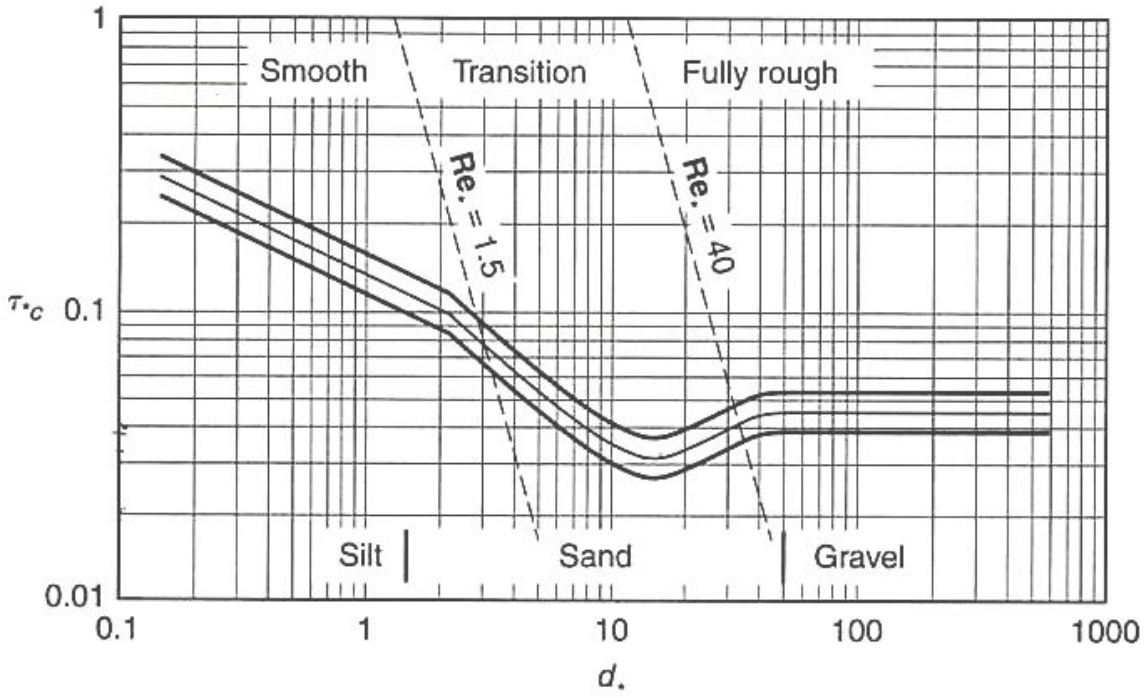

Figure 3.10 Shields diagram for direct determination of critical shear stress (Sturm 2001)

Substituting the critical values of velocity and shear stress into Equation 3.1, the result is an expression for critical velocity that depends on the critical value of Shields' parameter obtained from Figure 3.10 and is given by

$$V_c = 5.75\sqrt{\tau_{*c}\,(SG-1)\,g\,d_{50}}\,\log\left(\frac{12.2\,R}{k_s}\right) \qquad (3.4)$$

The value of critical velocity determined by Equation 3.4 is used in the scour calculations in Chapter 4.

3.4.3 Depth-averaged velocity assessment

To determine the depth-averaged velocities in the laboratory, a best-fit of the logarithmic velocity profile was applied to approximately 8 measured point velocities in the vertical. The depth-averaged velocity was then evaluated as the point velocity from the best-fit log relation at a relative distance above the bed of 0.4 times the depth (French 1986). Similarly, it can be shown that the average of the point velocities at relative depths of 0.2 and 0.8 measured below the free surface provide a good estimate of the depth-averaged velocity in each vertical profile as used by the USGS in field measurements of discharge.

3.4.4 HEC-RAS analysis

The Hydrologic Engineering Center's River Analysis System (HEC-RAS) developed at the Hydrologic Engineering Center of the US Army Corps of Engineers was created to calculate one-dimensional steady and unsteady flow.

When the main channel and floodplain geometry, information about bridge foundations including embankments, and data on stage and discharge are given, HEC-RAS can estimate flow characteristics such as discharge distribution in the channel and floodplain respectively, velocity distribution at each cross-section, flow depth, and

hydraulic radius. The output results were used to calculate the scour depth with the live bed contraction scour equation in prototype scale.

CHAPTER IV

RESULTS AND ANALYSIS

4.1 Introduction

A total of eight experimental runs were conducted in order to verify the relative contribution of contraction scour and local pier scour. The experimental results will show the scour time history, velocity time history, average contraction scour depth and depth-averaged cross-sectional velocity distributions. In the analysis, the computed scour depths and measured scour depths will be compared (both contraction and pier scour) to evaluate current scour prediction equations. Then the effect of piers on the contraction scour depth will be shown by the velocity time history and the change of discharge distribution across the approach cross section. Finally, measured laboratory scour depths will be compared with field measurements.

4.2 Time history

4.2.1 Time history with piers in place

As described in detail section 3.4.1, time development for contraction scour and pier scour was measured for three different discharges: 4.79cfs (65,000cfs), 5.83cfs

(79,200cfs), and 6.50cfs (88,300cfs). (Prototype values are shown in parentheses throughout this chapter). Time history graphs for contraction scour at four locations in the bridge cross sections and for pier scour at one location in front of the center pier were plotted to determine the time necessary to reach equilibrium scour conditions. Figures 4.1, 4.2 and 4.3 show plots of contraction scour time history at point C and pier scour time history at point A for discharges of 4.79cfs (65,000cfs), 5.83cfs (79,200cfs) and 6.50cfs (88,300cfs). (see Figure 3.8 in chapter III for locations of points A and C). For the pier scour time development, it required approximately 45hrs, 40hrs, and 30hrs to reach equilibrium for 4.79cfs (65,000cfs), 5.83cfs (79,200cfs) and 6.50cfs (88,300cfs) respectively. Contraction scour time development, however, required much longer times of approximately 90 hrs, 100 hrs, and 110 hrs to reach equilibrium for the three different discharges tested in increasing order of magnitude. The time scale for contraction scour was about two or three times larger than that for pier scour.

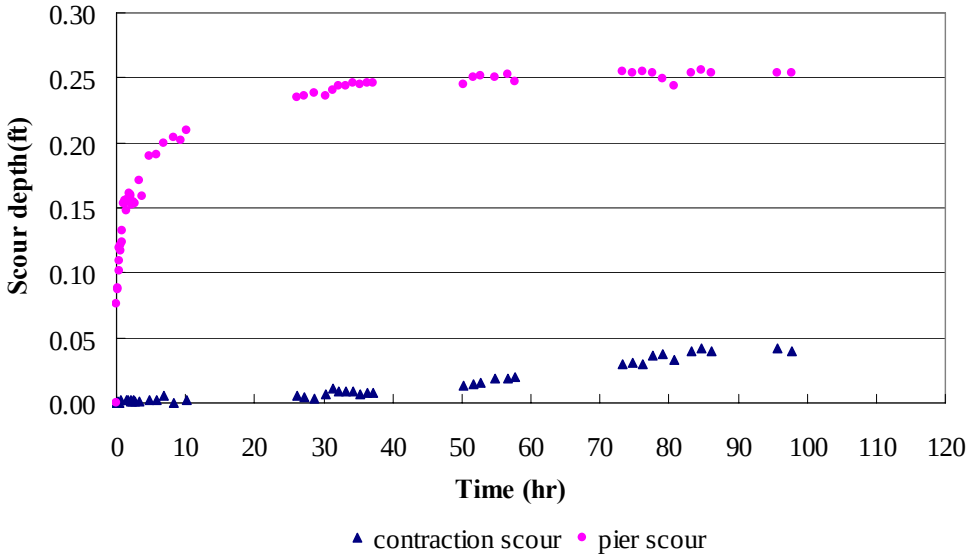

Figure 4.1 Pier scour time history at point A (x=45.72 ft, y=7.54 ft) and contraction scour time history at point C (x=45.92 ft, y=8.37 ft) for Q=4.79 cfs (65,000 cfs) and W.S. Elev.=2.078 ft (299.75 ft)

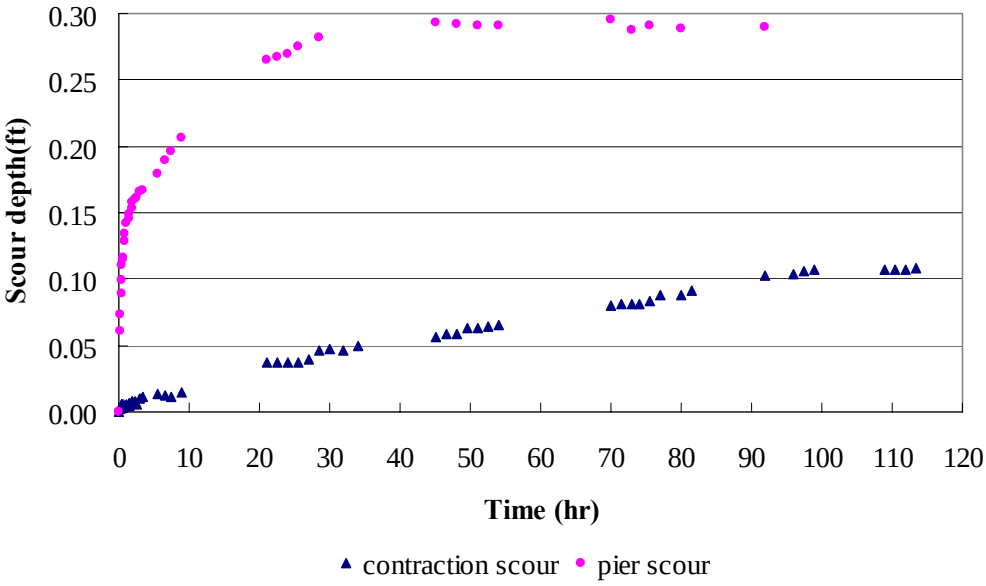

Figure 4.2 Pier scour time history at point A (x=45.72 ft, y=7.54 ft) and contraction scour time history at point C (x=45.92 ft, y=8.37 ft) for Q=5.83 cfs (79,200 cfs) and W.S. Elev.=2.109 ft (301.38 ft)

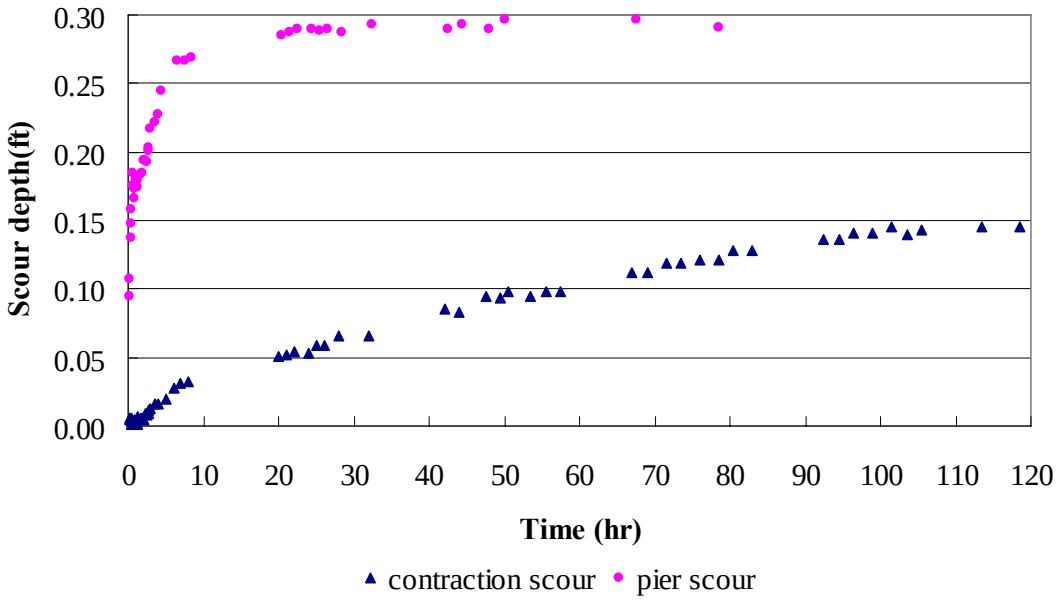

Figure 4.3 Pier scour time history at point A (x=45.72 ft, y=7.54 ft) and contraction scour time history at point C (x=45.9 2ft, y=8.37 ft) for Q=6.50 cfs (88,300 cfs) and W.S. Elev.=2.147 ft (302.95 ft)

4.2.2 Time history without piers in place

After finishing the scour experiments with the piers in place, the piers were removed and the experimental procedures were conducted in the same manner as the experiments including the piers in order to learn more about the interaction between pier scour and contraction scour. In this set of experiments, two different discharges were used. Figure 4.4 and Figure 4.5 show the time history for contraction scour at point C with discharges of 4.79 cfs (65,000 cfs) and 5.83 cfs (79,200 cfs) respectively. It takes about 65 hrs to reach equilibrium for the 4.79 cfs (65,000 cfs) case and 75 hrs for the 5.83

cfs (79,200 cfs) case. It requires about 25 hrs less time to reach equilibrium for the case without piers than for the case with the piers. The longer time required with the piers in place is likely due to interaction between pier and contraction scour. Furthermore, the time development of contraction scour without the piers shows more rapid development with time for about the first 10 hrs than for contraction scour with the piers in place.

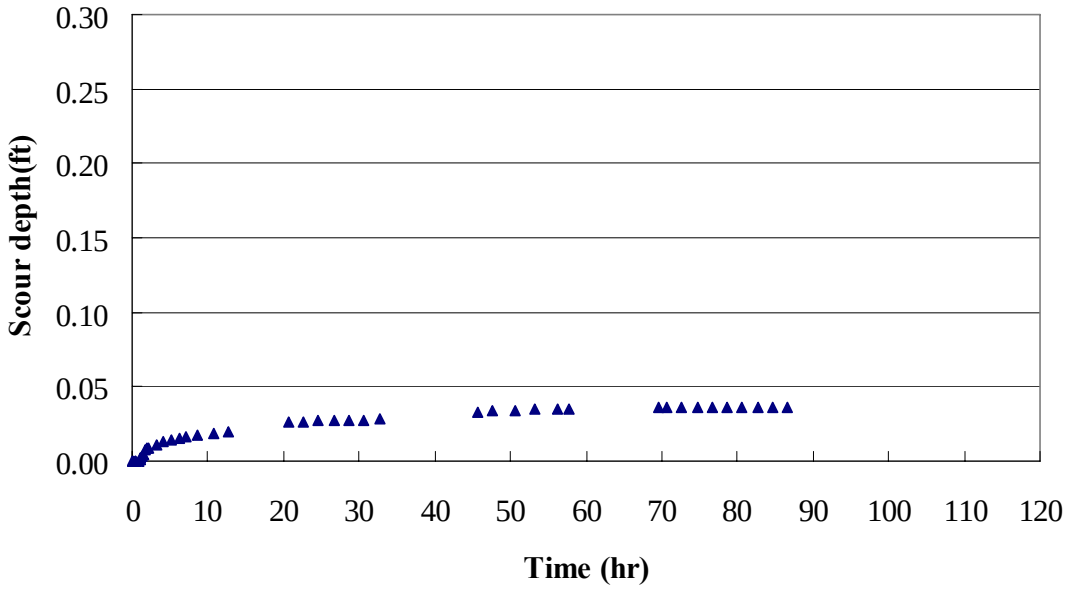

Figure 4.4 Contraction scour at point C (x=45.92 ft, y=8.37 ft) without piers for Q=4.79 cfs (65,000 cfs) and W.S. Elev.=2.078 ft (299.75 ft)

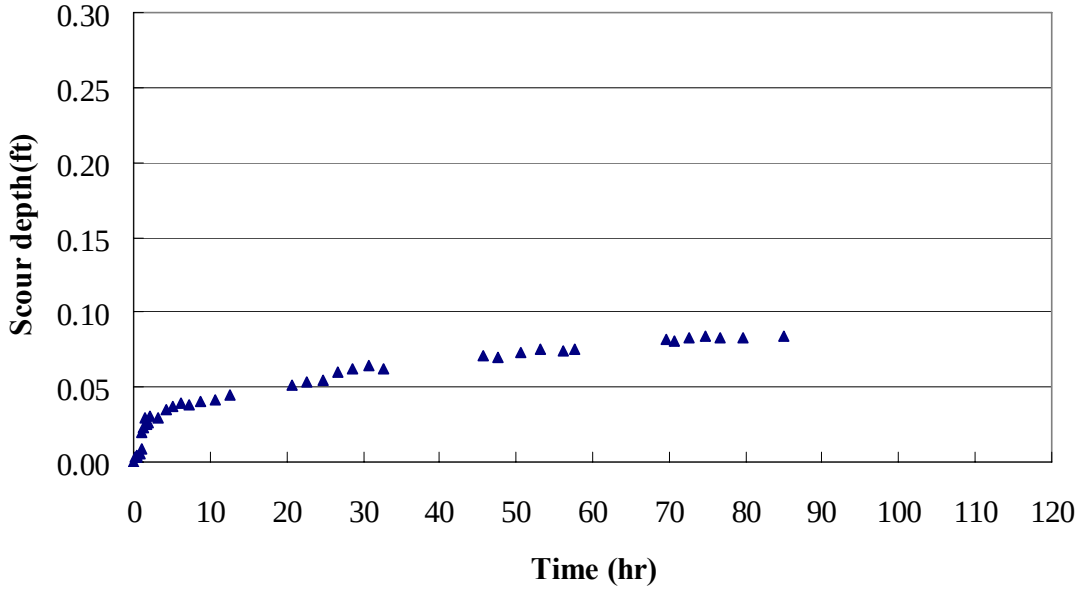

Figure 4.5 Contraction scour at point C (x=45.92 ft, y=8.37 ft) without piers for Q=5.83 cfs (79,200 cfs) and W.S. Elev.=2.109 ft (301.38 ft)

4.3 Raw scour depth data

Figures 4.6, 4.7 and 4.8 show the plan view of scour depth contours in the laboratory flume after finishing the experiments. To measure the scour depth, the initial bottom elevations were measured throughout the test section before the experiment and then the final bottom elevations were measured at all the same locations after finishing the experiment. These figures all show that maximum scour depth (negative values refer to scour) occurred around the side of the center pier rather in front of it because of the residual pier scour there. Further analysis is required to remove residual pier scour and residual contraction scour from the results.

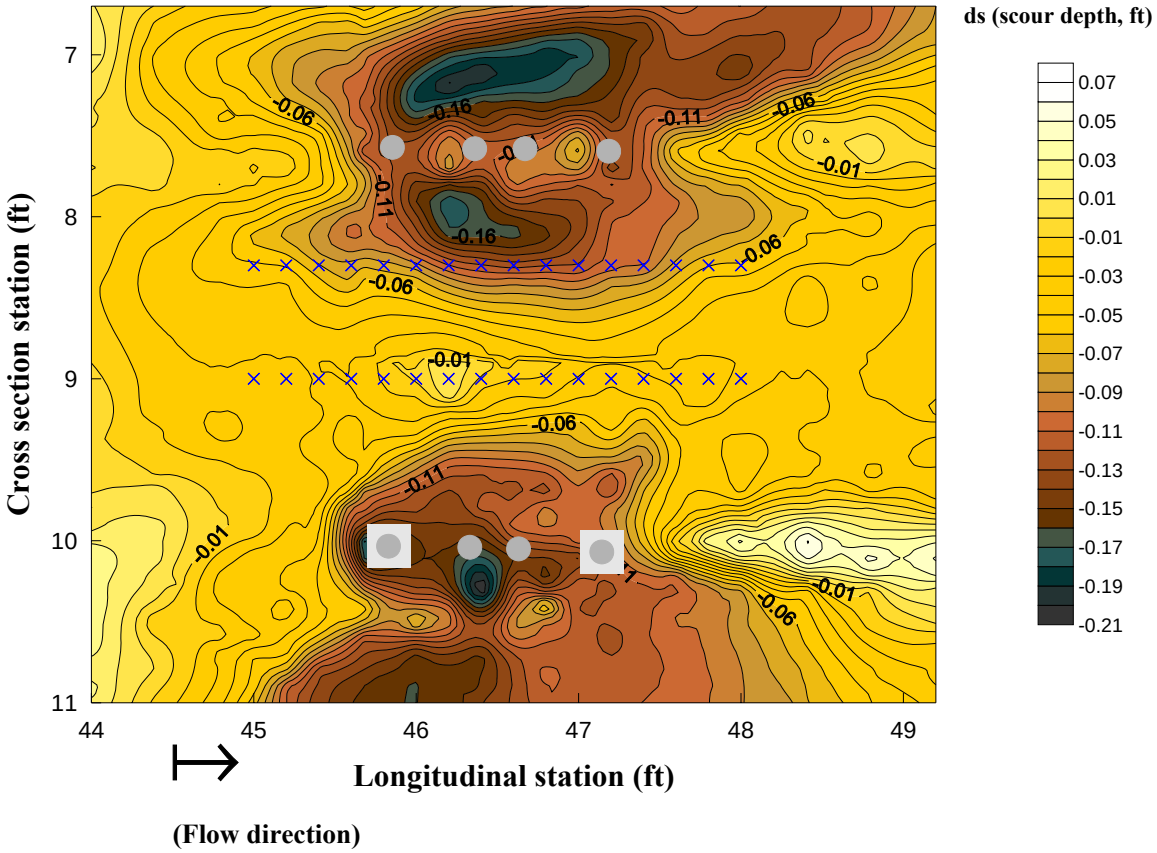

Figure 4.6 Plan view of laboratory raw scour depth contours for Q=4.79 cfs (65,000cfs).

Contour Using Scour depth

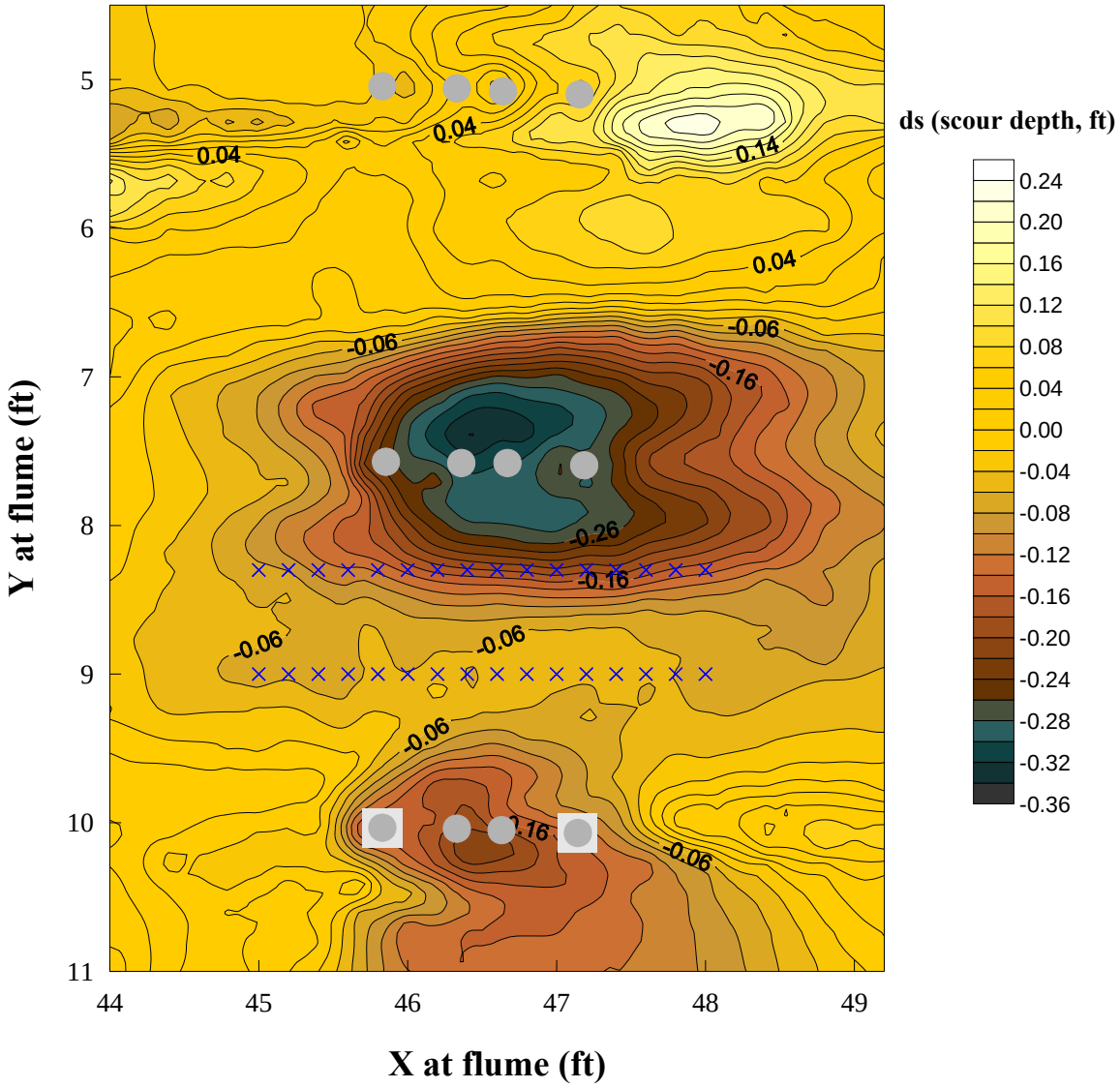

(Flow direction)

Figure 4.7 Plan view of laboratory raw scour depth contours for Q=5.83 cfs (79,200 cfs)

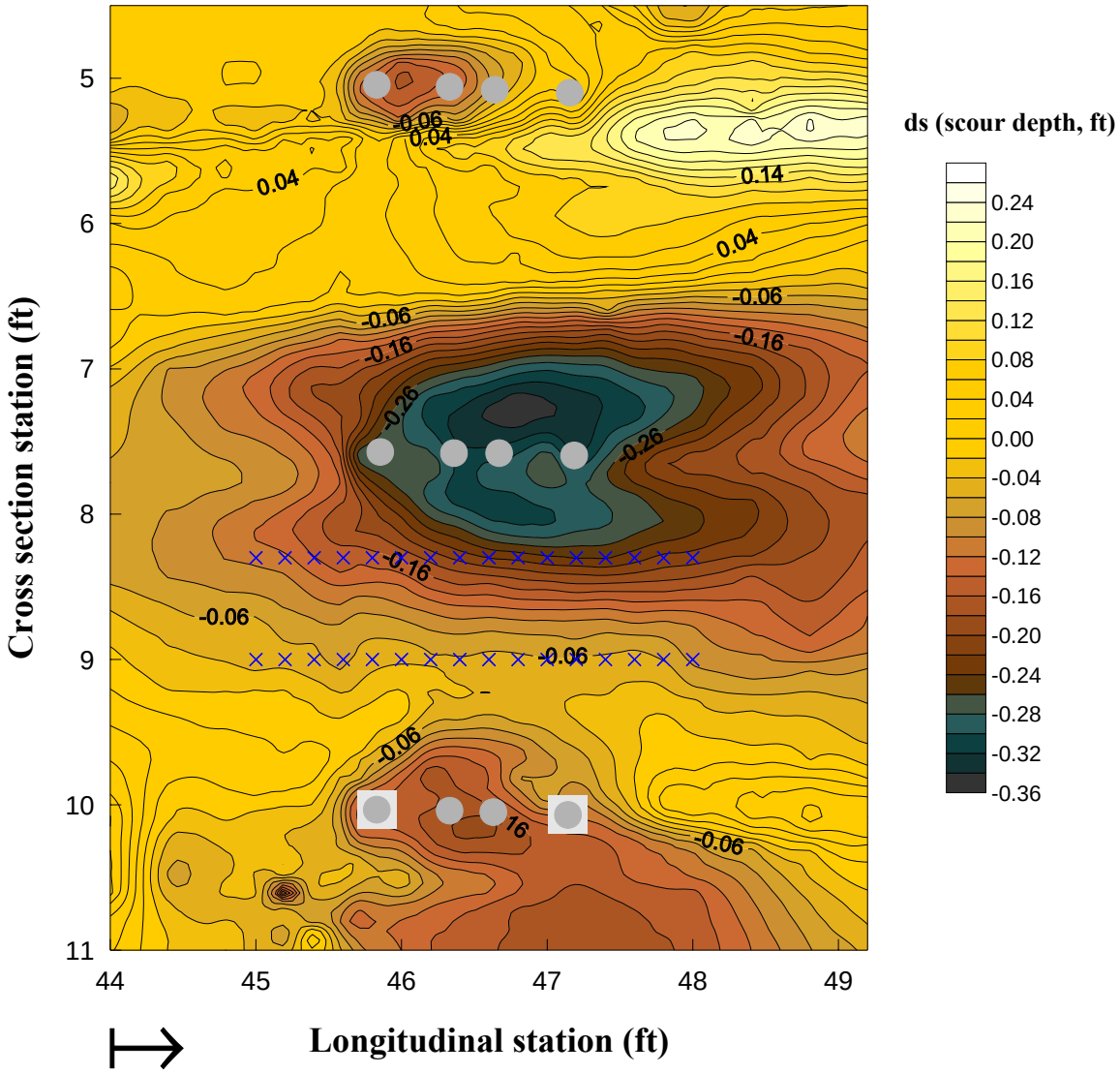

Figure 4.8 Plan view of laboratory raw scour depth contours for Q=6.50 cfs (88,300 cfs).

4.4 Contraction scour depth

4.4.1 Reference elevation

To measure the contraction scour depth, the reference elevation should be decided in advance such that residual contraction scour is removed. What is sought is an undisturbed bed profile that would have occurred without the bridge contraction in place. As mentioned in Chapter 2, the preferred method for determining the reference elevation for uncontracted conditions is to pass a line through the average streambed elevations of the upstream uncontracted section of the bridge to the downstream uncontracted section of the bridge. As a first step in this process, the upstream and downstream uncontracted cross sections have to be determined. Figure 4.9 shows the upstream cross-sections from R.S. 7.0 to R.S. 5.0 (R.S. = river section) on the same scale graph to check for residual scour depth. There was residual scour outside of the river bend from R.S. 7.0 to R.S. 5.0 (right corner of graph) because of the river meander. There was also residual meander scour in the main channel of R.S. 5.0. To establish an uncontracted cross section, the residual scour was removed as shown in Figure 4.10 which shows the adjusted R.S. 5.0 cross-section for contraction scour. Also shown in Figure 4.10 are the computed water surface elevations at R.S. 5.0 from HEC-RAS for each of the three test discharges. From each of these water surface elevations,

the average depth of flow in the main channel can be determined from a spatial integration of the cross-sectional area. In addition, the average main channel bed elevation can be calculated by integration based on the bank-full water surface elevation. There are adjusted cross section profile data for all the cross section in the Appendix E.

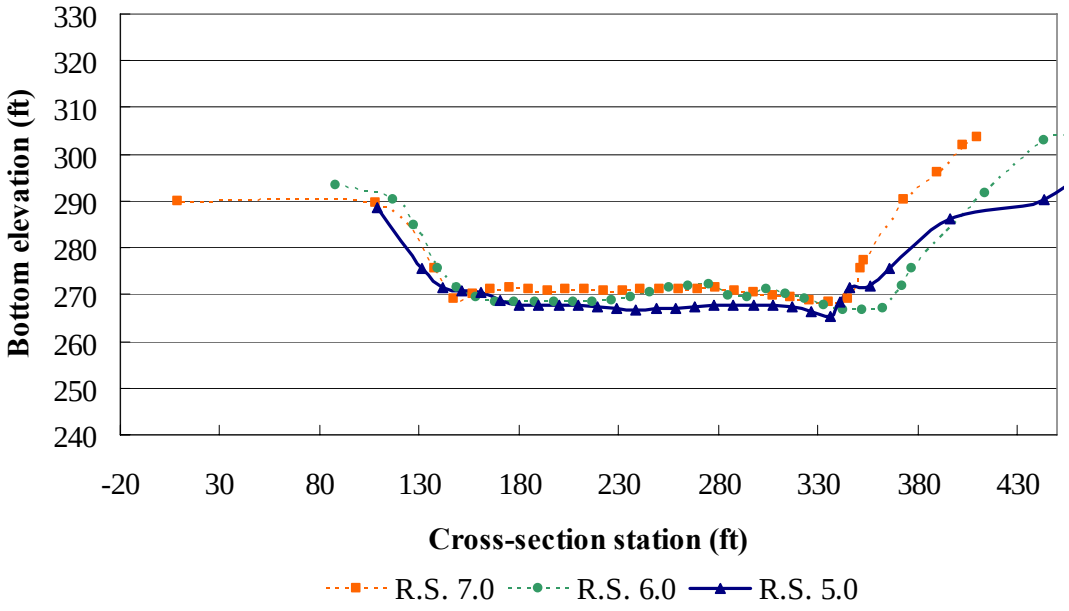

Figure 4.9 Cross section comparison from R.S. 7.0 to R.S. 5.0

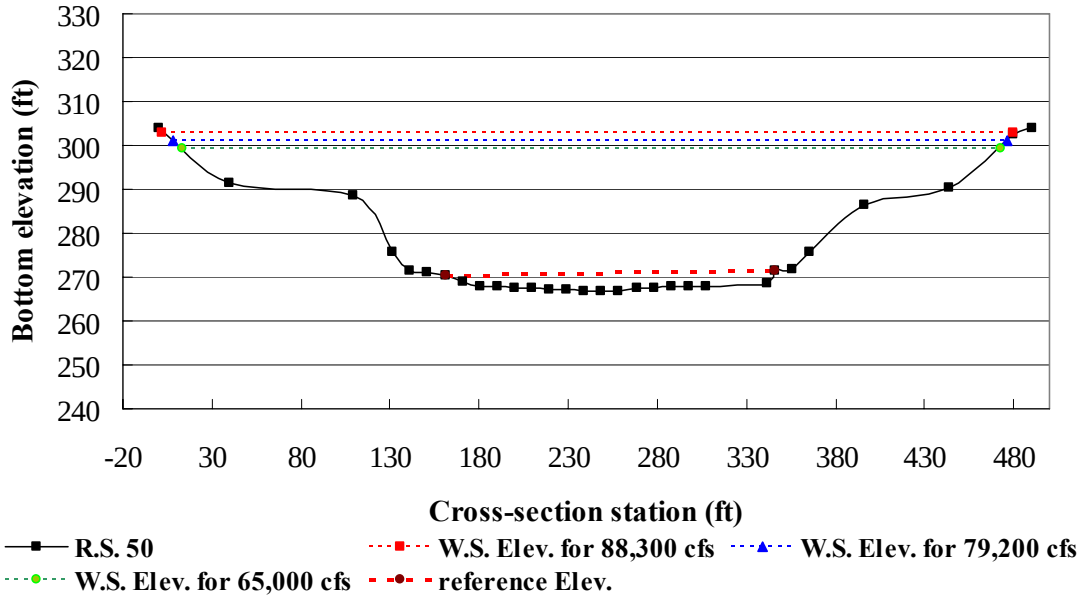

Figure 4.10 Adjusted approach cross section at R.S. 5.0 for contraction scour

Using the same technique as that for adjusting upstream cross sections, Figure 4.11 shows the cross-section comparison for the cross sections downstream of the bridge from R.S. 3.0 to R.S. 1.0. There was no change of main channel bed elevation from R.S. 2.0 to R.S. 1.0. However, near the toe of the right bank of R.S. 2.0 there was local residual scour because of a slight river meander. In order to create an uncontracted downstream cross section, this residual scour was removed and Figure 4.12 shows the adjusted R.S. 2.0 cross section.

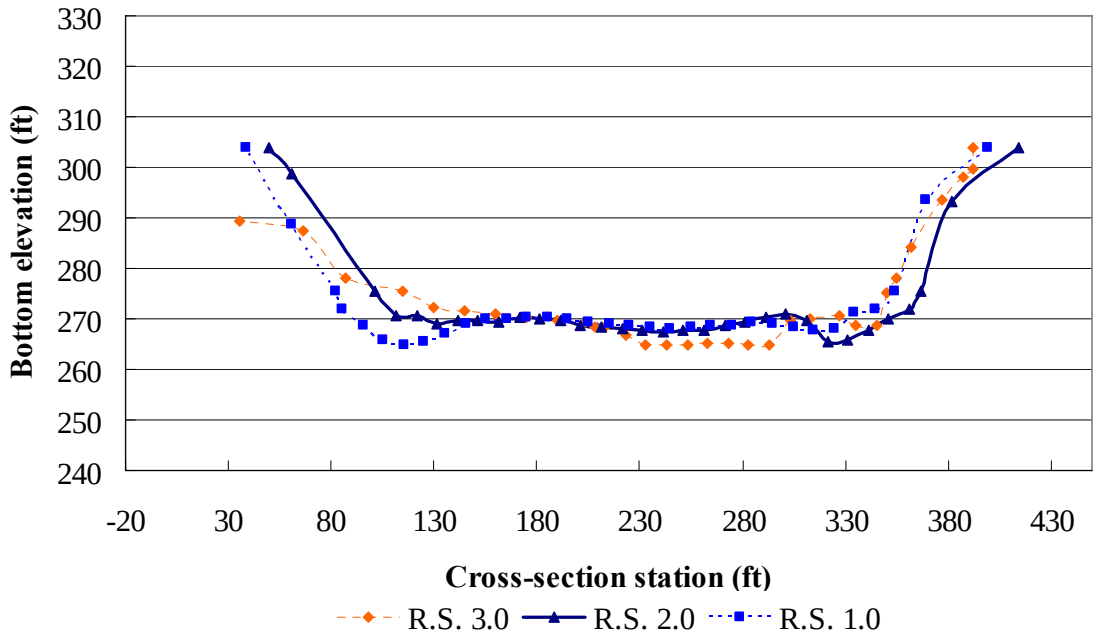

Figure 4.11 Cross section comparison from R.S. 3.0 to R.S. 1.0

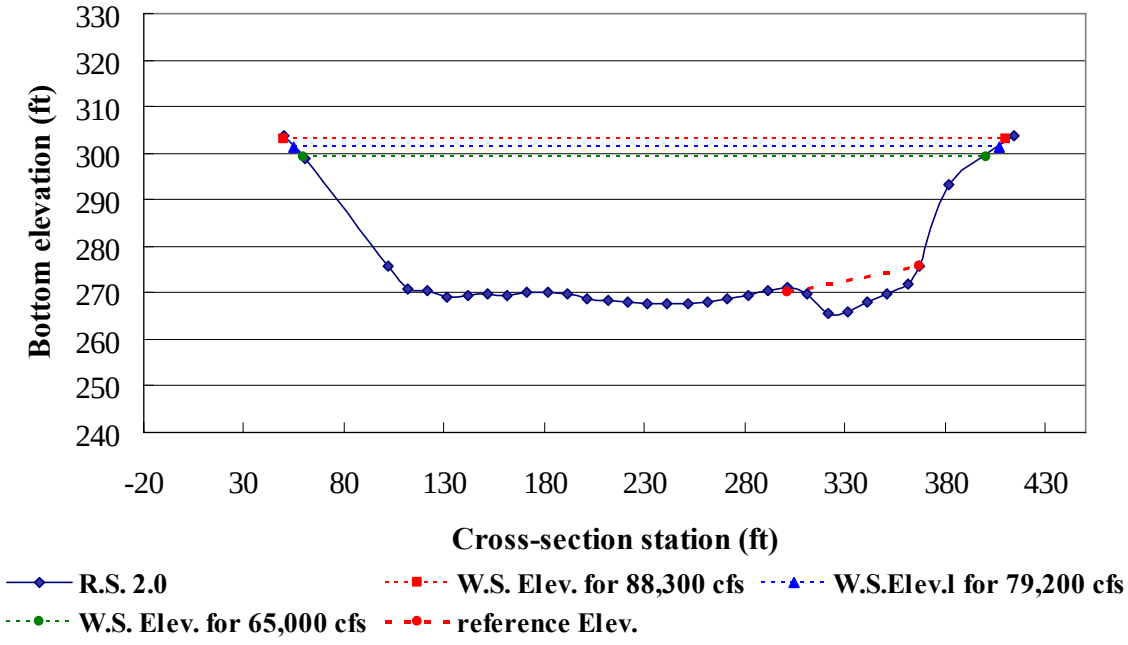

Figure 4.12 Adjusted downstream cross section at R.S. 2.0

Figure 4.13 depicts the average streambed profile after making the adjustments just described for residual scour. This figure also shows an adjusted bed formed by a straight line profile drawn from R.S. 7.0 to R.S. 1.0. The straight line is in close agreement with the adjusted uncontracted upstream cross sections (R.S. 7.0, R.S. 6.0, and R.S. 5.0) and adjusted uncontracted down stream cross sections (R.S. 2.0 and R.S. 1.0). Figure 4.13 illustrates the residual contraction scour that is present from R.S. 5.0 to R.S. 3.0. The dashed bed profile is then taken as the reference elevation for contraction scour at the bridge section (R.S. 4.0), and the corresponding average reference elevation is 1.477 ft (272.665 ft) at R.S. 4.0 by interpolation.

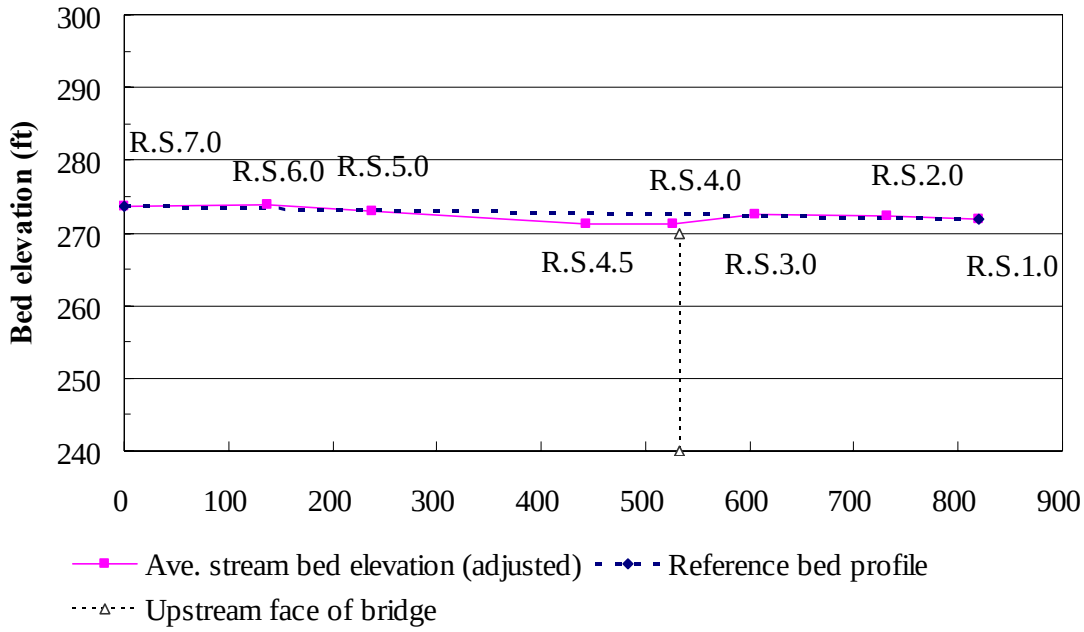

Figure 4.13 Adjusted average stream bed elevation and reference bed profile for contraction scour

For calculation of contraction scour, the approach river cross section has to be determined. Figure 4.14 shows the mean velocity in the main channel along the river profile for each of the three test discharges from the HEC-RAS output. The velocity decreases from R.S. 7.0 to R.S. 5.0 and then starts to increase from R.S. 5.0 to the bridge section at R.S. 4.0. The velocity data seem to indicate that the acceleration caused by the contraction begins at R.S. 5.0. In addition, the bed is dropping from R.S. 5.0 to R.S. 4.0 as shown previously in Figure 4.13, and the channel width at the water surface is clearly largest at R.S. 5.0 as shown in Figure 4.15 for Q = 65,000 cfs. Superimposed on the width changes are the longitudinal changes in the main channel velocity along the river in Figure 4.15, and the results show the lowest velocity and largest width occurring at R.S. 5.0. Based on these results R.S. 5.0.is assumed to be the approach uncontracted section for contraction scour.

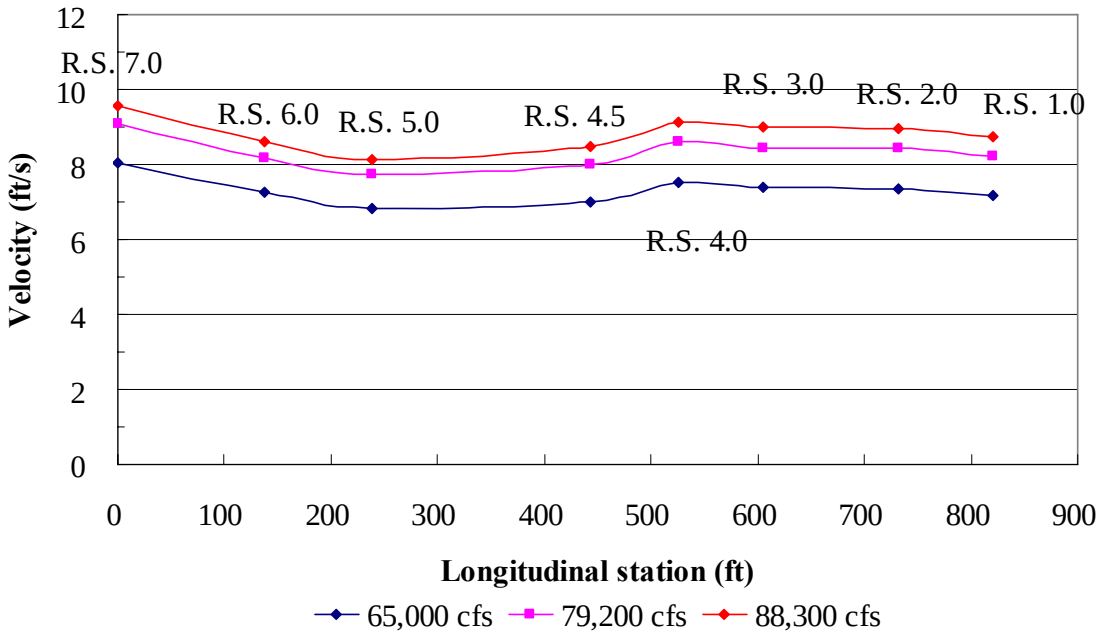

Figure 4.14 Main channel velocity variation from R.S. 7.0 to R.S. 1.0

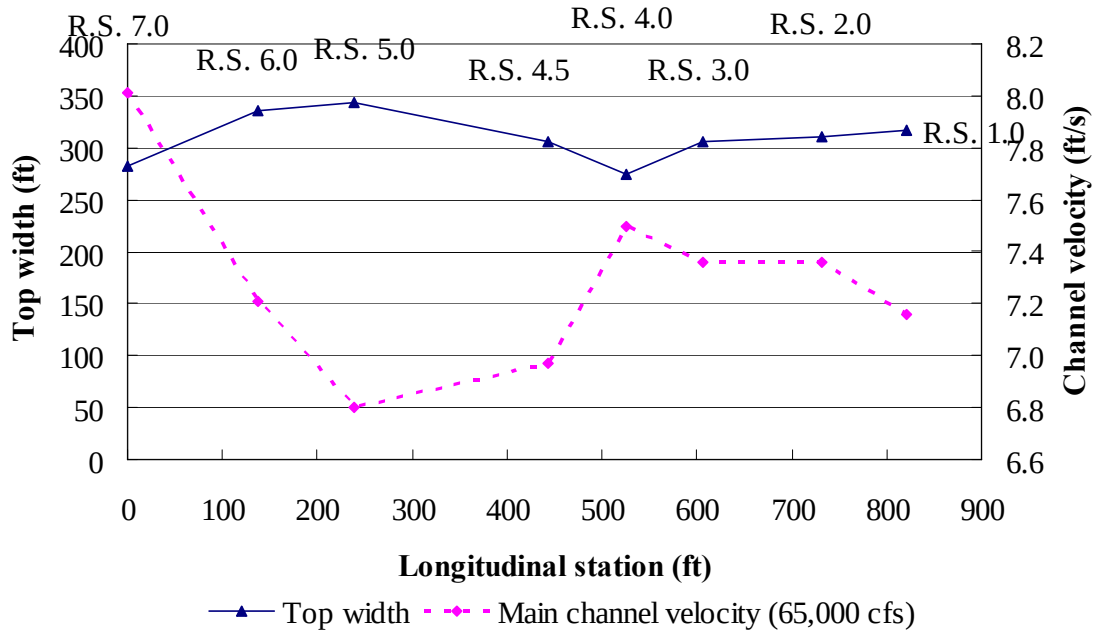

Figure 4.15 Top width and main channel velocity profile at 65,000 cfs

Table 4.1 shows the average water depth for the cross sections at R.S. 5.0, R.S. 4.0 (bridge), and R.S. 2.0. The computed water surface elevations from HEC-RAS were used to calculate average water depth relative to the adjusted reference bed surface for contraction scour at each cross section for each of the 3 test discharges.

Table 4.1 Average water depth at each cross-section before scouring
(The value in the parenthesis is prototype value)

Discharge (cfs)	Average water depth (ft)		
	R.S. 5.0	R.S. 2.0	R.S. 4.0
4.79 (65,000)	0.593 (26.69)	0.607 (27.32)	0.601 (27.05)
5.83 (79,200)	0.625 (28.13)	0.639 (28.76)	0.633 (28.49)
6.50 (88,300)	0.665 (29.93)	0.679 (30.56)	0.673 (30.29)

4.4.2 Average contraction scour depth with piers

The average water depth was calculated at R.S. 4.0 after scour depth reached equilibrium by integrating water depths over the entire equilibrium bed cross section. However, to consider the scour depth due to the contraction only, local pier scour was first removed from the equilibrium cross section. Figures 4.16 (A), (B), and (C) show the bed cross section elevations at the end of the scour experiments and the adjusted bed elevation after removing local pier scour for each of the 3 test discharges. The

adjusted bed elevations were used to calculate the average water depth at the contracted section (R.S. 4.0) after scour from which the average water depths based on the reference bed elevations were subtracted to obtain the average contraction scour depth. Table 4.2 shows the average contraction scour depth results.

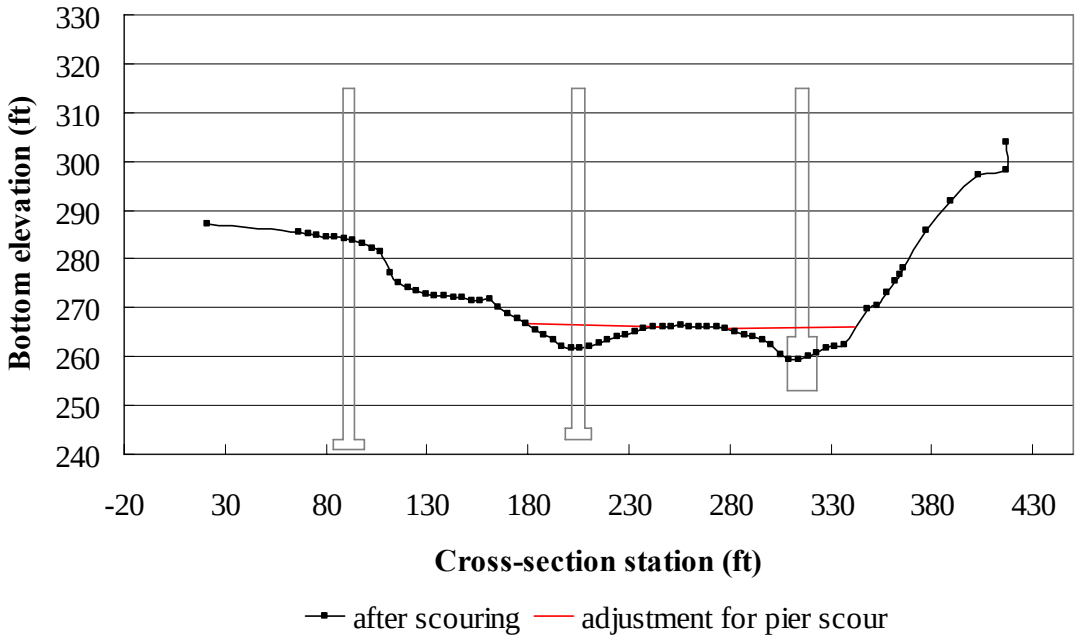

Figure 4.16 (A) Cross section at R.S. 4.0 adjusted for pier scour after scouring for Q=4.79 cfs (65,000 cfs)

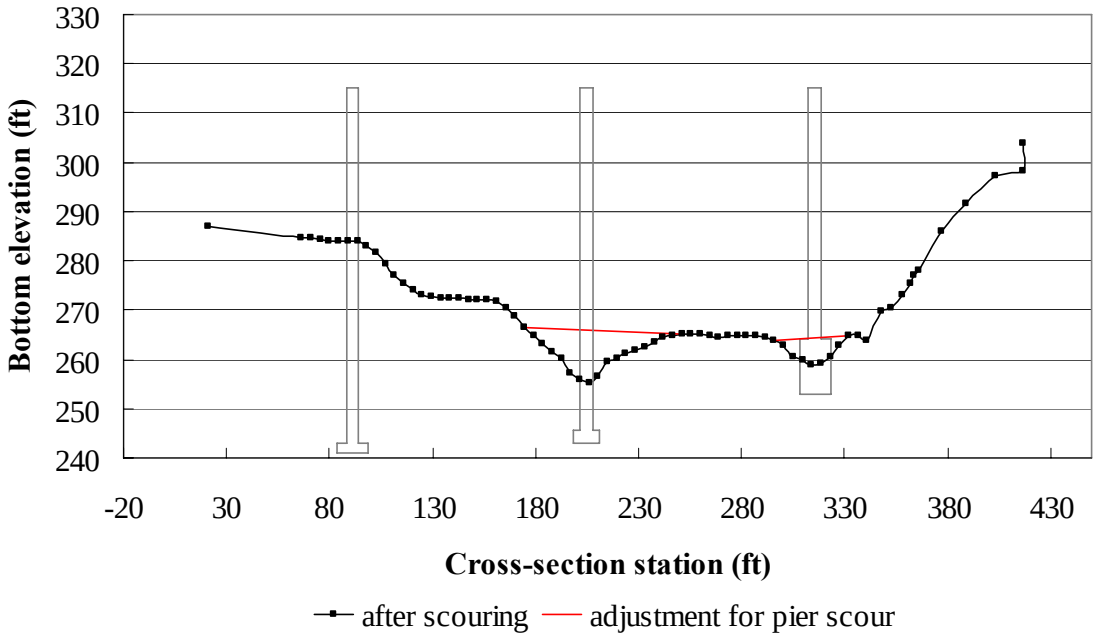

Figure 4.16 (B) Cross section at R.S. 4.0 adjusted for pier scour after scouring for Q=5.83 cfs (79,200 cfs)

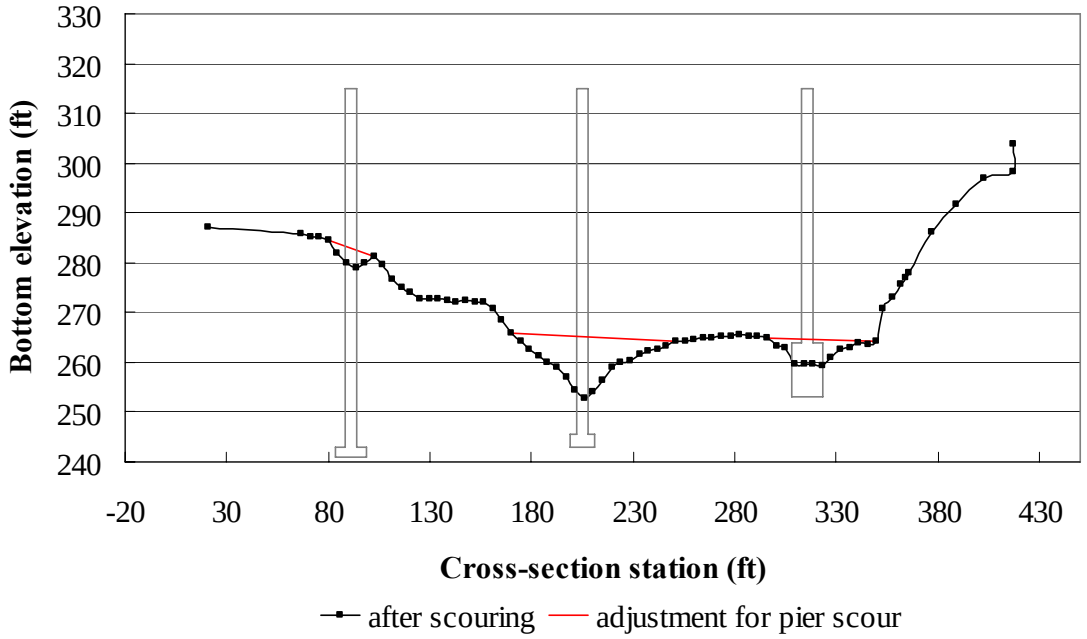

Figure 4.16 (C) Cross section at R.S. 4.0 adjusted for pier scour after scouring for Q=6.50 cfs (88,300 cfs)

Table 4.2 Average contraction scour depth at R.S. 4.0

(y_{2ref} =average water depth at reference bottom elevation, y_2 =average water depth after scouring for contraction scour, d_{sc} =average contraction scour depth (y_2 - y_{2ref}))

Discharge (cfs)	y_{2ref} (ft)	$y_2(w)$ (ft) (with piers)	d_{sc} (ft)
4.78 (65,000)	0.601 (27.05)	0.669 (30.77)	0.068 (3.06)
5.83 (79,200)	0.633 (28.49)	0.715 (32.18)	0.082 (3.69)
6.50 (88,300)	0.673 (30.29)	0.778 (35.01)	0.105 (4.73)

4.4.3 Average contraction scour depth without piers

The average water depth at the uncontracted approach upstream cross-section and downstream cross-section were assumed to be the same as in cases with the piers for determination of the contraction scour without piers. Figures 4.17 (A), (B), and (C) show the bed elevations at R.S. 4.0 at the end of scour experiments conducted without the piers in place. To show the difference between contraction scour depths with and without piers, the bed elevations for the two cases are plotted in the same figure. For the bed elevations after scouring with the piers in place, the local pier scour has been removed to isolate the contraction scour in Figure 4.17. The results shown in Figure 4.17 suggest that contraction scour without the piers in place is slightly larger than with the piers in place. This point will be discussed further in subsequent sections. Table 4.3

gives the average contraction scour depth results without the piers in place.

Table 4.3 Average contraction scour depth at R.S. 4.0 without piers

(y_{2ref} =average water depth at reference bottom elevation, y_2 =average water depth after scouring for contraction scour, d_{sc} =average contraction scour depth (y_2 - y_{2ref}))

Discharge (cfs)	y_{2ref} (ft)	y_2 (ft) (without piers)	d_{sc} (ft)
4.79 (65,000)	0.601 (27.05)	0.686 (30.87)	0.085 (3.83)
5.83 (79,200)	0.633 (28.49)	0.735 (33.08)	0.102 (4.59)

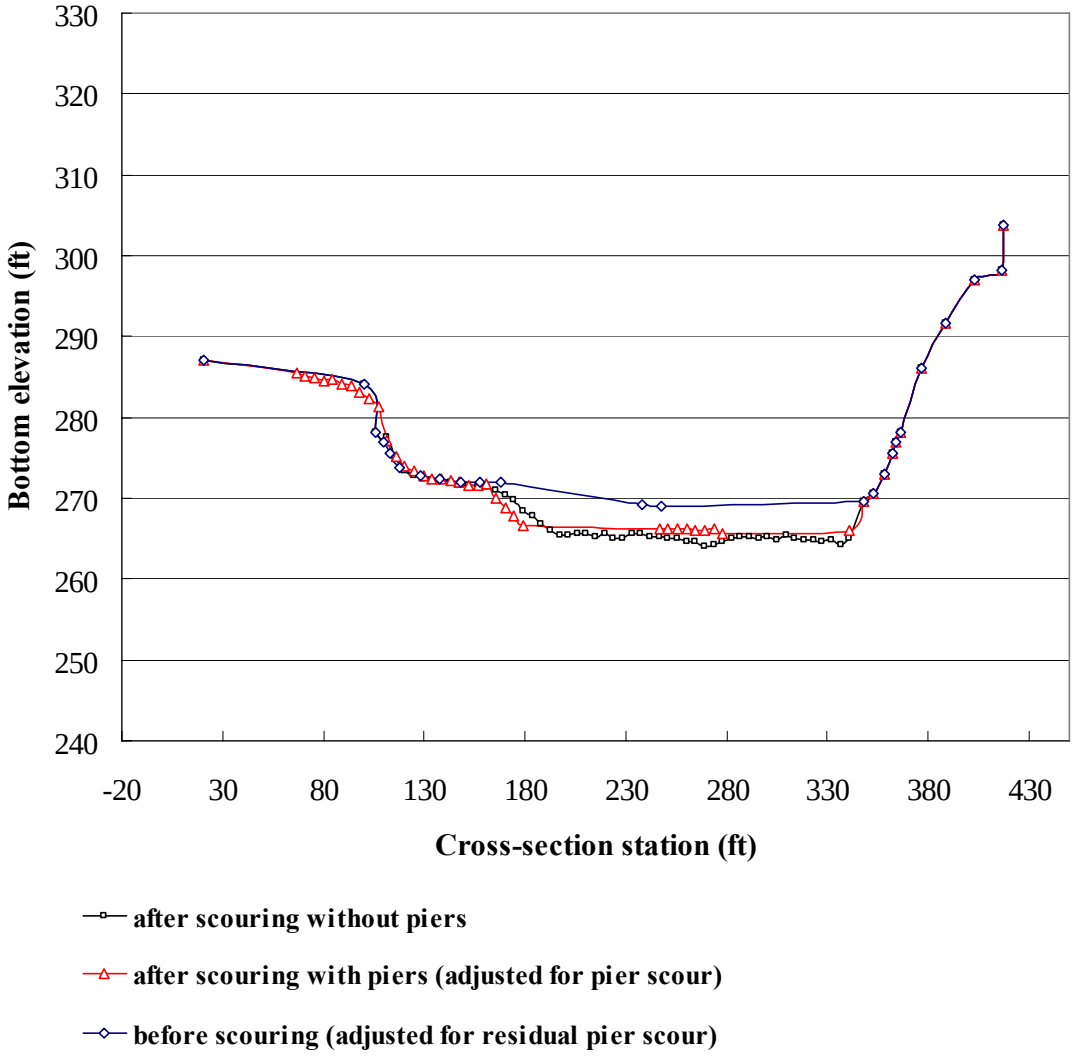

Figure 4.17 (A) Comparison of contraction scour at R.S. 4.0 with and without piers for Q=4.79 cfs (65,000 cfs)

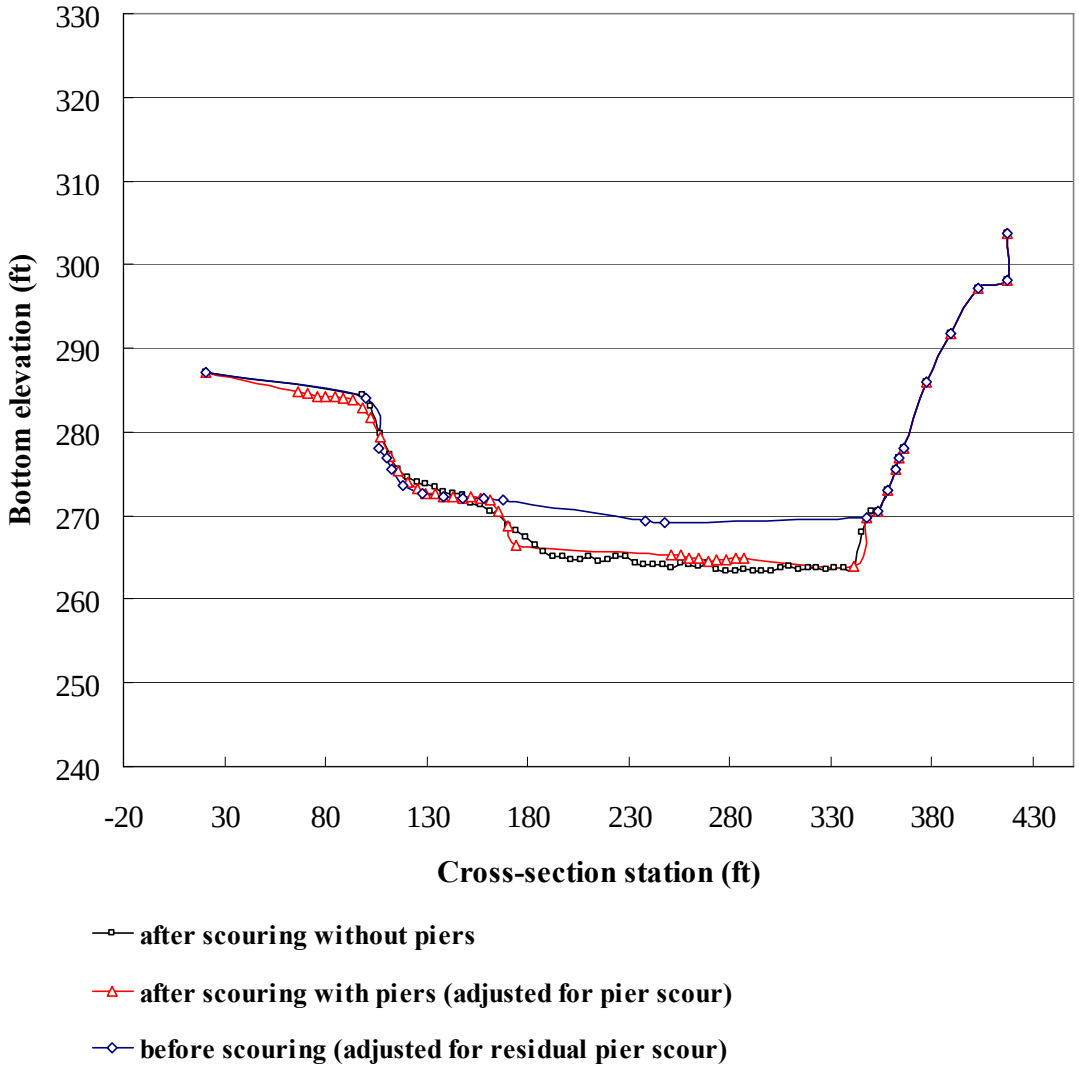

Figure 4.17 (B) Comparison of contraction scour at R.S. 4.0 with and without piers for Q=5.83 cfs (79,200 cfs)

4.5 Measured laboratory model velocity distributions

4.5.1 Velocity distribution at the bridge with the piers in place

Velocities were measured across the channel at R.S. 4.0. before and after the scouring. At this time, about 10 point velocities were measured vertically to determine the depth-averaged velocity at 25 points laterally across the cross section. The purpose of measuring the velocities at R.S. 4.0 was twofold. The first purpose was to determine the accuracy of the Froude number modeling approach by comparing the velocities obtained in the experiments with the velocities measured in the field. The second purpose was to compare the changes in the velocity and specific discharge distributions before and after scouring. Figure 4.18 shows the comparison between velocities in the laboratory and field after scouring for the historic discharge of 65,000cfs. Tables B.1, B.2, and B.3 in Appendix B show the mean velocity, water depth and specific discharge data at R.S. 4.0 for the 3 different test discharges after scouring

In the field study, the velocities were measured a short time after the occurrence of the peak discharge for the historic flood event of 65,000cfs, that is, when the measured discharge was 49,000 cfs. Thus, the velocity data from the USGS in Figure 4.18 have smaller values because of the difference in discharges, but they are only slightly smaller because the rate of change in velocity with stage is small for these higher discharges. The

change in mean velocities for these two discharges of 49,000 cfs and 65,000 cfs is a 15% larger velocity for 65,000 cfs than for 49,000 cfs. It is important to note that the shape of the two velocity distributions is very similar which seems to verify the validity of the Froude number scaling used in the model.

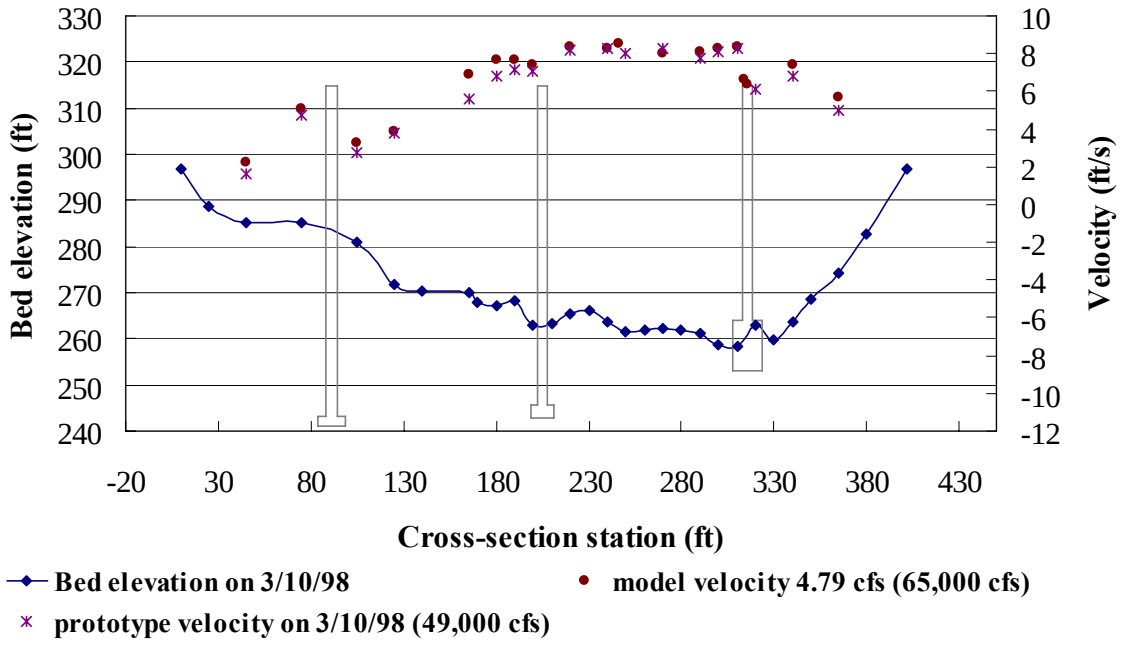

Figure 4.18 Velocity comparison at R.S. 4.0 after scouring between prototype (49,000cfs) and model (65,000cfs)

4.5.2 Approach velocity distribution and velocity along the piers for a fixed bed

Approach velocities and the approach water depths for contraction scour were measured across R.S. 5.0 for the 3 test discharges with a fixed bed. Figure 4.19 shows the velocity distributions across R.S. 5.0 using the prototype coordinates. The velocity and depth data are given in Tables D.1, D.2, and D.3 in Appendix D for the 3 different test discharges. At the bottom of each table is given the mean velocity and mean water depth in the main channel.

The measured laboratory velocity distributions in Figure 4.19 given as prototype values indicate velocity magnitudes between 8 and 9 ft/sec over a wide portion of the main channel. The prototype channel is clearly in the live-bed scour regime at the peak discharge for each of the three floods.

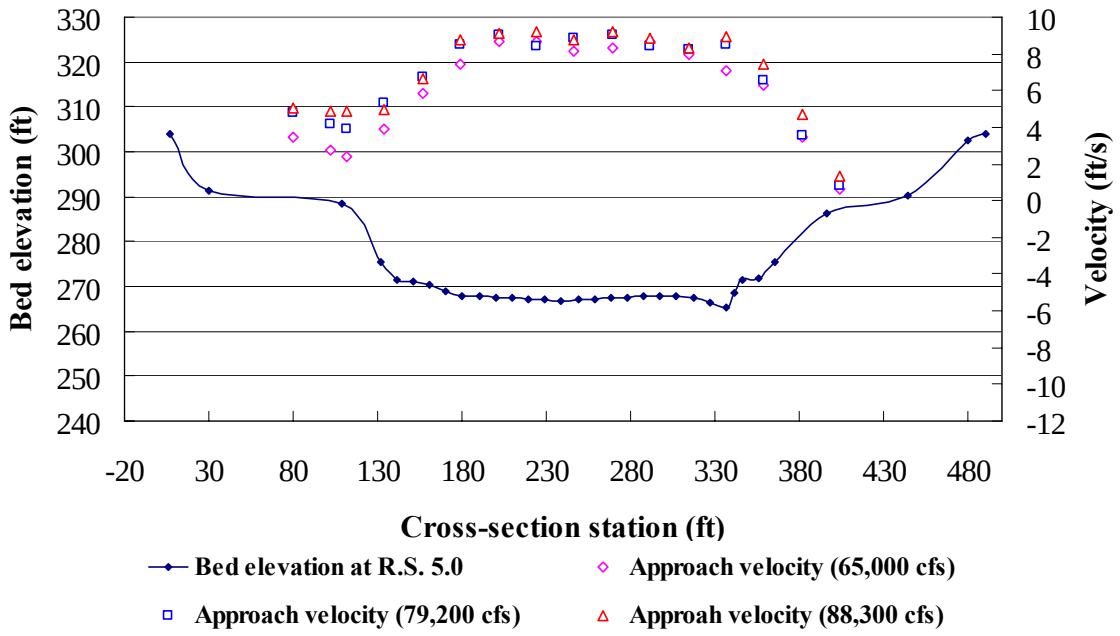

Figure 4.19 Measured model velocity distribution for contraction scour at R.S. 5.0 for three different discharges: 4.79cfs (65,000cfs), 5.83cfs (79,200cfs) and 6.50cfs (88,300cfs)

In order to gage the potential for contraction scour in the laboratory model, the depth-averaged velocities were measured through the bridge along the line at y = 8.3 ft and y = 9.0 ft between pier bent #2 and pier bent #3 with a fixed bed prior to scour. Figure 4.20 shows the locations of the measured streamwise velocities through the bridge.

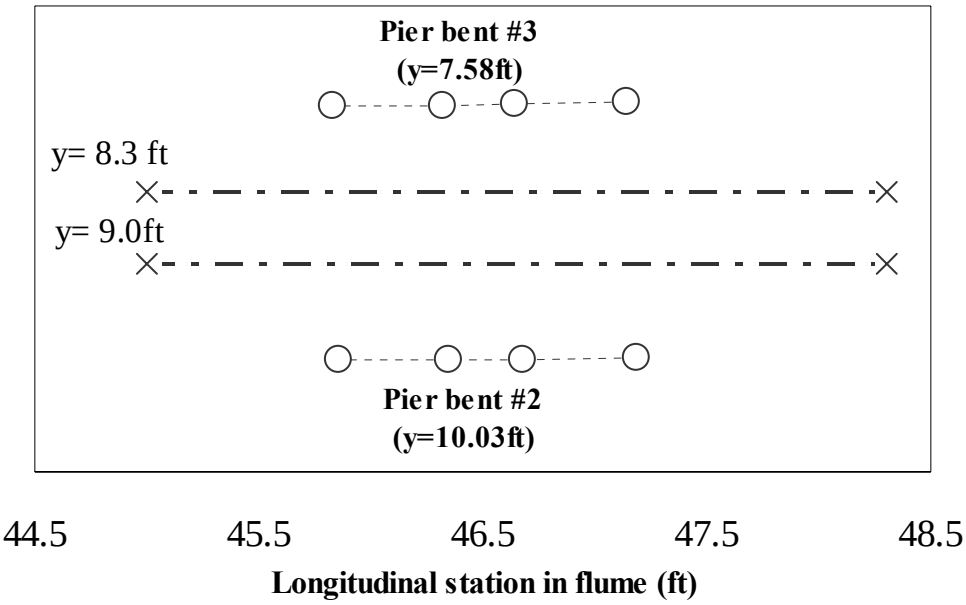

Figure 4.20 Locations of measured streamwise velocities through the bridge (*y* = lateral distance from left flume wall)

Point streamwise velocities were measured with the ADV at relative heights above the bed of approximately 0.01, 0.02, 0.04, 0.08, 0.1, 0.2, 0.4, and 0.6 times the flow depth and then the depth-averaged velocity at each measuring location was calculated by regression analysis using the logarithmic velocity distribution. Figure 4.21 shows the streamwise velocity relative to critical velocity for initiation of motion V_c in the laboratory model using the laboratory sediment for 3 different discharges. These results show that conditions for contraction scour ($V/V_c > 1.0$) were reached for all three discharges between pier bent #2 and pier bent #3. Figure 4.21 validates the choice of model sediment size such that model velocities determined by the Froude number

modeling criterion were sufficiently large to achieve contraction scour. In addition, it is apparent that the upstream depth-averaged velocities at the selected lateral positions between pier bents #2 and #3 approach conditions of incipient live-bed scour for the discharges of 79,200 cfs (50-yr) and 88,300 cfs (100-yr) for the chosen sediment size of 1.1 mm in the model. The bed elevations through the bridge after scour are also shown in Fig. 4.21 indicating a drop in the bed corresponding to the increase in velocity. These elevations were taken from the scour contours in Figures 4.6, 4.7, and 4.8. This point will be discussed further in Chapter 5.

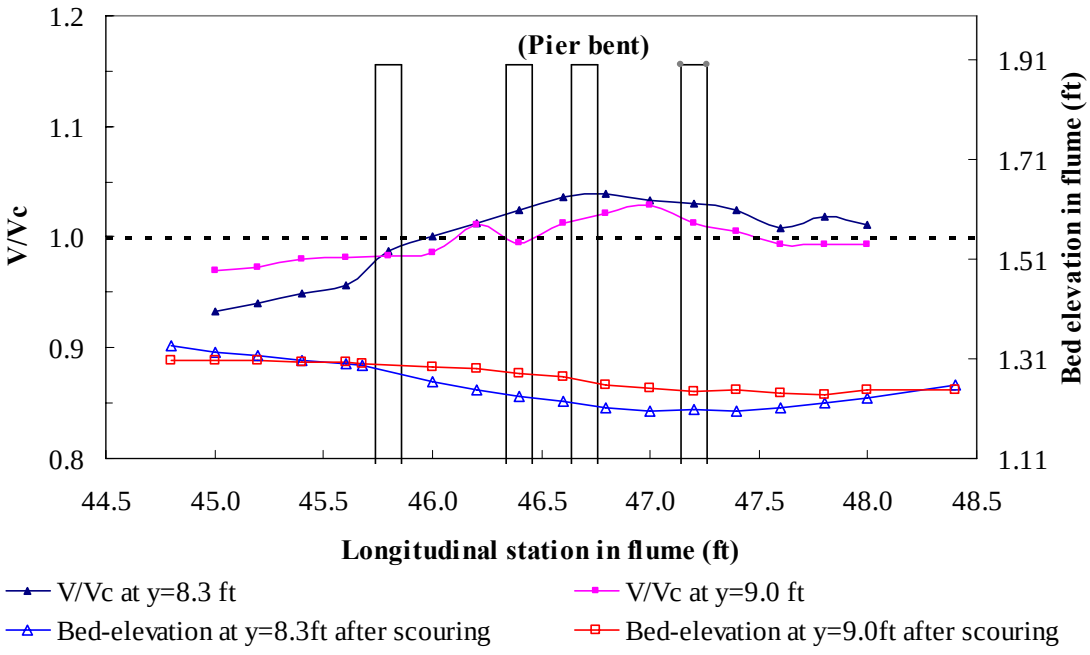

Figure 4.21 (A) Streamwise depth-averaged velocity relative to critical velocity in the flume through the bridge for Q=4.79cfs (65,000cfs) and W.S. Elev.=2.078ft (299.75ft)

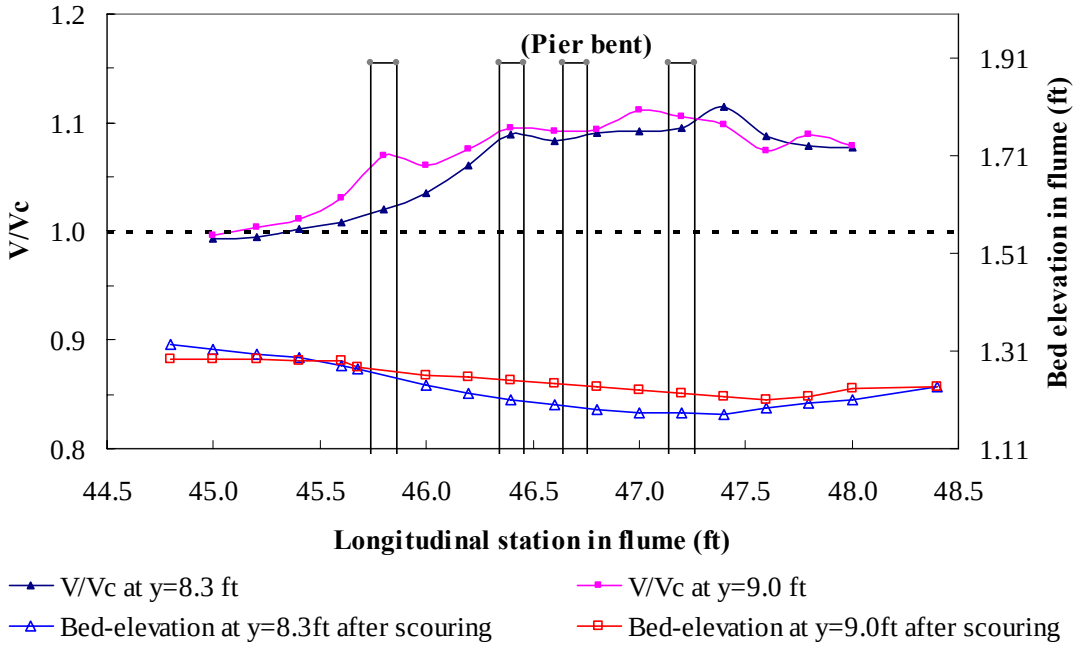

Figure 4.21 (B) Streamwise depth-averaged velocity relative to critical velocity in the flume through the bridge for Q=5.83cfs (79,200cfs) and W.S. Elev.=2.109ft (301.38ft)

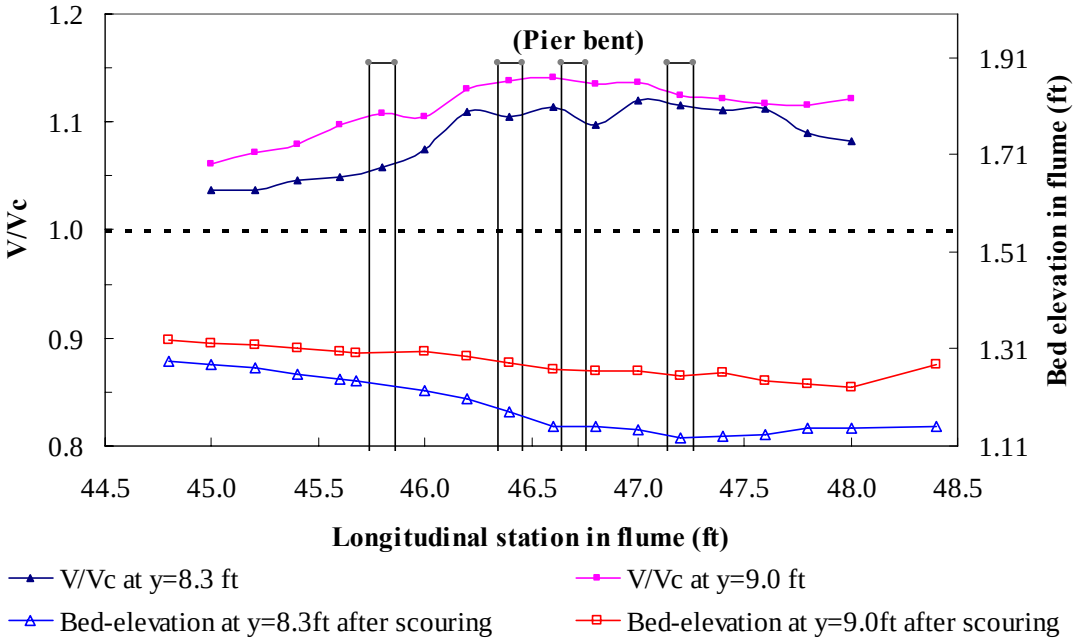

Figure 4.21 (C) Streamwise depth-averaged velocity relative to critical velocity in the flume through the bridge for Q=6.50cfs (88,300cfs) and W.S. Elev.=2.147ft (302.95ft)

4.6 Analysis and discussion of laboratory results

4.6.1 Comparison of predicted and measured contraction scour in the laboratory

Measured laboratory model data for the Ocmulgee River are presented in Table 4.4 for the 3 test discharges. The critical velocity in the sediment mobility factor V_1 / V_c was calculated from Keulegan's equation given previously as Equation 3.4 with an equivalent sand-grain roughness of $k_s = 2\,d_{50}$ and applied to laboratory depths and the laboratory sediment having d_{50} = 1.1 mm. The approach velocity V_1 is the mean cross-sectional velocity at the approach section for contraction scour at R.S. 5.0. The contraction scour depths with the piers and without the piers are defined as the average contraction scour depths at the upstream face of the bridge (R.S. 4.0). The contraction scour depth in the prototype scale was calculated from Laursen's live-bed contraction scour equation given previously as Equation 2.3. The HEC-RAS output data presented in Table 4.5 were used to calculate the contraction scour depth in the prototype scale.

Table 4.4 Experimental data table

(Q=discharge, V_1 =approach flow velocity, V_c =critical velocity, Fr =approach Froude number, y_1 =approach flow depth, y_{2ref} = reference flow depth at reference bridge section, $y_2\,(w)$ =flow depth at bridge section with pier after scouring, $y_2\,(w/o)$ =flow depth at bridge section without pier after scouring)

Q (cfs)	scale ratio	V_1 (ft/s)	V_c (ft/s)	V_1/V_c	Fr	y_1 (ft)	y_{2ref} (ft)	$y_2\,(w)$ (ft)	$y_2\,(w/o)$ (ft)
4.79	1/45	1.022	1.289	0.793	0.236	0.593	0.601	0.669	0.686
5.83	1/45	1.102	1.307	0.843	0.246	0.625	0.633	0.715	0.735
6.50	1/45	1.147	1.321	0.868	0.248	0.665	0.673	0.778	

Table 4.5 HEC-RAS results for contraction scour computation

(Q_t =total discharge, Q_c =contraction scour approach section main channel discharge, B_2=bridge section top width, B_1=approach section top width, y_1 =contraction scour approach flow depth)

Q_t (cfs)	Q_c (cfs)	B_2 (ft)	B_1 (ft)	y_1 (ft)
65,000	62,828	274.5	343	26.76
79,200	76,005	274.5	343	28.68
88,300	84,309	274.5	343	30.17

Table 4.6 shows the measured laboratory results for contraction scour depth with the piers, without the piers and the predicted contraction scour depth calculated by Laursen's live-bed contraction scour equation with the aid of the HEC-RAS output in

Table 4.5. The measured laboratory contraction scour depth without the piers is larger than the contraction scour depth with the piers by about 25% as shown in Table 4.6. Furthermore, the contraction scour depth predicted by Laursen's live-bed formula is greater than the measured laboratory contraction scour depth for the case of the piers installed by a factor of approximately 30-60% with better agreement obtained for higher discharges. Figure 4.22 plots the comparison between laboratory measured contraction scour depth and computed contraction scour depth and shows that all the computed values overpredict scour depth relative to the laboratory measured values.

One likely reason for the observed larger contraction scour in the laboratory model without the piers in comparison to the case of the piers in place is the interaction between pier and contraction scour and the associated redistribution of discharge that occurs. This issue is explored further in section 4.6.3.

Overprediction of scour by Laursen's live-bed equation may be related to the fact that the laboratory results were obtained under clear-water scour conditions, although incipient live-bed scour was approached, while the field conditions were live-bed and the live-bed formula was used. This matter will be taken up in section 4.6.4

Table 4.6 Measured and predicted contraction scour results

($d_{sc}(w)$ =contraction scour depth with pier, $d_{sc}(w/o)$ =contraction scour depth without pier, $d_{sc}(c)$ =calculated contraction scour depth, $del = d_{sc}(w/o) - d_{sc}(w)$; the value inside the parenthesis is prototype value)

Q (cfs)	$d_{sc}(w)$ (ft)	$d_{sc}(w/o)$ (ft)	$d_{sc}(c)$ (ft)	del (ft)
4.79 (65,000)	0.068 (3.06)	0.085 (3.83)	(5.01)	0.017 (0.77)
5.83 (79,200)	0.082 (3.69)	0.102 (4.59)	(5.58)	0.020 (0.90)
6.50 (88,300)	0.105 (4.73)	-	(6.03)	-

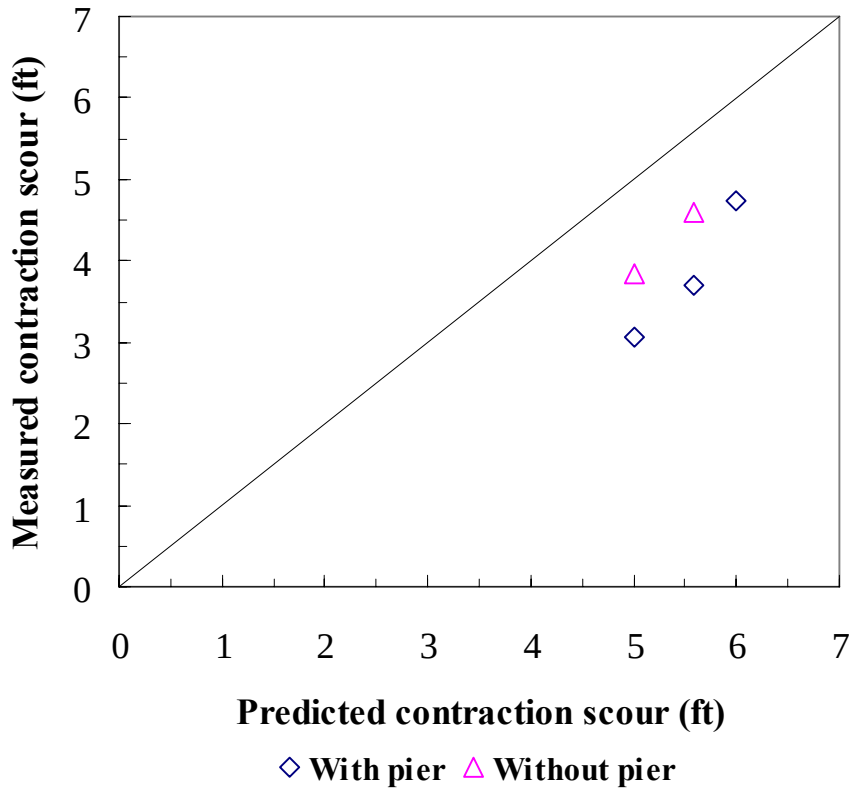

Frgure 4.22 Comparison between measured laboratory contraction scour and predicted contraction scour using the Laursen live-bed formula

4.6.2 Comparison of predicted and measured total scour in the laboratory model

Table 4.7 shows the HEC-RAS output variables required for the pier scour depth computation. The pier scour depth is calculated by the pier scour equation recommended in HEC-18 (Richardson and Davis 1995). To calculate the total scour depth, the pier scour depth and contraction scour depth are calculated separately and those values are then summed. Table 4.8 gives the total scour depth comparison, while Figure 4.23 depicts graphically the comparison between predicted total scour depth and measured total scour depth in the laboratory. These results show that the local pier scour depth calculated by the recommended HEC-18 equation predicts the laboratory scour depth very closely (within about 2%). However, because the contraction scour depth calculated by Laursen's live-bed formula was overpredicted, the total scour depth was still overpredicted.

Table 4.7 HEC-RAS results for pier scour computation

(Q = total discharge, y_1 =pier scour approach flow depth b =pier width, Fr_1 =pier scour approach Froude number, K_s =pier shape factor, K_θ =pier alignment factor, V_1 =pier scour approach velocity, d_{50} =median sediment size)

Q (cfs)	y_1 (ft)	y_1/b	Fr_1	K_s	K_θ	V_1/V_c	b/d_{50}
65,000	29.62	4.94	0.23	1.00	1.00	2.34	2613
79,200	31.50	5.25	0.25	1.00	1.00	2.59	2613
88,300	32.96	5.49	0.26	1.00	1.00	2.69	2613

Table 4.8 Total scour depth comparison

Discharge (cfs)	Measured scour depth (ft)			Computed scour depth (ft)		
	Pier	Contraction	Total	Pier	Contraction	Total
4.79 (65,000)	0.273 (12.29)	0.068 (3.06)	0.341 (15.35)	12.27	5.01	17.28
5.83 (79,200)	0.293 (13.19)	0.082 (3.69)	0.375 (16.88)	12.98	5.58	18.56
6.50 (88,300)	0.292 (13.14)	0.105 (4.73)	0.397 (17.87)	13.42	6.03	19.45

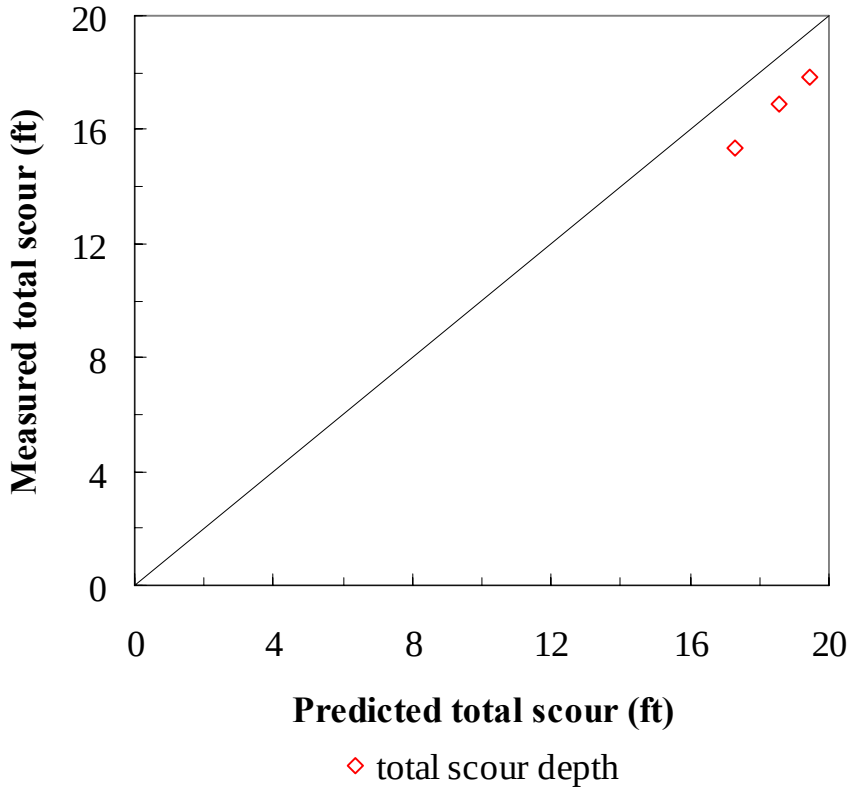

Figure 4.23 Comparison of measured total scour in the laboratory to predicted total scour

4.6.3 Interaction of pier scour and contraction scour

4.6.3.1 Change in velocity time history

Figure 4.24 and Figure 4.25 show the time history for contraction scour, pier scour, and velocity for discharges of 79,200 cfs (50 year) and 88,300 cfs (100 year). The contraction scour time history and velocity time history were measured at the exact same point (Point C in Figure 3.8). It is important to note that the velocity decrease with time in Figures 4.24 and 4.25 corresponds to the pier scour depth increase, not to

the contraction scour increase. During the first 5 or 10 hrs, the abrupt decrease in velocity is due to the abrupt increase of pier scour depth. As the slope of the pier scour time history curve decreases, the slope of the velocity time history also decreases. After the time of equilibrium for the pier scour is reached, the velocity does not change appreciably as a function of time. After the pier scour reached equilibrium conditions the velocity time history plot should have followed the contraction scour time history because the contraction scour continued to increase. However, because the contraction scour depth increases very slowly and the amount is relatively small, the measured depth-averaged velocity was insensitive to additional contraction scour within the uncertainty of the experimental measurements of velocity.

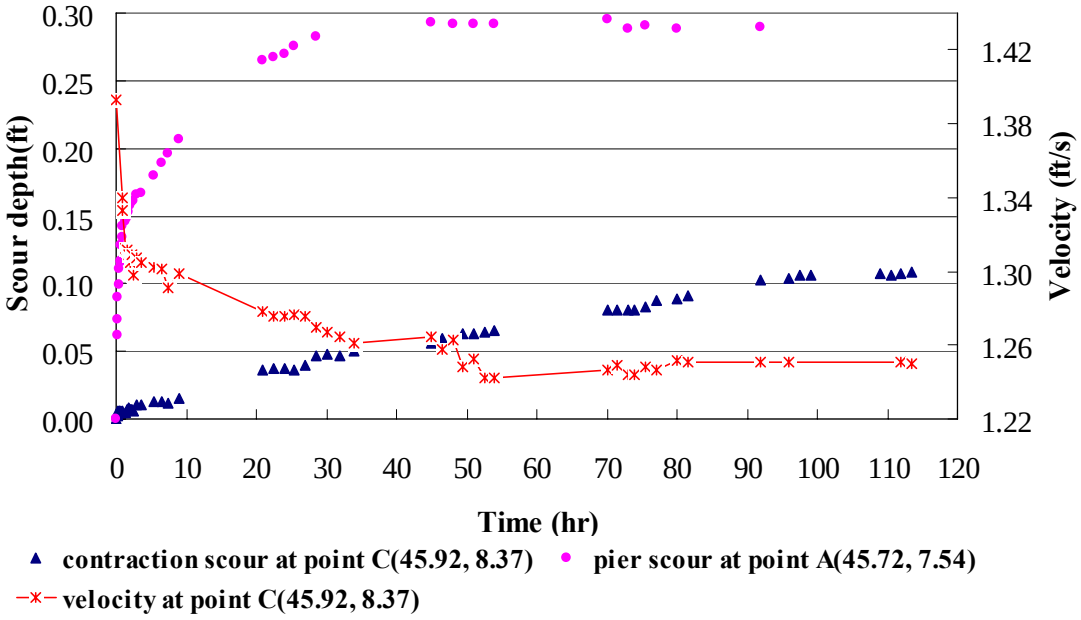

Figure 4.24 Pier effect on the velocity at point C in the contraction scour region (Q=5.83cfs (79,200cfs)/ with pier, W.S. Elev.=2.109ft (301.38ft))

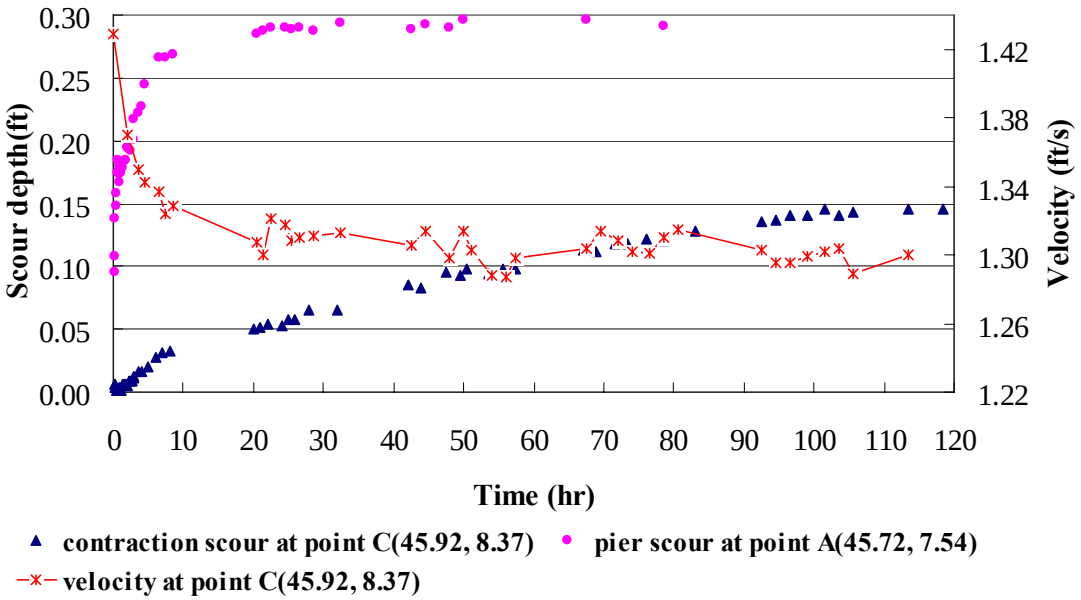

Figure 4.25 Pier effect on the velocity at point C in the contraction scour region (Q=6.50cfs (88,300cfs)/ with pier, W.S. Elev.=2.147ft (302.95ft))

Figure 4.26 and Figure 4.27 provide additional evidence for the interaction between pier scour and contraction scour, or more precisely, the lack thereof when the piers are removed. In Figure 4.26 and Figure 4.27, the time history of the contraction scour and the velocity at point C in the contraction region between pier bents is shown after removing the piers from the bridge cross section. The only difference between Figures 4.24 and 4.26 is whether there are piers in the flume or not. The velocity time history measured with the piers in place followed the trend of the pier scour time history as noted previously in Figure 4.24. However, upon removing the piers, the time history for velocity corresponds to the time history for contraction scour as shown in Figure 4.26 at the same discharge of 79,200 cfs. The case of contraction scour without the piers in place for a discharge of 65,000 cfs confirms that the velocity time history corresponds to the contraction scour time history as shown in Figure 4.27, although the magnitude of the changes with time are smaller for this smaller discharge.

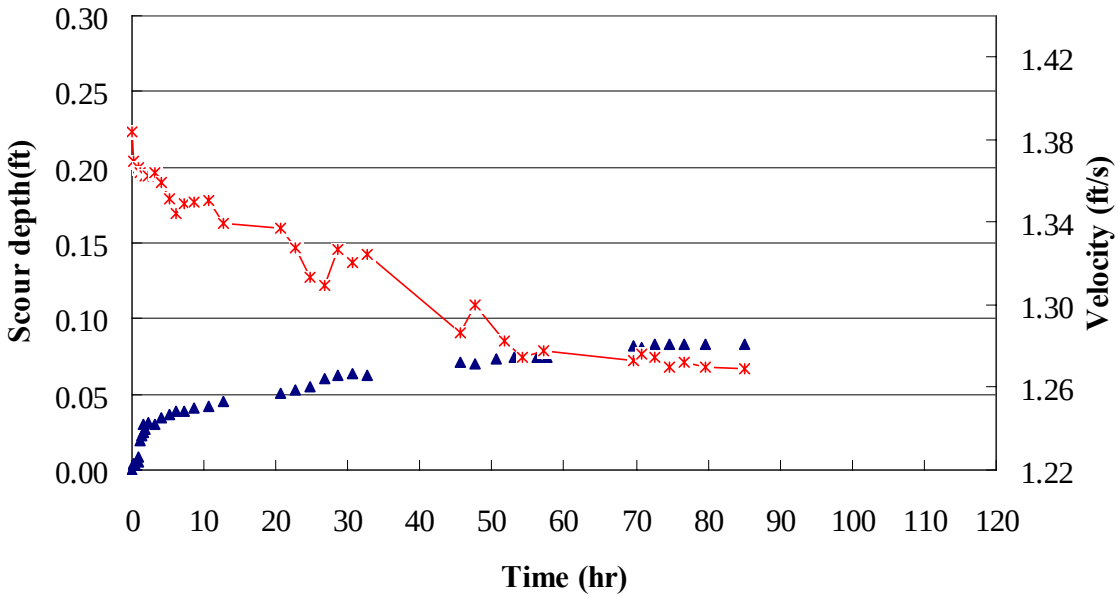

Figure 4.26 Contraction scour effect on velocity time history without the piers (Q=5.83cfs (79,200cfs) / without pier, W.S. Elev.=2.109ft (301.38ft))

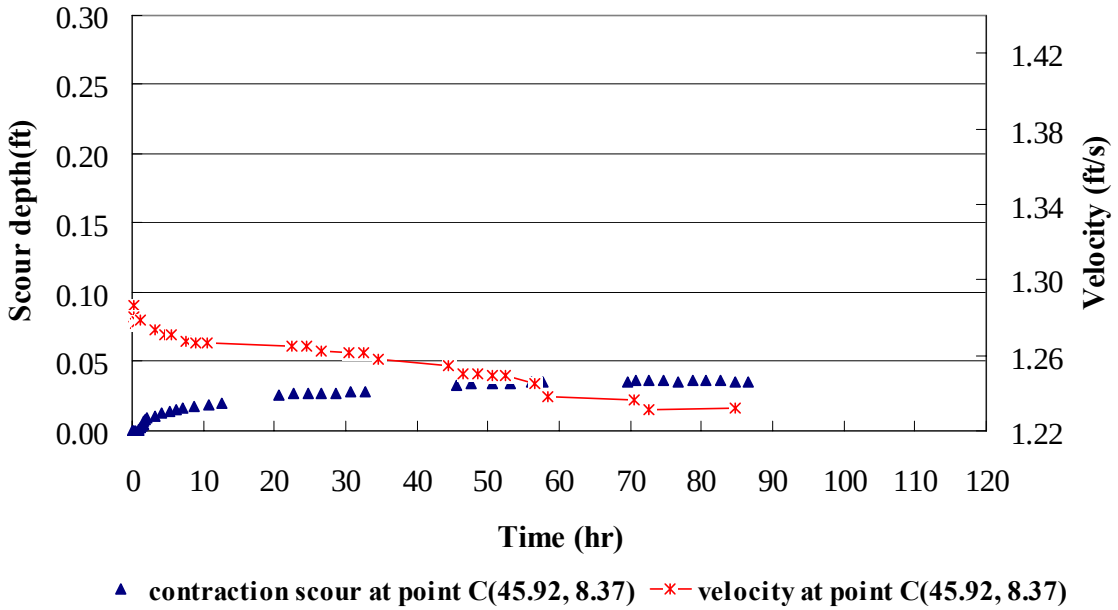

Figure 4.27 Contraction scour effect on velocity time history without the piers (Q=4.79cfs (65,000cfs)/ without pier, W.S. Elev.=2.078ft (299.75ft))

4.6.3.2 Change in discharge distribution

Previously in this chapter, results for the time development of the contraction scour and pier scour were given in Figure 4.1, Figure 4.2 and Figure 4.3. These figures show that the pier scour develops faster than the contraction scour with each discharge. Whereas the pier scour depth reached about 90% of its final value (equilibrium condition) after 40 hrs, the contraction scour just reached 40% of its final value for the same duration of time. This result suggested that the more rapid development of pier scour may change the discharge distribution across the bridge cross section before the contraction scour has had time to fully develop. In other words, the discharge that flows outside the scour hole region is reduced with respect to the initial discharge in the contraction scour region between pier bents due to discharge redistribution into the scour hole region although the total discharge remains constant.

A discharge redistribution across the bridge cross section may explain why the contraction scour depth measured without the piers is larger than the contraction scour depth measured with the piers in place as given preciously in Table 4.6. If the discharge in the contraction scour region is less due to the interaction with pier scour, then removal of the piers would tend to increase the discharge between the piers and increase the contraction scour.

That the discharge redistribution just hypothesized actually occurs is evidenced by the measured specific discharge data given in Figure 4.28, Figure 4.29, and Figure 4.30. Specific discharge, or local discharge per unit width, was calculated as the depth-averaged velocity times water depth at each measuring location across the cross section. Figure 4.28, Figure 4.29 and Figure 4.30 show the specific discharge change before and after scouring for the 3 different test discharges. Contrary to the assumption that specific discharge might be expected to be a constant before and after scour, the specific discharge in the region of local pier scour in front of the middle pier bent is observed to increase significantly after scour as shown in Figures 4.29 and 4.30 because of the larger increase in local water depth due to the pier scour compared to the decrease in velocity. Conversely, it can be observed in Figures 4.28 and 4.29 that the specific discharge distribution before scour and after scour without the piers in place is approximately the same. With respect to the specific discharge in the contraction scour region between the pier bents, it decreased noticeably for the higher discharge in Figure 4.30 but remained relatively unchanged in Figures 4.28 and 4.29 perhaps because the change was too small to measure precisely.

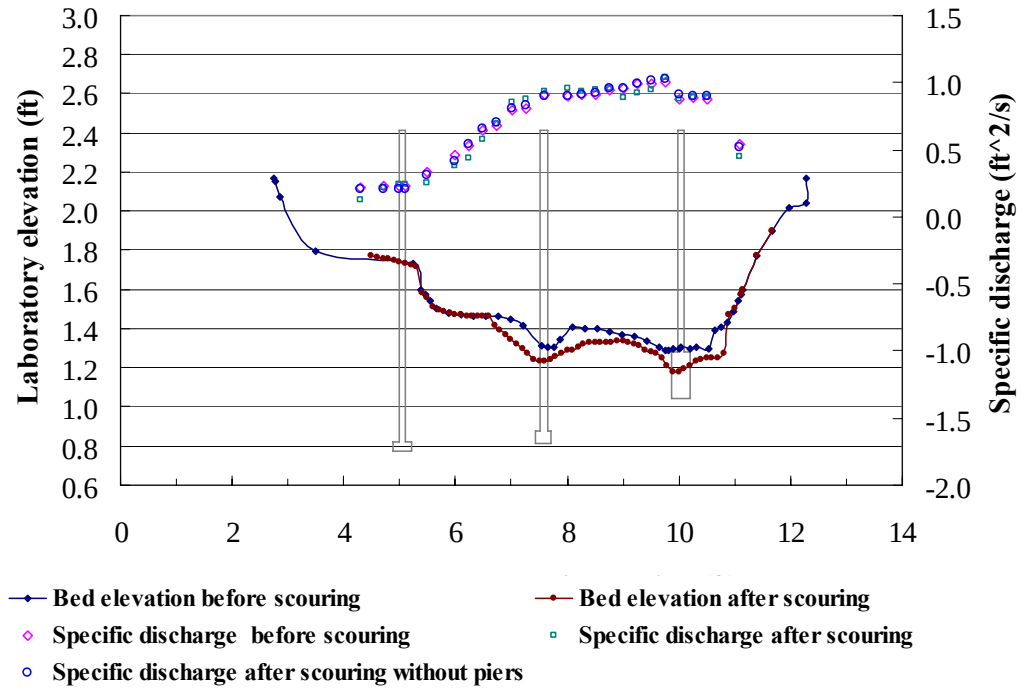

Figure4.28 Specific discharge distribution at R.S. 4.0 (immediately upstream of bridge for Q=4.79 cfs (65,000 cfs), W.S. Elev.=2.078 ft (299.75 ft))

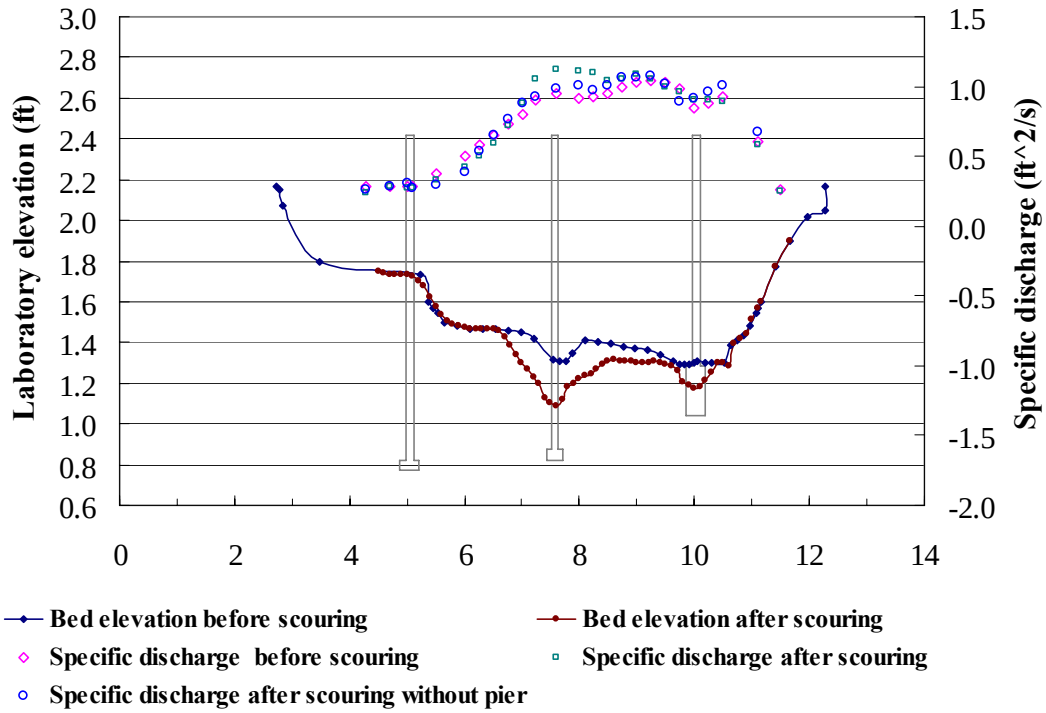

Figure4.29 Specific discharge distribution at R.S. 4.0 (immediately upstream of bridge for Q=5.83 cfs (79,200 cfs), W.S. Elev.=2.109 ft (301.38 ft))

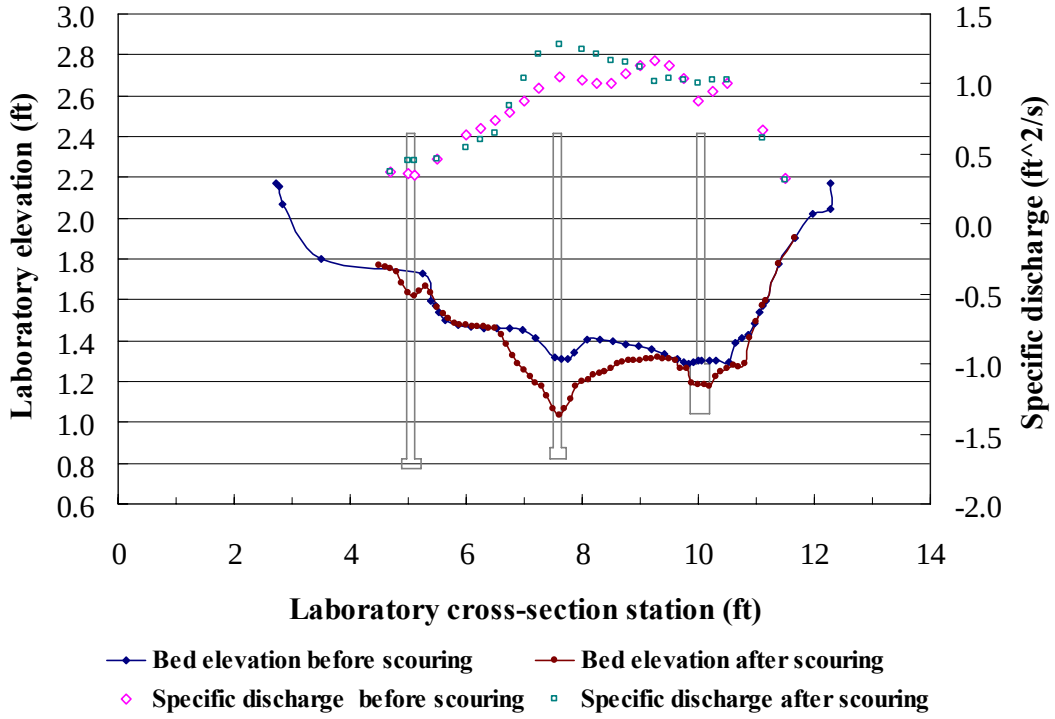

Figure4.30 Specific discharge distribution at R.S. 4.0 (immediately upstream of bridge for Q=6.50 cfs (88,300 cfs), W.S. Elev.=2.147 ft (302.95 ft))

4.6.4 Comparison between live-bed scour and clear-water contraction scour

In the field, the flow condition was live-bed scour for all 3 flood discharges. As a result, to predict the scour depth with prototype values of the independent variables, the live-bed scour equation was used to compute the contraction scour depths given in Table 4.6. However, in the laboratory, the experiment was conducted under clear-water conditions by appropriate choice of the laboratory sediment size such that the sediment mobility parameter, V_1/V_c, approached unity, or incipient live-bed scour. This modeling approach proved to be quite successful in reproducing field

measurements of pier scour as shown in the next section. However, the advisability of this modeling approach for contraction scour should be investigated separately. It is possible that this approach may account for overprediction of the measured laboratory contraction scour by use of the field live-bed scour formula.

Figure 4.31 shows the comparison between the computed results for contraction scour using the live-bed equation and the measured results from the clear-water contraction scour experiments in the laboratory. The results are given in terms of the water depth after scour in the contracted section y_2 in ratio to the approach flow depth y_1. (Note that it is usually assumed that differences in velocity head are small so that $d_{sc}/y_1 = y_2/y_1 - 1$, where d_{sc} is the contraction scour depth.) The figure shows that there is a discrepancy between these two results as given previously in Table 4.6 with respect to contraction scour depths.

Also shown in Figure 4.31 is the calculated contraction scour depth using the clear-water contraction scour formula for comparison with the laboratory results. The contraction scour formula for the clear-water case is different from the formula for live-bed contraction scour. Clear-water contraction scour is assumed to reach equilibrium when the shear stress in the contracted section becomes equal to the critical shear stress for initiation of motion resulting in Equation 2.8. The live-bed contraction

scour formula, on the other hand, assumes that at equilibrium scour, the rate of sediment transport is the same in the approach and contracted sections resulting in Equation 2.3.

Figure 4.32 shows the contraction scour depth plotted relative to the value of the sediment mobility parameter, V_1/V_c, which is different in the laboratory than the field because of the necessity to choose a larger sediment size in the laboratory than exact similarity of sediment mobility allows. The experiment results for the clear water contraction scour depth agree very closely with the computed result from the clear-water contraction scour equation using c_n = 0.039 and τ_{*c} = 0.035 (See equation 2.8). Based on these calculations alone, it appears that as V_1/V_c approaches unity in the lab, there is reasonable agreement between the calculated clear-water contraction scour and the calculated live-bed contraction scour for field conditions. In other words, the lab results are approaching the predicted field results so it would appear that this is a successful modeling strategy if V_1/V_c =1.0 in the laboratory. However, the measured field contraction scour for 65,000 cfs is shown in both Figure 4.31 and 4.32, and both clear-water and live-bed scour predictions as well as laboratory measurements are less than this value. This point will be discussed further in section 4.7.

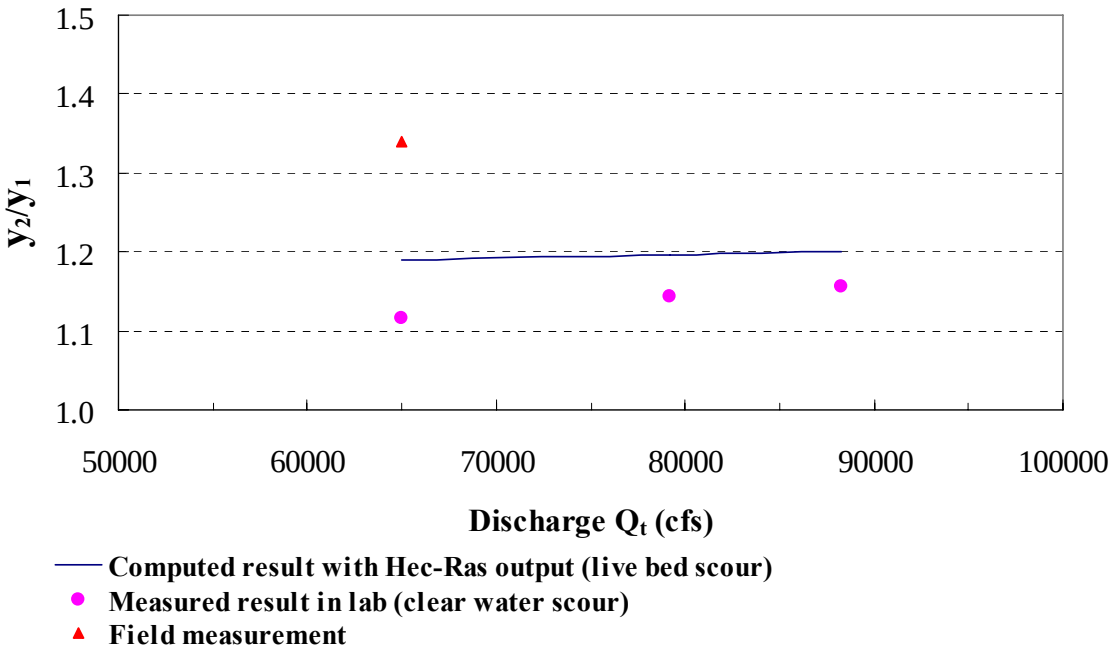

Figure 4.31 Comparison between the results from the live-bed contraction scour equation and clear-water experiments

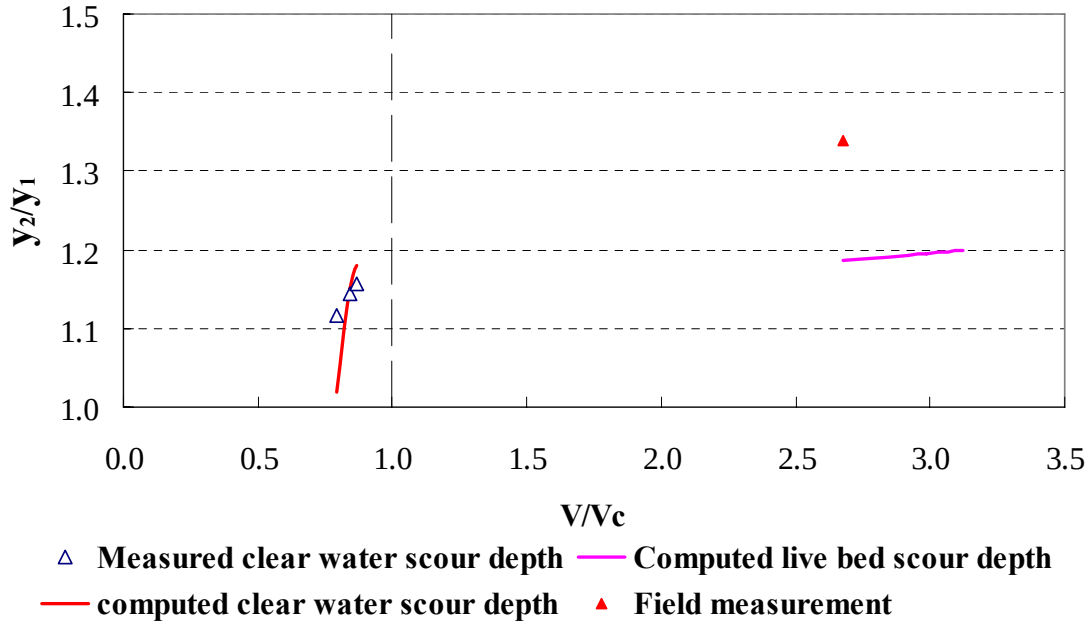

Figure 4.32 Contraction scour depth results computed by the clear-water scour equation and live-bed scour equation compared with contraction scour depths measured in the lab

It should be noted that the computed live-bed scour values in Figure 4.31 and Figure 4.32 appear to increase very slowly with discharge or with the sediment mobility parameter. This is because the primary dependence of the calculated contraction scour ratio is on the ratio of the total discharge to the main channel discharge in the approach section, Q_t/Q_c, which varies slowly over the tested discharge range as shown in Figure 4.33. Based on HEC-RAS results, Figure 4.33 shows only about a 1.5% change in Q_t/Q_c over the range of discharges from 65,000 cfs to 88,300 cfs.

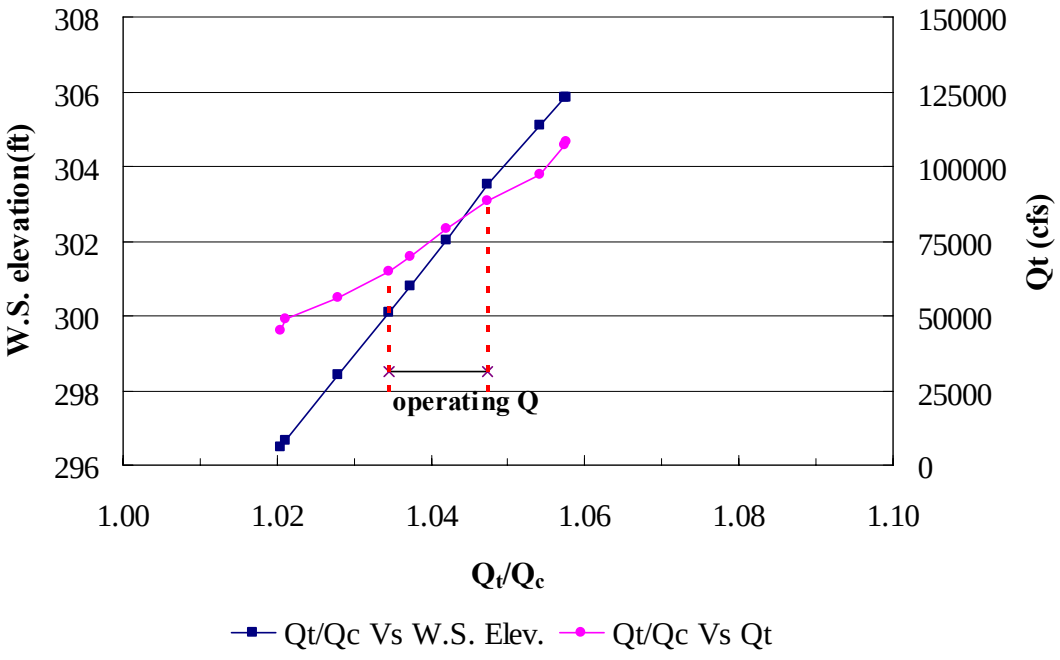

Figure 4.33 Variability of Q_t/Q_c with stage and discharge. (Q_t is the total discharge and Q_c is main channel discharge.)

4.7 Comparison between field and laboratory results

The river cross sections in the laboratory model were constructed based on the field data measured at the Ocmulgee River at Macon on February 23, 2002 by the USGS[1]. A historic discharge measurement of 65,000 cfs was made by the USGS in March of 1998 including velocities and cross-section bed elevations at the upstream side of the bridge.

Figure 4.34 shows the upstream bed elevation comparisons for different discharges based on field measurements in 2003 and during the historic flood of 1998. These cross sections are taken just upstream of the bridge at R.S. 4.0. The cross section dated February 23, 2002 was taken at base flow and represents the initial bed elevations before scour in the laboratory model for this location. In addition, the bed elevations after scour in the laboratory model are given in Figure 4.34 for the flood of 1998.

Figure 4.34 shows that the measured laboratory contraction scour depths between pier bents #2 and #3 just upstream of the bridge do not seem to agree with the field measurements for the 1998 historic discharge (65,000cfs) although the agreement of bed elevations between pier bents #4 and #3 is quite close. Overall, the adjusted

[1]River cross sections in this chapter were provided by the USGS as part of a joint research project with Georgia Tech funded by Georgia DOT (see Sturm et al. 2004).

average field contraction scour depth is 8.62 ft compared to 3.06 ft of laboratory contraction scour for this event as shown previously in Figure 4.32. On the other hand, it can be seen that for pier scour, the laboratory scour depth agrees very closely with the field measurement for both pier bents #2 and #3. The minimum bed elevation at pier bent #2 was 259.4 ft in the model and 259 ft in the prototype, while the corresponding minimum bed elevation at pier bent #3 was 261.7ft in the model and 262.5 ft in the prototype.

The other cross sections shown in Figure 4.34 indicate that from February 2002 until March 2003, the cross section on the upstream side of the bridge filled in, perhaps because of upstream sediment mobilization and deposition in the bridge opening due to the river discharge of 19,400 cfs (< 2-year recurrence interval discharge of 28,500 cfs) in March 2003. The two subsequent cross sections taken in May and July of 2003 display minor fluctuations about some mean bed cross section previously established. These results indicate that the bed is very dynamic even in response to small flood events.

It was initially postulated that the discrepancy between field and laboratory contraction scour depths between pier bents #2 and #3 might be attributed to residual scour from Tropical Storm Alberto, which occurred in 1994 with a peak discharge of

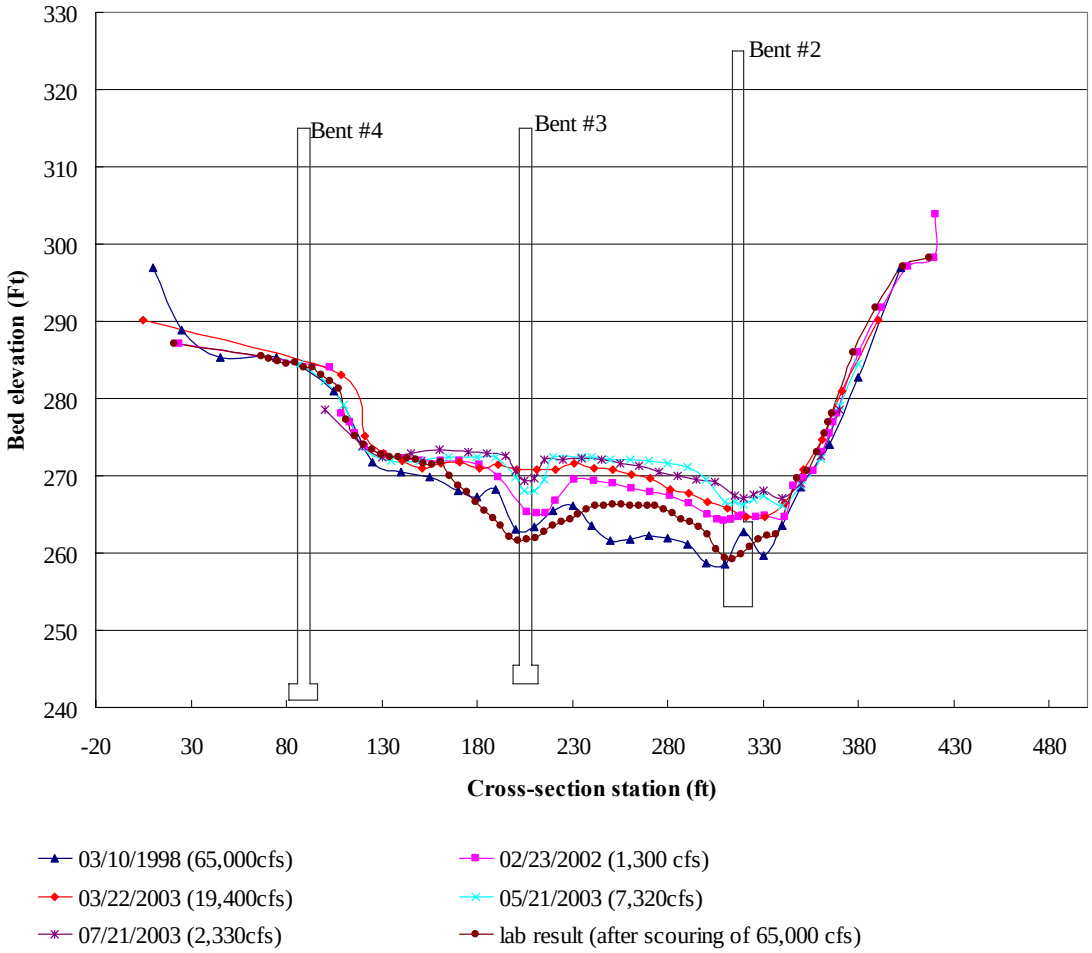

Figure 4.34 Comparison of field cross-sections upstream of the bridge in 2002 and 2003 and after the 1998 flood with the laboratory cross section after scour for the 1998 flood

107,000 cfs (just less than the 500-yr recurrence interval flood peak). Table 4.9 gives the annual peak discharges for the Ocmulgee River at Macon from 1994 through 2004, and it can be seen that from 1995 to 1997, the annual peak discharges are of the order of 30,000 cfs, which is comparable to the 2-yr recurrence interval flood. As a result, it would seem reasonable to assume that Alberto left behind residual contraction scour

that never filled back in by the time of the 1998 flood. However, Figure 4.35 compares cross-sections taken just upstream of the bridge in February 1998 before the March 1998 historic flood modeled in the laboratory, and it is clear that in the interim period from 1994 to 1998, the cross section had filled back in to an elevation of around 270 ft between pier bents #2 and #3 which is comparable to the in-fill bed elevations in the March, May, and June 2003 cross sections shown previously in Figure 4.34.

Table 4.9 Peak stream flow data, Ocmulgee river at Macon, GA

Date	Discharge (cfs)	W.S. Elev. (ft)
Jul.06, 1994	107,000	305.2
Feb.13, 1995	28,600	292.46
Oct.07, 1996	28,900	292.54
Mar.02, 1997	30,100	292.85
Mar.09, 1998	65,600	297.70
Feb.01, 1999	12,000	287.08
Jan.24, 2000	6,710	283.93
Mar.16, 2001	21,700	290.60
Apr.02, 2002	9,630	285.87

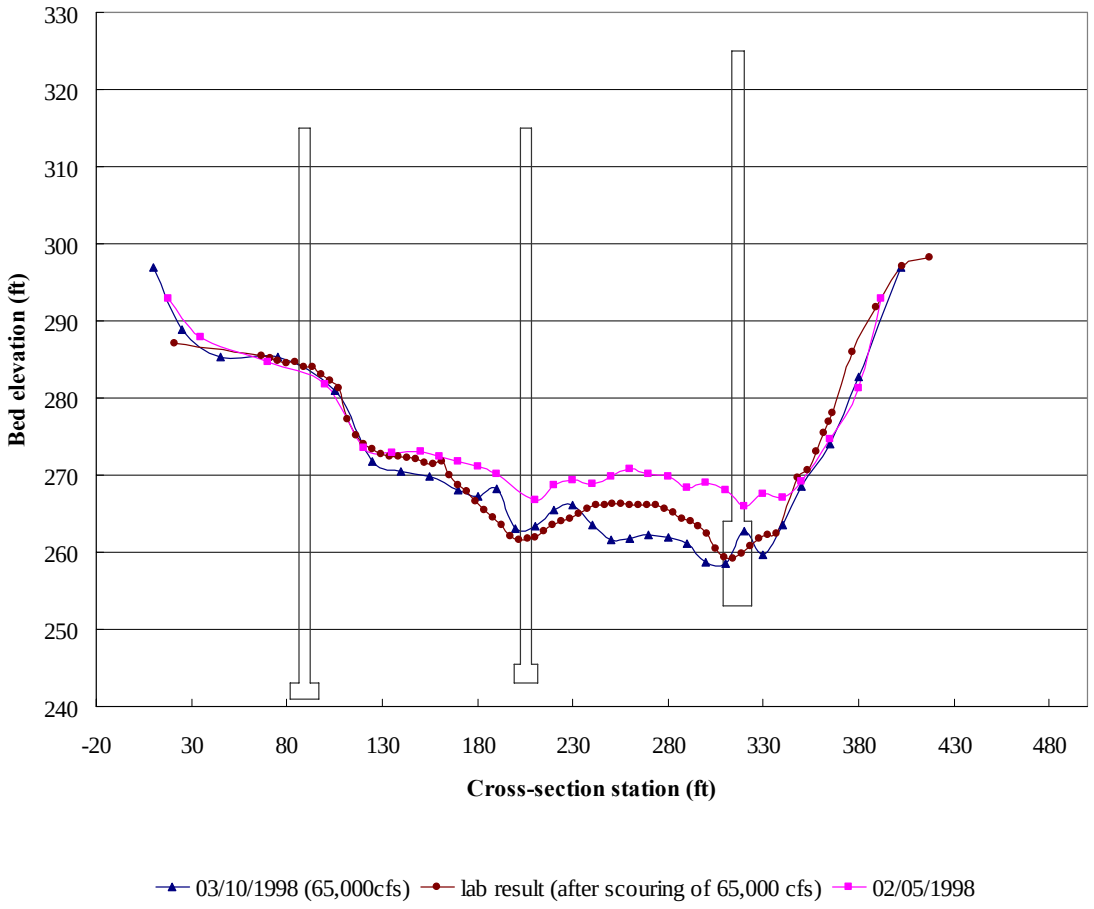

Figure 4.35 Comparison of field cross-sections upstream of the bridge before and after the 1998 flood with the laboratory cross section after scour

A second consideration in the comparison of field and laboratory contraction scour is that contraction scour is likely to vary through the bridge itself so that comparisons made only at the upstream side of the bridge may be misleading. Cross sections immediately downstream of the bridge are compared in Figure 4.36.

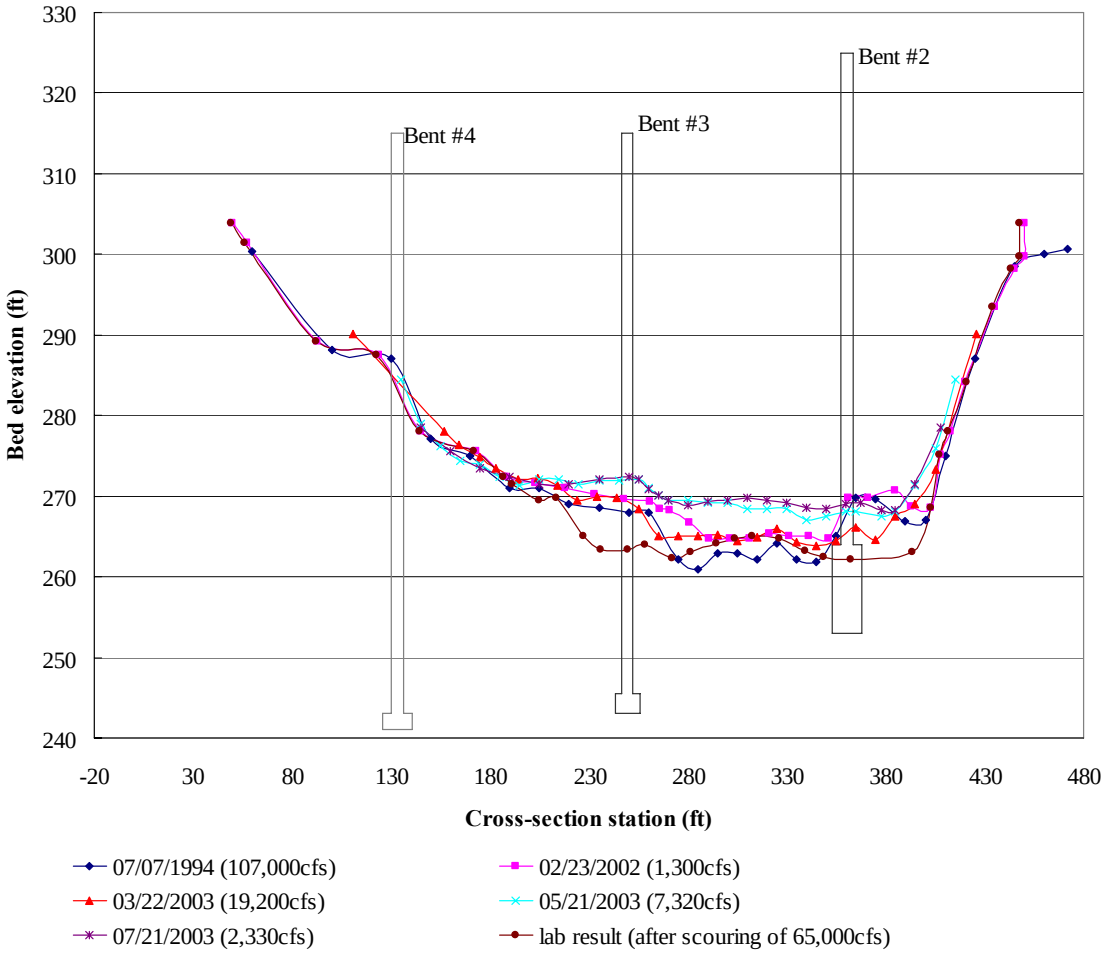

Figure 4.36 Comparison of cross-sections just downstream of the bridge in 2002 and 2003 with the 1994 flood and with the laboratory cross section after scour for the 1998 flood.

In comparing cross sections upstream and downstream of the bridge in 2002 and 2003 as shown in Figures 4.34 and 4.36, it is immediately obvious that while the March 2003 discharge of 19,400 cfs caused no change upstream of the bridge, it did cause significant scour just downstream of the bridge. In fact, the bed elevations between pier bents #2 and #3 downstream of the bridge are comparable in February

2002 and March 2003. In addition, the laboratory measured cross section after the 1998 flood (65,000 cfs) is only 1 to 2 ft above the downstream cross section for the 1994 Alberto flood discharge (107,000 cfs) between pier bents #2 and #3. In general, for the February 2002, March 2003, and the laboratory measured cross sections for the 1998 flood, the bed elevations between pier bents #2 and #3 are several feet lower on the downstream side of the bridge in comparison to the upstream side. This observation is consistent with the laboratory measurements of increasing velocity as flow passes through the bridge as shown previously in Figure 4.21, and it highlights the weakness of theoretical contraction scour formulas that assume a very long contraction.

The question now arises as to whether some of the differences between scour depths on the upstream and downstream sides of the bridge could be caused by bed forms as they pass through the bridge. Calculations were made using the bedform formulations of Van Rijn (1984) for the peak discharge of the 1998 flood (65,000 cfs). These calculations produced a value of van Rijn's transport parameter T of 23 for a dimensionless particle diameter of $d_* = 18.8$. The resulting bedform predicted is dunes with an amplitude of approximately 0.4 ft, but the prediction point is approaching the washout to a plane bed. As a result, bedform fluctuations associated with larger flood discharges seem to be smaller than the observed differences in bed elevation upstream

and downstream of the bridge.

In summary, while part of the discrepancy between the laboratory measured contraction scour and the field contraction scour immediately upstream of the bridge for the 1998 flood can be attributed to the fact that the model conditions were at less than incipient live-bed scour conditions (see Figure 4.32), other contributing factors must be present. Residual contraction scour due to Alberto does not seem to be the reason for the remaining discrepancy, nor does the relatively small amplitude of bedforms at the peak flood discharge when the field cross section was measured. The most probable cause for discrepancy is the unsteady nature of the incoming sediment transport to the contraction during the flood and the spatial variability of the contraction scour through the bridge itself.

CHAPTER V

CONCLUSIONS AND RECOMMENDATIONS

5.1 Conclusions

The physical mechanisms of the bridge scour process are very complex. Furthermore, the variability of the site conditions and the potential interaction of the various components of scour make predicting the scour depth using general formulas based on the assumption of a very long contraction and uniform sediment a tricky problem. For example, the contraction scour in the field actually develops in an abrupt contraction with a non-uniform sediment bed. The Federal Highway Administration (FHWA) gives practical equations to predict local and contraction scour depths. However, as discussed in Chapter II the suggested methods introduce the problem of overprediction in comparison to field measurements. The result can be overdesigned bridge foundations that increase the cost of the bridge. This project has addressed these concerns and the experiments were conducted to investigate the interactions between pier scour and contraction scour that are usually assumed to be independent in the calculation of total scour depth.

The experiments were conducted in three different sets. In the first set of experiments, the entire river bathymetry and the bridge piers were modeled. The second set of experiments was conducted by modeling river bathymetry but without the piers in place. Finally, the third set of experiment was conducted with a fixed bed to measure the initial velocity distribution. The experimental results show the important interaction between pier scour and contraction scour.

With the piers in place, the velocity time history was measured at the same point where the contraction scour time history was measured. The results show that if there are piers in the river, the average mean velocity time history trend at the location where the contraction scour occurred was dependent on the pier scour. On the other hand, in the case study of removing the piers in the model, the average mean velocity time history trend at the same point as before was dependent only on the time development of contraction scour. The velocity, one of the most important variables used to predict the scour depth, at the point where the contraction scour occurred, must be affected by the existence of the piers.

It was observed that the local scour developed more rapidly than the contraction scour. Furthermore, the local scour resulted in a large scour hole in front of and alongside the pier bents. Measurements of the specific discharge distribution

showed an increase just upstream of the local pier scour hole and a small decrease in the region between pier bents. The result is a reduction in contraction scour because of interaction with the piers.

The contraction scour depth measured in the laboratory model without the piers was about 25% larger than the contraction scour depth measured in the model with the piers in place. This provides further evidence of the reduced contraction scour depth that occurs due to interaction with the local pier scour.

The current guidelines recommended by HEC-18 assume that contraction and local scour processes are independent and so they are determined separately and summed to estimate total scour depth. This study shows that independent scour processes cannot be assumed. Thus, the practice of assuming independence may result in significant overestimations of scour depth.

The modeling of contraction scour in the clear-water regime at incipient live-bed conditions produced good agreement with the clear-water contraction scour equation in the model but the live-bed scour equation overestimated the contraction scour in the model as just discussed. One of the most important factors in comparing predicted and measured contraction scour is the determination of a reference contraction scour bed elevation that does not include residual local and contraction

scour.

Although comparisons between laboratory and field measurements of local pier scour were quite good, the field contraction scour on the upstream side of the bridge was larger than measured in the laboratory model for one particular historic flood event with a recurrence interval of approximately 20 years. Better agreement was obtained on the downstream side of the bridge. The field results indicate that contraction scour is very dynamic and constantly adjusting to the incoming sediment load, and that the assumption of a long contraction that underpins the theoretical contraction scour formulas is not entirely accurate.

5.2 Recommended future study

This study shows that contraction scour and pier scour are not independent. However, to assess the relative contribution of contraction scour and local pier scour to the final design value of the bridge foundation depth, more field and laboratory data are needed. In particular, both temporal and spatial distributions of bed elevations during a significant scour event need to be measured in both the field and laboratory for a specific bridge in order to make useful comparisons and to suggest improvements in contraction scour predictions. The unrealistic assumption of a long contraction and the sensitivity of

contraction scour to temporal changes in upstream sediment discharges especially need to be addressed.

It would be very helpful to explore further the issue raised by Figure 4.32 in which clear-water contraction scour measurements in the laboratory are compared with live-bed contraction scour predictions. Additional experiments near V/V_c = 1.0 would help resolve this modeling issue.

A review of the literature found 29 references with mention of contraction and (or) abutment scour data, but only one presented detailed data collected during floods (Mueller and Wagner, 2005). Additional field data for contraction scour are needed in great enough detail that a corresponding laboratory model study can be used to better understand the contraction scour process and improve the reliability of bridge foundation design methodology.

APPENDIX A

Initial cross sections before scour

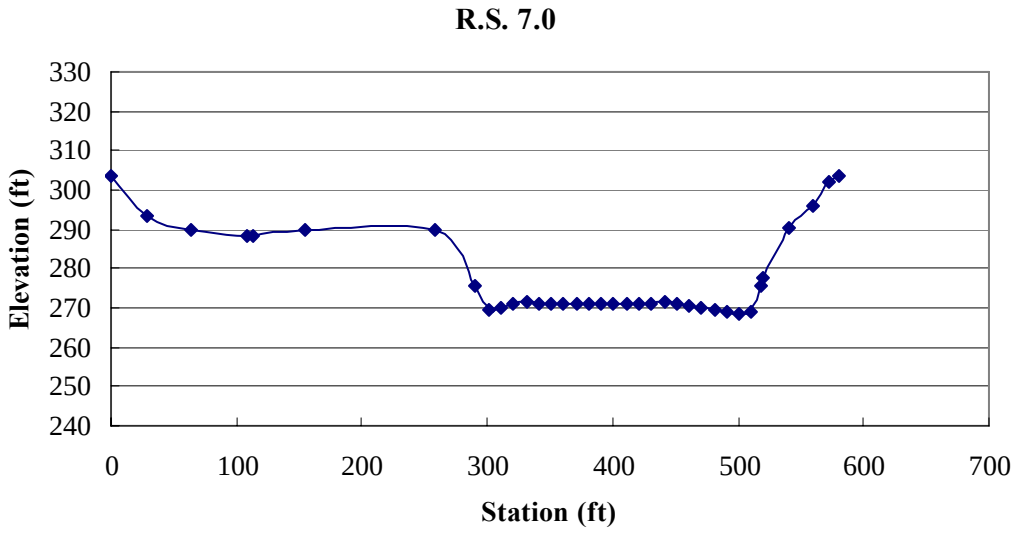

Figure A.1 Initial cross section before scour at R.S. 7.0

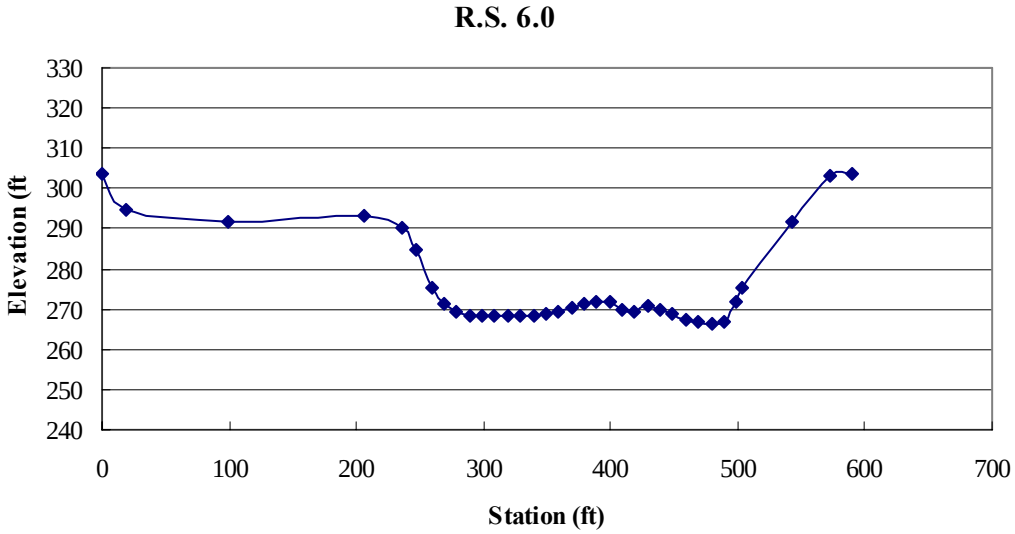

Figure A.2 Initial cross section before scour at R.S. 6.0

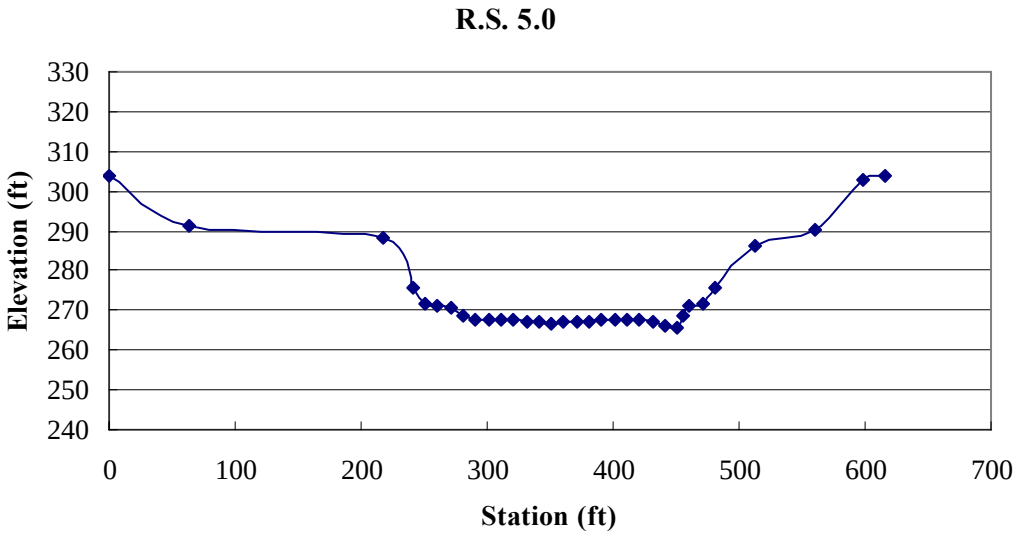

Figure A.3 Initial cross section before scour at R.S. 5.0

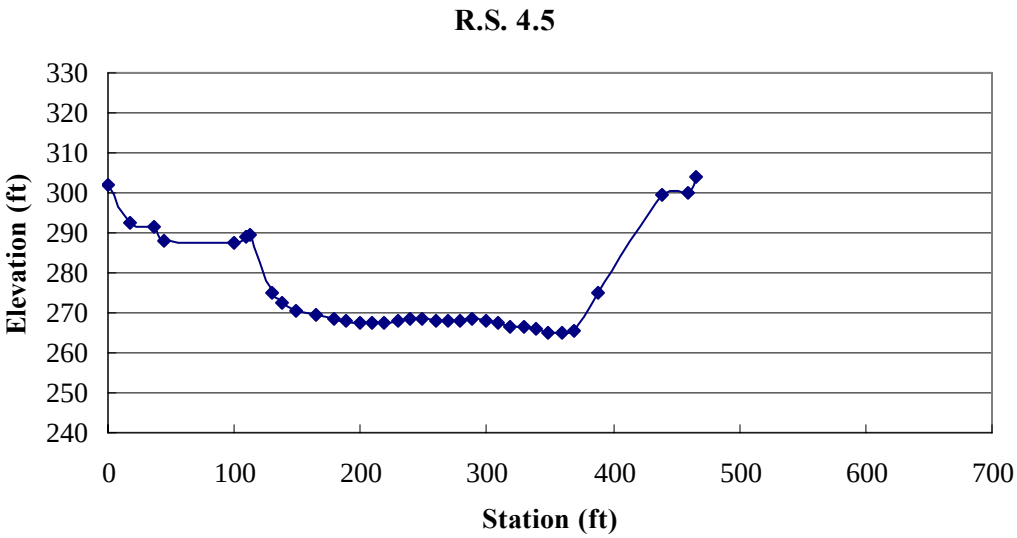

Figure A.4 Initial cross section before scour at R.S. 4.5

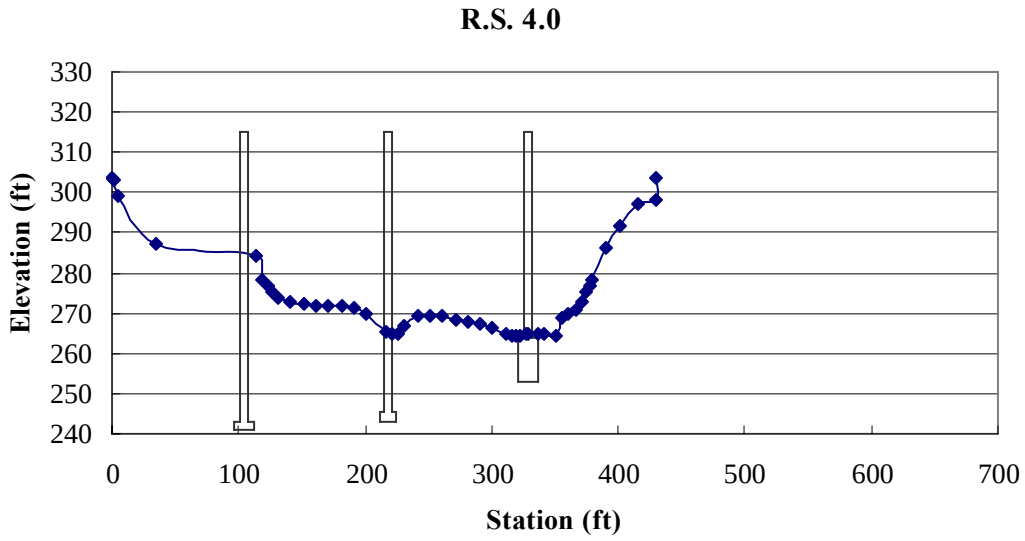

Figure A.5 Initial cross section before scour at R.S. 4.0

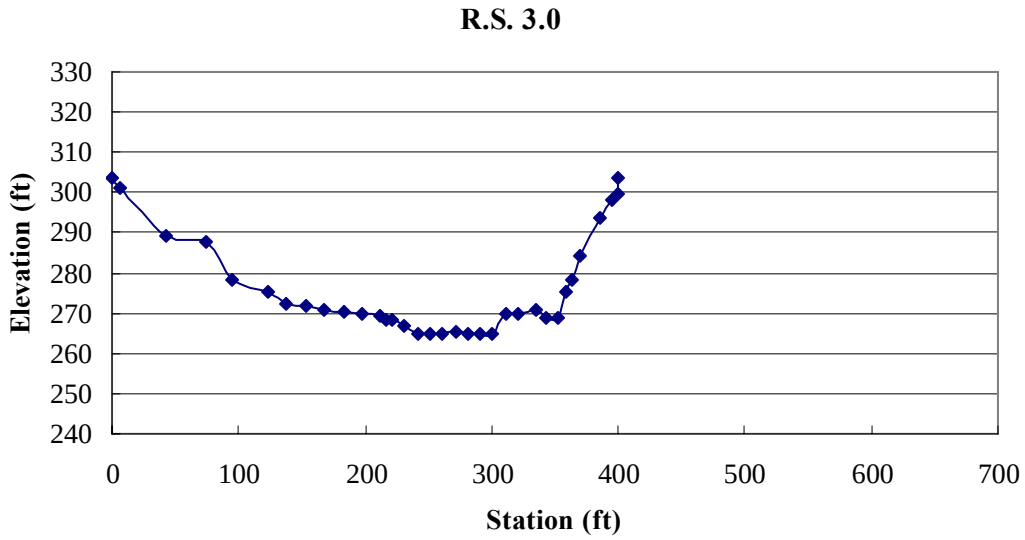

Figure A.6 Initial cross section before scour at R.S. 3.0

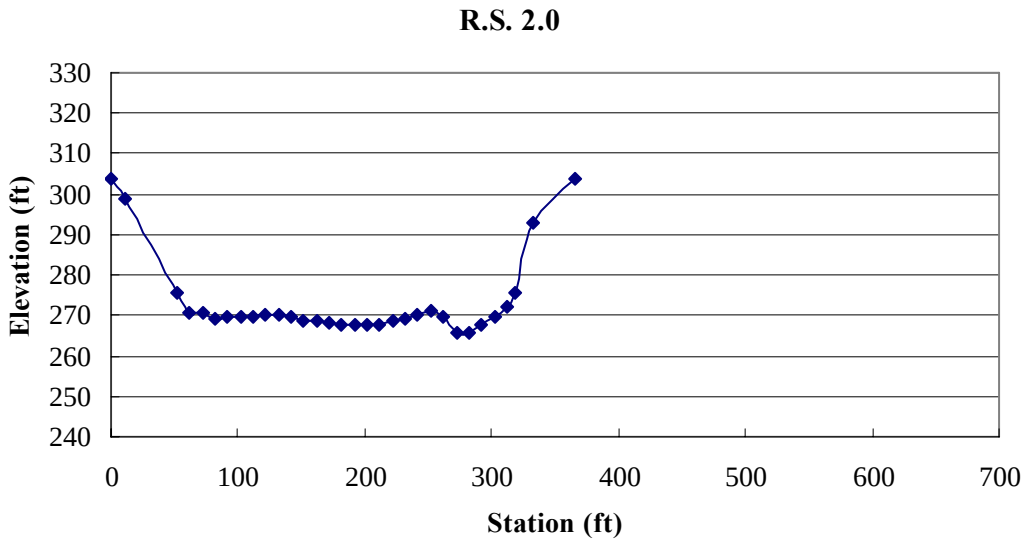

Figure A.7 Initial cross section before scour at R.S. 2.0

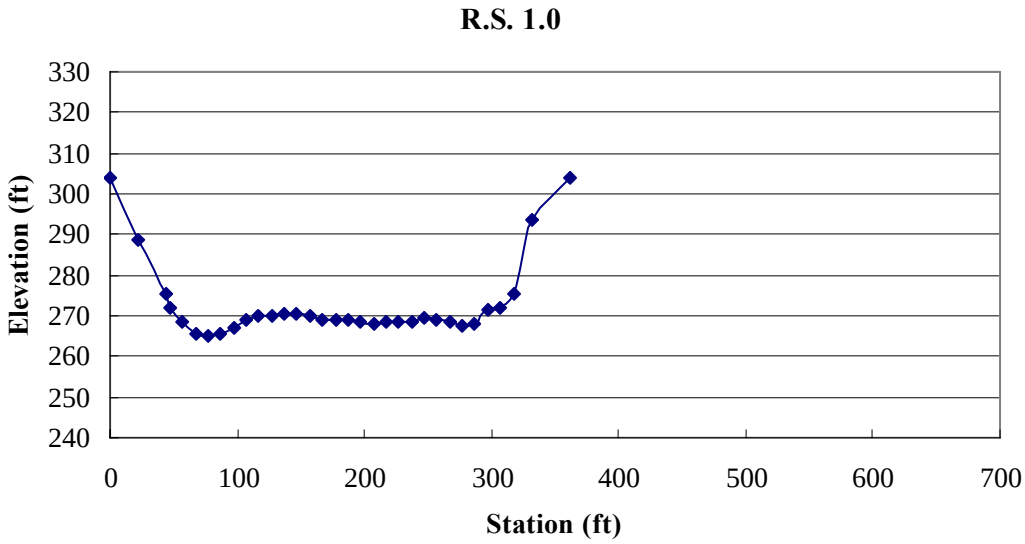

Figure A.8 Initial cross section before scour at R.S. 1.0

APPENDIX B

Velocity, water depth and specific discharge distribution after scouring at R.S. 4.0

Table B.1 Velocity, water depth and specific discharge distribution across the R.S. 4.0 (4.79cfs)

(a = distance from left wall (looking downstream), V = point mean velocity, y = water depth at the point, q = specific discharge)

a (ft)	V (ft/s)	y (ft)	q (ft^2/s)
4.30	0.427	0.307	0.131
4.70	0.694	0.313	0.217
5.00	0.720	0.327	0.235
5.10	0.711	0.336	0.239
5.50	0.494	0.515	0.254
6.00	0.636	0.599	0.381
6.25	0.720	0.606	0.436
6.50	0.949	0.610	0.579
6.75	1.025	0.670	0.687
7.00	1.174	0.726	0.852
7.25	1.138	0.766	0.871
7.60	1.118	0.836	0.935
8.00	1.227	0.783	0.960
8.25	1.230	0.758	0.932
8.50	1.273	0.739	0.941
8.75	1.293	0.738	0.955
9.00	1.210	0.734	0.888
9.25	1.223	0.756	0.925
9.50	1.207	0.786	0.949
9.75	1.232	0.843	1.039
10.00	0.983	0.891	0.876
10.25	1.043	0.847	0.884
10.50	1.080	0.821	0.887
11.10	0.893	0.499	0.446

Table B.2 Velocity, water depth and specific discharge distribution across the R.S. 4.0 (5.83cfs)

(a = distance from left wall (looking downstream), V = point mean velocity, y = water depth at the point, q = specific discharge)

a (ft)	V (ft/s)	y (ft)	q (ft^2/s)
4.30	0.670	0.347	0.232
4.70	0.766	0.375	0.287
5.00	0.717	0.379	0.272
5.10	0.720	0.384	0.277
5.50	0.620	0.534	0.331
6.00	0.669	0.635	0.425
6.25	0.779	0.645	0.502
6.50	0.918	0.647	0.594
6.75	1.027	0.702	0.721
7.00	1.083	0.811	0.878
7.25	1.168	0.898	1.049
7.60	1.102	1.020	1.123
8.00	1.246	0.891	1.110
8.25	1.280	0.856	1.096
8.50	1.288	0.804	1.036
8.75	1.313	0.802	1.053
9.00	1.337	0.813	1.087
9.25	1.293	0.810	1.047
9.50	1.222	0.815	0.996
9.75	1.091	0.878	0.958
10.00	0.959	0.939	0.900
10.25	1.017	0.887	0.902
10.50	1.111	0.807	0.896
11.10	1.074	0.539	0.579
11.50	0.933	0.267	0.249

Table B.3 Velocity, water depth and specific discharge distribution across the R.S. 4.0 (6.50cfs)

(a = distance from left wall (looking downstream), V = point mean velocity, y = water depth at the point, q = specific discharge)

a (ft)	V (ft/s)	y (ft)	q (ft^2/s)
4.70	0.938	0.397	0.372
5.00	0.881	0.514	0.453
5.10	0.845	0.530	0.448
5.50	0.783	0.587	0.459
6.00	0.798	0.675	0.539
6.25	0.879	0.683	0.600
6.50	0.940	0.687	0.646
6.75	1.062	0.800	0.849
7.00	1.167	0.895	1.044
7.25	1.251	0.970	1.213
7.60	1.155	1.113	1.285
8.00	1.304	0.952	1.242
8.25	1.319	0.920	1.214
8.50	1.317	0.885	1.165
8.75	1.337	0.860	1.150
9.00	1.318	0.848	1.117
9.25	1.219	0.837	1.020
9.50	1.229	0.841	1.034
9.75	1.161	0.888	1.031
10.00	1.042	0.963	1.003
10.25	1.085	0.950	1.031
10.50	1.158	0.887	1.027
11.10	1.065	0.579	0.617
11.50	1.020	0.307	0.313

APPENDIX C

Velocity, water depth and specific discharge distribution with fixed bed at R.S. 4.0

Table C.1 Velocity, water depth and specific discharge distribution across the R.S. 4.0 (4.79cfs)

(a = distance from left wall (looking downstream), V = point mean velocity, y = water depth at the point, q = specific discharge)

a (ft)	V (ft/s)	y (ft)	q (ft^2/s)
4.30	0.694	0.307	0.213
4.70	0.720	0.320	0.230
5.00	0.697	0.330	0.230
5.10	0.699	0.327	0.229
5.50	0.645	0.522	0.337
6.00	0.766	0.606	0.464
6.25	0.876	0.607	0.532
6.50	1.055	0.608	0.641
6.75	1.123	0.610	0.685
7.00	1.266	0.630	0.797
7.25	1.210	0.670	0.810
7.60	1.202	0.761	0.915
8.00	1.346	0.670	0.902
8.25	1.359	0.666	0.905
8.50	1.367	0.670	0.916
8.75	1.373	0.688	0.945
9.00	1.371	0.701	0.961
9.25	1.384	0.714	0.988
9.50	1.321	0.750	0.990
9.75	1.282	0.780	1.000
10.00	1.143	0.770	0.880
10.25	1.148	0.770	0.884
10.50	1.132	0.770	0.872
11.10	1.276	0.499	0.637

Table C.2 Velocity, water depth and specific discharge distribution across the R.S. 4.0 (5.83cfs)

(a = distance from left wall (looking downstream), V = point mean velocity, y = water depth at the point, q = specific discharge)

a (ft)	V (ft/s)	y (ft)	q (ft^2/s)
4.30	0.829	0.347	0.288
4.70	0.796	0.360	0.286
5.00	0.779	0.370	0.288
5.10	0.757	0.367	0.278
5.50	0.675	0.562	0.379
6.00	0.784	0.646	0.506
6.25	0.891	0.647	0.576
6.50	1.007	0.648	0.653
6.75	1.125	0.650	0.732
7.00	1.199	0.670	0.803
7.25	1.275	0.710	0.905
7.60	1.187	0.801	0.951
8.00	1.282	0.710	0.910
8.25	1.306	0.706	0.922
8.50	1.334	0.710	0.947
8.75	1.361	0.728	0.991
9.00	1.392	0.741	1.032
9.25	1.374	0.754	1.036
9.50	1.302	0.790	1.029
9.75	1.203	0.820	0.987
10.00	1.051	0.810	0.851
10.25	1.092	0.810	0.885
10.50	1.139	0.810	0.923
11.10	1.124	0.539	0.606
11.50	0.995	0.267	0.266

Table C.3 Velocity, water depth and specific discharge distribution across the R.S. 4.0 (6.50cfs)

(a = distance from left wall (looking downstream), V = point mean velocity, y = water depth at the point, q = specific discharge)

a (ft)	V (ft/s)	y (ft)	q (ft^2/s)
4.70	0.939	0.400	0.376
5.00	0.876	0.410	0.359
5.10	0.868	0.407	0.353
5.50	0.769	0.602	0.463
6.00	0.920	0.686	0.631
6.25	0.996	0.687	0.684
6.50	1.080	0.688	0.743
6.75	1.151	0.690	0.794
7.00	1.233	0.710	0.875
7.25	1.288	0.750	0.966
7.60	1.246	0.841	1.048
8.00	1.366	0.750	1.024
8.25	1.347	0.746	1.005
8.50	1.335	0.750	1.001
8.75	1.399	0.768	1.074
9.00	1.451	0.781	1.133
9.25	1.462	0.794	1.161
9.50	1.360	0.830	1.129
9.75	1.213	0.860	1.043
10.00	1.036	0.850	0.881
10.25	1.110	0.850	0.944
10.50	1.176	0.850	1.000
11.10	1.160	0.579	0.672
11.50	1.065	0.307	0.327

APPENDIX D

Mean velocity and water depth with fixed bed at R.S. 5.0

Table D.1 Mean velocity and water depth across the R.S. 5.0 (4.79cfs) (a = distance from left wall (looking downstream), V = point mean velocity, y = water depth at the point)

a (ft)	V (ft/s)	y (ft)
3.5	0.526	0.215
4.0	0.565	0.269
4.5	0.520	0.262
5.0	0.404	0.285
5.5	0.356	0.280
6.0	0.587	0.474
6.5	0.873	0.638
7.0	1.114	0.687
7.5	1.290	0.705
8.0	1.292	0.708
8.5	1.210	0.726
9.0	1.244	0.721
9.5	1.295	0.719
10.0	1.190	0.727
10.5	1.055	0.758
11.0	0.932	0.625
11.5	0.522	0.446
12.0	0.093	0.316
average	1.022	0.585

Table D.2 Mean velocity and water depth across the R.S. 5.0 (5.83cfs) (a = distance from left wall (looking downstream), V = point mean velocity, y = water depth at the point)

a (ft)	V (ft/s)	y (ft)
4.3	0.696	0.301
4.5	0.715	0.294
5.0	0.620	0.317
5.5	0.581	0.312
6.0	0.789	0.506
6.5	1.003	0.670
7.0	1.273	0.719
7.5	1.344	0.737
8.0	1.252	0.740
8.5	1.322	0.758
9.0	1.347	0.753
9.5	1.253	0.751
10.0	1.232	0.759
10.5	1.265	0.790
11.0	0.978	0.657
11.5	0.526	0.478
12.0	0.117	0.348
average	1.102	0.625

Table D.3 Mean velocity and water depth across the R.S. 5.0 (6.50cfs) (a = distance from left wall (looking downstream), V = point mean velocity, y = water depth at the point)

a (ft)	V (ft/s)	y (ft)
3.5	0.750	0.298
4.0	0.761	0.307
4.5	0.750	0.304
5.0	0.724	0.327
5.5	0.726	0.352
6.0	0.736	0.546
6.5	0.992	0.710
7.0	1.306	0.759
7.5	1.365	0.777
8.0	1.369	0.780
8.5	1.304	0.798
9.0	1.375	0.793
9.5	1.320	0.791
10.0	1.242	0.799
10.5	1.327	0.830
11.0	1.107	0.697
11.5	0.698	0.518
12.0	0.196	0.388
average	1.147	0.665

APPENDIX E

Adjusted cross sections for residual scour

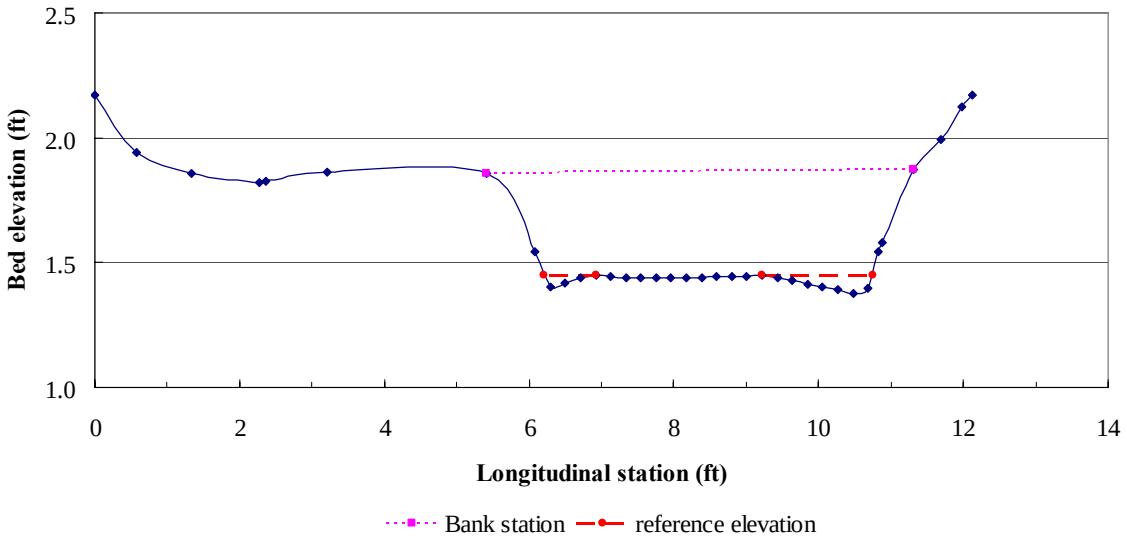

Figure E.1 Adjusted cross sections for residual scour at R.S. 7.0

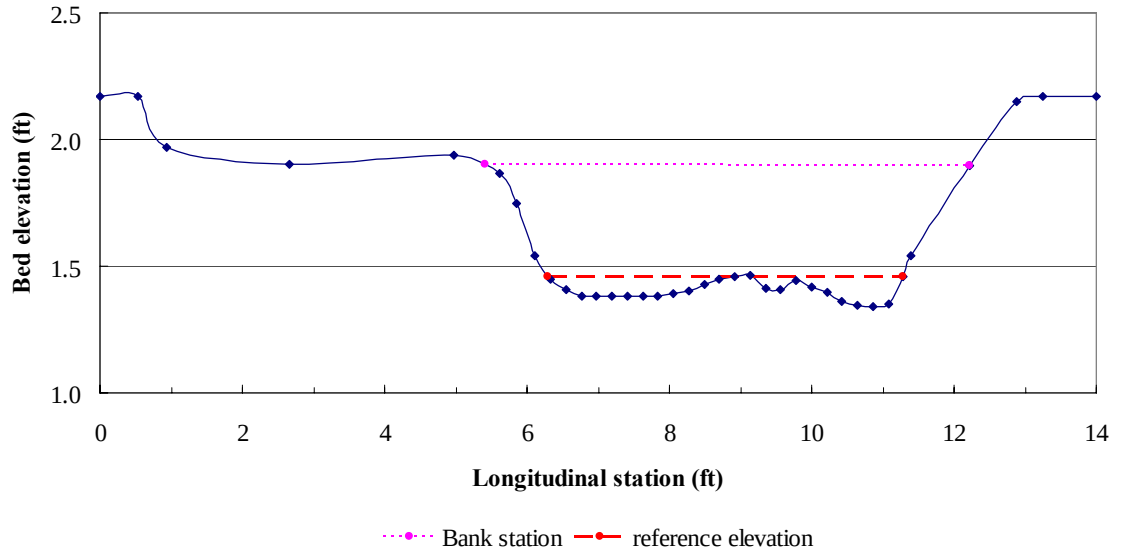

Figure E.2 Adjusted cross sections for residual scour at R.S. 6.0

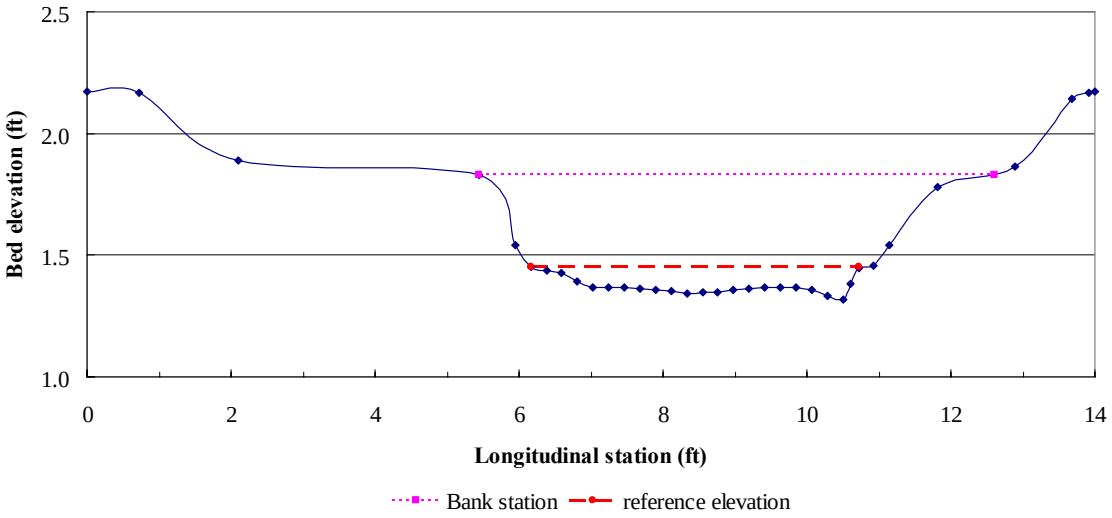

Figure E.3 Adjusted cross sections for residual scour at R.S. 5.0

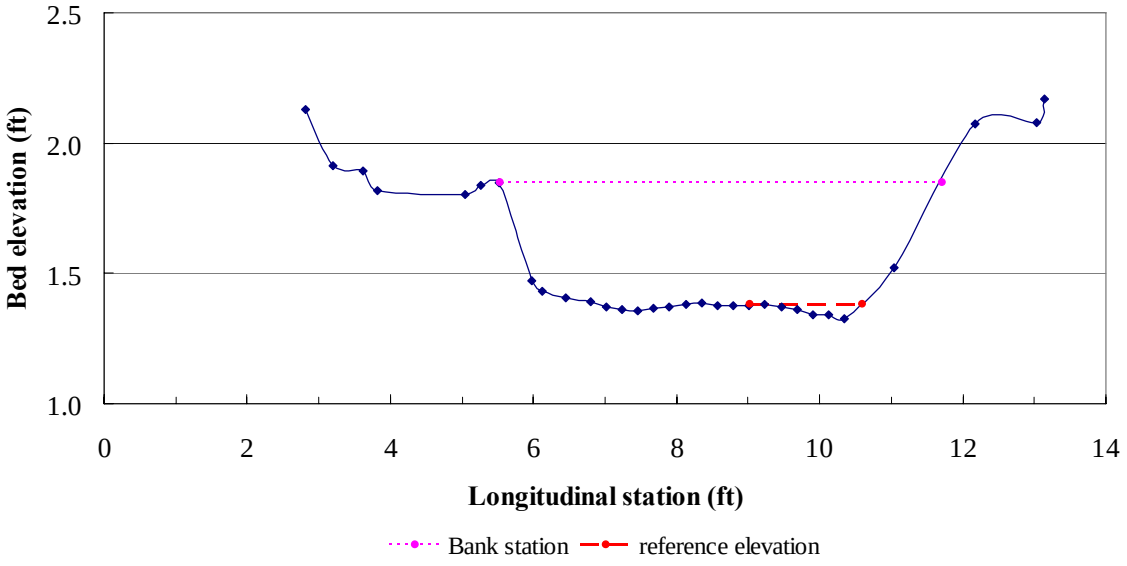

Figure E.4 Adjusted cross sections for residual scour at R.S. 4.5

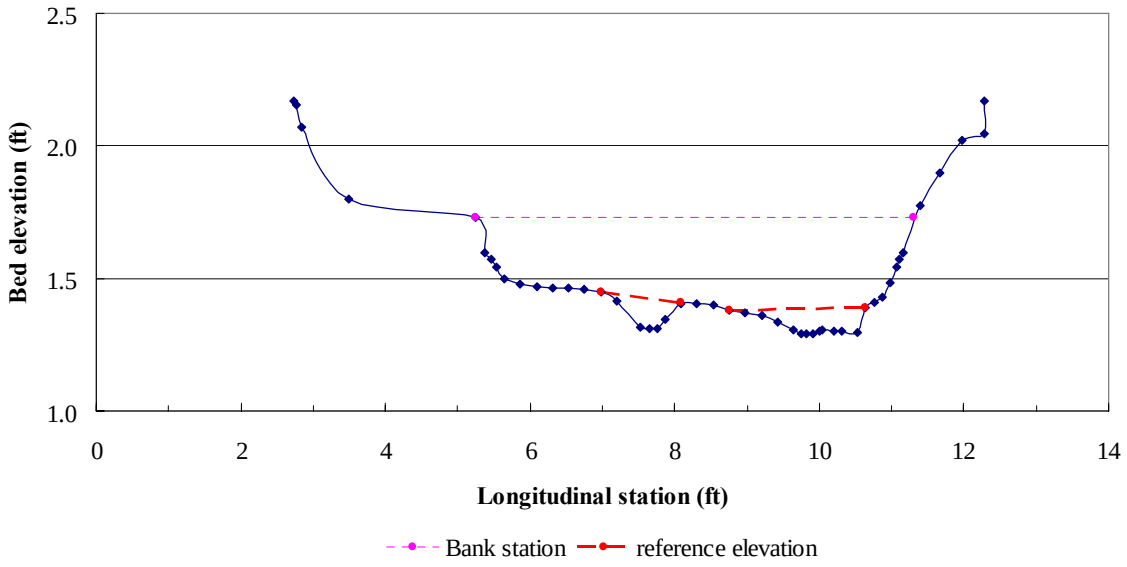

Figure E.5 Adjusted cross sections for residual scour at R.S. 4.0

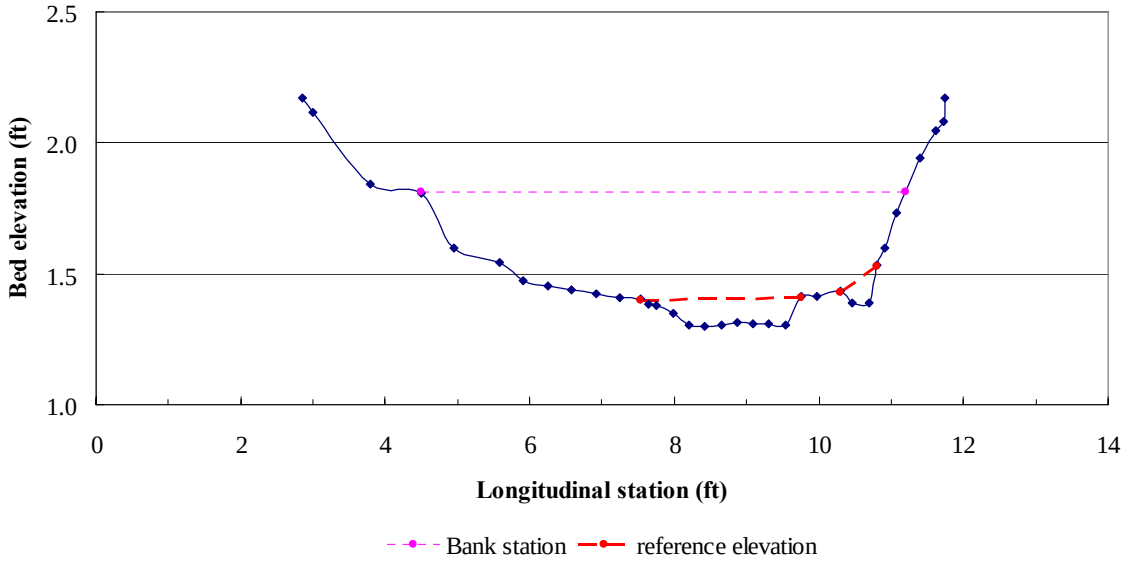

Figure E.6 Adjusted cross sections for residual scour at R.S. 3.0

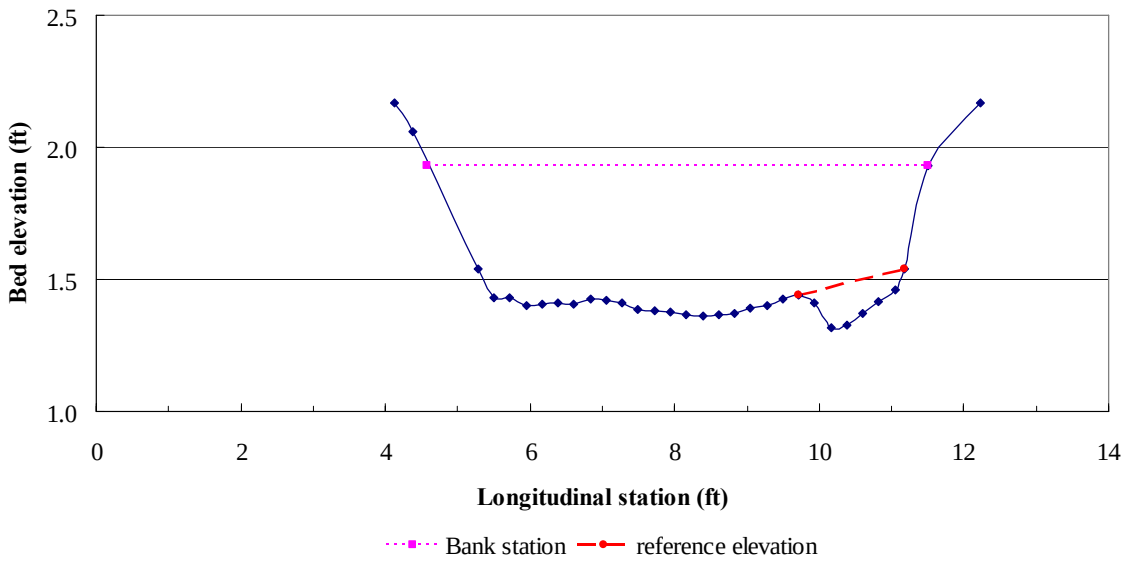

Figure E.7 Adjusted cross sections for residual scour at R.S. 2.0

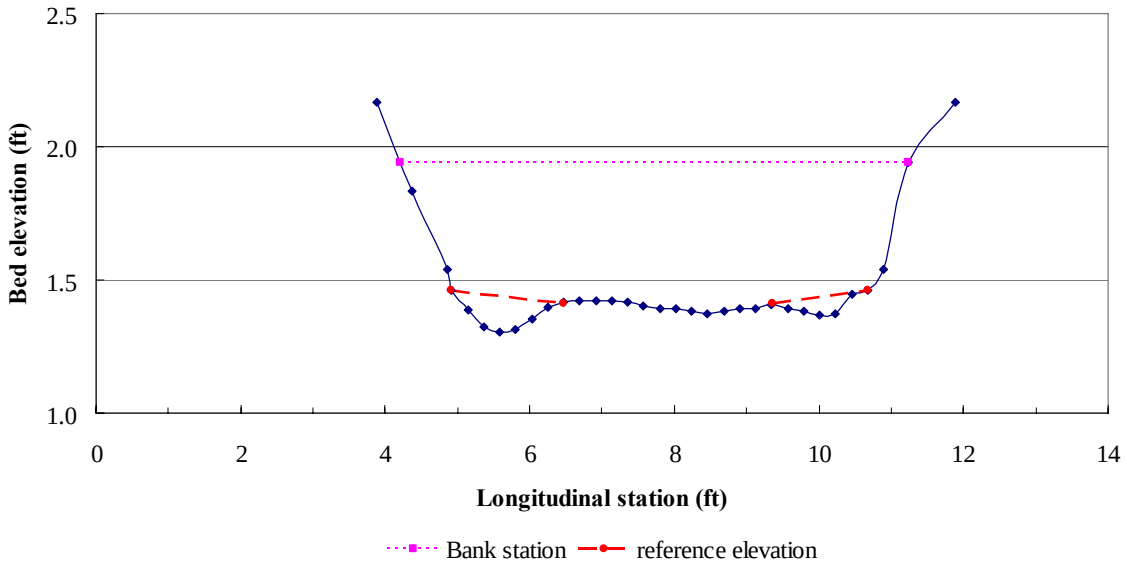

Figure E.8 Adjusted cross sections for residual scour at R.S. 1.0

REFERENCES

Arneson, Larry A., and Abt, Steven R. (1998). “Vertical contraction scour at bridges with water flowing under pressure conditions.”, Journal of Transportation Research Record, n 1647, pp.10-17

Benedict, S.T. and Caldwell, A.W. (1998). “The collection of clear-water contraction and abutment scour data at selected bridges sites in the coastal plain and piedmont of South Carolina” Water Resources Engineering, ASCE, Menphis, TN, pp.216-222

Blodgett, J.C. and Harris Carroll D. (1993). “Measurement of bridge scour at the SR-32 crossing of the Sacramento river at Hamilton City, California, 1987-92” Proc.,Hydraulic Engineering, ASCE, San Francisco, CA, pp.1860-1865

Brabets, T.P. (1994). “Scour assessment at bridges from flag point to Million Dollar Bridge, Copper River Highway, Alaska.”, Anchorage, AK, U.S. Geological Survey Water-Resources Investigations Report 94-4073

Brabets, T.P. (1995). “Application of surface geophysical techniques in a study of the geomorphology of the lower Copper River, Alaska”, Anchorage, AK, U.S. Geological Survey Water-Resources Investigations Report 94-4165

Fischer, Edward E. (1993). “Scour at bridge over the Weldon river, Iowa.” Proc., Hydraulic Engineering, ASCE, San Francisco, CA, pp.1854-1859

Fischer, Edward E. (1994). “Contractions scour at a bridge over the Iowa river.” Proc., Hydraulic Engineering, ASCE, Buffalo, NY, pp. 31-35

Fischer, Edward E. (1995). “Contractions scour at a bridge over Wolf creek, Iowa.” Proc., Water Resources Engineering V1, ASCE, San Antonio, TX, pp. 430-434

French, Richard H. (1986). Open Channel Hydraulic. Text book series in Water resources and Environmental Engineering, McGraw-Hill, NY.

Froehlich, David C. (1989). “Local scour at bridge abutments.”, Proc. National Conference of Hydraulic Engineering, ed. M.A. Ports, ASCE, New Orleans, LU pp.13-18

Froehlich, David C. (1995). “Armor-limited clear water contraction scour at bridge.”, Journal of Hydraulic Engineering. V121, n 6, pp.490-493

Hayes, D.C. (1996). “Scour at bridge sites in Delaware, Maryland, and Virginia”, Richmond, VA, U.S. Geological Survey Water-Resources Investigations Report 96-4089

Hunt, B.E. et al (1998). “Scour monitoring of the Woodrow Wilson bridge” Water Resources Engineering, ASCE, Memphis, TN, pp.57-62

Holnbeck, Stephen R., Parrett, Charles., and Tillinger, Todd N. (1993). “Bridge scour and change in contracted section, Razor Creek.” Proc., Hydraulic Engineering, ASCE, San Francisco, CA, pp.2249-2255

Laursen, E.M. (1958a) “Scour at bridge crossings.” Iowa Highway Research Board Bulletin No. 8. Iowa City: Iowa Institute of Hydraulic Research, University of Iowa

Laursen, E.M. (1958b) “The total sediment load of streams.”, Journal of Hydraulic Div., ASCE 54, no. HY1, pp.1-36

Laursen, E.M. (1960) “Scour at bridge crossings.”, Journal of Hydraulic Div., ASCE 86, no. HY2, pp.39-54

Laursen, E.M. (1963) “An analysis of relief bridge scour.”, Journal of Hydraulic Div., ASCE 89, no. HY3, pp.93-117

Landers, M.N., and Mueller, D.S. (1993). “Reference surfaces for bridge scour depths.” Proc., National Conference on Hydraulic Engineering, ASCE, San Francisco, CA, pp.2075-2080

Lane, S.N., Biron, P.M., Bradbrook, K.F., Butler, J.B., Chander, J.H., Crowell, M.D., Mclelland, S.J., Richards, K.S., and Roy, A.G. (1998). “Three-dimensional measurment of river channel flow processes using Acoustic Doppler Velocimetry.” Earth Surface Processes and Landforms, 23, pp.1247-1267

Lim, Siow-yong., and Cheng, Nian-Sheng. (1998). “Scouring in long contraction.”, Journal of Irrigation and Drainage Engineering, V 124, n 5, pp.258-261

Martin, V., Fisher, T.S.R., Millar, R.G., and Quick, M.C. (2002). “ADV data analysis for turbulent flows: low correlation problem.”, Hydraulic Measurement and Experiment Methods 2002, Proc. Of the Specialty Conf., ed. By T.L. Wahl, C.A. Pugh, K.A. Oberg, and T.B. Vermeyen, ASCE, Reston, VA

Melville, B.W., and Coleman, S.E. (2000). Bridge Scour. Water Resources Publications, Highlands Ranch, Colorado.

Morris, J.L., and Pagan-Ortiz, J.E. (1999). “Bridge scour evaluation program in the United States.”, Stream Stability and Scour at Highway Bridges, E.V. Richardson and P.F. Lagasse, eds., ASCE, pp.61-70

Mueller, D.S. and Hitchcock, H.A. (1998). “Scour measurements at contracted highway crossing in Minnesota, 1997” Water Resources Engineering, ASCE, Menphis, TN, pp.210-215

Mueller, D.S. and Wagner, C.R. (2005). “Field observation and evaluations of streambed scour at bridges.” Lousiville, KY, U.S. Department of Transportation FHWA-RD-03-052

Niezgoda, Sue L., and Johnson, Peggy A. (1999). “Abutment scour at small severly contracted bridges.” Proc., Cold Regions Engineering ‘Putting Into Practice’., ASCE, Lincoln, NH, pp.600-611

Norman, V.W. (1975). “Scour at selected bridge sites in Alaska”, Anchorage, AK, U.S. Gelolgacal Survey Water-Resources Investigations Report 32-75.

Parola, A.C., Hagerty, D.J., Mueller, D.S., Melville, B.W., Parker, G., and Usher, J.S.(1997b). “The need for research in scour at bridge crossings.” Proc., Of XXVII IAHR Congress, Managing Water: Coping with Scarcity and Abundance, San Francisco, CA, pp. 124-129

Pagan-ortiz,J.E. (1998). “Status of the scour evaluation of bridges over waterways in the United States”, Water Resources Engineering, ASCE, Memphis, TN, pp.2-4

Richardson, E.V. and Richardson, J.R. (1999). “Determining contraction scour”, In Stream Stability and Scour at Highway Bridges, ed. E. V. Richardson and P.F. Lagasse, ASCE, pp. 483-491

Richardson, E.V. and Davis, S.R. (2001). “Evaluating scour at bridges, Fourth edition”, Hydraulic engineering circular No.18, Federal Highway Administration, U.S. Department of Transportation Report No. FHWA NHI 01-001 HEC-18.

Schreider, Mario., Scacchi, Graciela., Franco, Felipe., and Romano, Carlos. (2001). “Contraction and abutment scour in relief bridge in a flood plain.” Proc., Wetlands Engineering and River Restoration, ASCE, Reno, NV, pp.1375-1386

Shields, A. (1936). “Application of similarity principles and turbulence research to bed-load movement. trans.”, W.P. ott and J.C. van Uchelen. Hydrodynamics Laboratory Publ. No. 167. Pasadena: USDA, Soil Conservation Service Cooperative Laboratory, California Institute of Technology.

SonTek (2001). “Acoustic Doppler Velocimeter (ADV) principles of operation.” SonTek Technical Notes, SonTek, San Diego, CA.

Sturm, T.W. (1999). “Abutment scour in compound channels.” In Stream Stability and Scour at Highway Bridges, ed. E. V. Richardson and P.F. Lagasse, ASCE, pp. 443-456

Sturm T.W. (1999). “Abutment scour studies for compound channels.” Washington, DC, Federal Highway Administration, U.S. Department of Transportation Report No. FHWA-RD-99-156

Sturm, T.W. (2001). Open Channel Hydraulic. Text book series in Water resources and Environmental Engineering, McGraw-Hill, NY.

Sturm, T. W. et al (2004). “Laboratory and 3D numerical modeling with field monitoring of regional bridge scour in Georgia”, Atlanta, GA, Georgia Department of Transportation Final Project, Project No. 2002

U.S. Army Corp of Engineers. (1998). HEC-RAS Hydraulic Reference Manual, Version 2.2. Davis, CA: U.S. Army Corps of Engineers, Hydrologic Engineering Center.

Van Rijn, L.C. (1984a) “Sediment transport, Part I: Bed load transport.”, Journal of Hydraulic Engineering, ASCE 110, no. 10, pp. 1431-56

Van Rijn, L.C. (1984b) “Sediment transport, Part II: Suspended load transport.”, Journal of Hydraulic Engineering, ASCE 110, no. 11, pp. 1613-41

Van Rijn, L.C. (1984c) “Sediment transport, Part III: Bed form and alluvial roughness.”, Journal of Hydraulic Engineering, ASCE 110, no. 12, pp. 1733-54

Wahl, T. (2002). “Analyzing ADV data using WinADV.”, Hydraulic Measurements and Experiemts Methods 2002, Proc. Of the Specialty Conf., ed. By T.S. Wahl, C.A. Pugh, K.A. Oberg, and T.B. Vermey

White, F.M. (1991). Viscous Fluid Flow second edition. Text book series in Mechanical Engineering, McGraw-Hill, NY.